

REPORT DOCUMENTATION PAGE

Form Approved
OMB No. 0704-0188

Pulic reporting burden for this collection of information is estimated to average 1 hour per response, including the time for reviewing instructions, searching existing data sources, gathering and maintaining the data needed, and completing and reviewing the collection of information. Send comments regarding this burden estimate or any other aspect of this collection of information, including suggestions for reducing this burden, to Washington Headquarters Services, Directorate for information Operations and Reports, 1215 Jefferson Davis Highway, Suite 1204, Arlington, VA 22202-4302, and the Office of Management and Budget, Paperwork Reduction Project (0704-0188), Washington, DC 20503.

1. AGENCY USE ONLY (Leave Blank)		2. REPORT DATE 12/28/02	3. REPORT TYPE AND DATES COVERED Phase I Final Report 3/20/02 - 9/20/02	
4. TITLE AND SUBTITLE Detection, Tracking and Classification of Multiple Targets using Advanced Beamforming and Classification Methods			5. FUNDING NUMBERS DAAE3002C1058	
6. AUTHOR(S) M.R. Azimi-Sadjadi and K. Khorasani				
7. PERFORMING ORGANIZATION NAME(S) AND ADDRESS(ES) Information Systems Technologies, Inc. 5412 Hilldale Court Fort Collins, CO 80526			8. PERFORMING ORGANIZATION REPORT NUMBER IST000F	
9. SPONSORING/MONITORING AGENCY NAME(S) AND ADDRESS(ES) US Army TACOM-ARDEC AMSTA-AR-FSF-R, Bldg 407 Picatinny Arsenal, NJ 07806-5000			10. SPONSORING/MONITORING AGENCY REPORT NUMBER	
11. SUPPLEMENTARY NOTES				
12a. DISTRIBUTION/AVAILABILITY STATEMENT Approved for public release; distribution unlimited.			12b. DISTRIBUTION CODE	
13. ABSTRACT (Maximum 200 words) Report developed under SBIR contract for topic A01-020. Detection, tracking and localization of ground targets, e.g. trucks and tanks, using unattended passive acoustic sensor arrays is considered. Several factors complicate this problem. These include: non-stationary target signatures, loss of coherence and fading, wind noise and weather/environmental effects, competing clutter, lack of any prior knowledge about the number of targets, and presence of multiple targets in tight formations. The goal of this Phase I research was to develop fast and accurate direction of arrival (DOA) estimation and source separation algorithms to localize and resolve multiple closely spaced targets. The array geometry was considered to develop two classes of algorithms. The first class is based upon high-resolution subspace-based DOA estimation methods that can be used to localize and track the targets. The second class, however, is based upon source separation methods using variants of independent component analysis for determining the number of potential targets. Of particular importance was to investigate target detection and information extraction in spatially aliased data due to the sparse nature of the array. Testing and benchmarking of the algorithms was done on real and synthesized data sets containing multiple target scenarios in abreast, staggered, or single-file formations.				
14. SUBJECT TERMS SBIR Report			15. NUMBER OF PAGES 75	
			16. PRICE CODE	
17. SECURITY CLASSIFICATION OF REPORT Unclassified	18. SECURITY CLASSIFICATION OF THIS PAGE Unclassified	19. SECURITY CLASSIFICATION OF ABSTRACT Unclassified	20. LIMITATION OF ABSTRACT	

Standard form 298 (Rev.2-89)
Prescribed by ANSI Std. Z39-18
298-102

20030109 162

Final Report

**Detection, Tracking and Classification of Multiple Targets using
Advanced Beamforming and Classification Methods**

PI: Dr. M. R. Azimi-Sadjadi

CO-PI Dr. K. Khorasani

Information System Technologies, Inc.
5412 Hilldale Court
Fort Collins, CO 80526
Tel: (970) 226-6706
E-mail: infosyst@aol.com

Submitted to :

Mr. Robert Wade
US Army TACOM-ARDEC
AMSTA-AR-FSF-R, Bldg 407
Picatinny Arsenal, NJ 07806-5000
Tel : (973) 724-5356
E-mail: rwade@pica.army.mil

Contract No.: DAAE30-02-C-1058

Duration of Effort : March 20, 2002 - September 20, 2002

Contents

1	Introduction and Objectives of Phase I Research	1
2	Identification of Barrier Issues & Review of Existing Methods	2
2.1	Narrowband Direction-of-Arrival (DOA) Estimation	3
2.2	Wideband DOA Estimation	4
2.3	DOA Estimation for Non-uniform Arrays	4
2.4	DOA Estimation for Multiple Invariance Arrays	6
2.5	DOA Estimation for Non-Gaussian Sources	7
2.6	DOA Estimation Under Missing Data/Array Scenarios	8
2.7	DOA Estimation using Independent Component Analysis and Blind Source Separation	8
2.8	Multiple Target Tracking and DOA Estimation for Unattended Ground Sensors	8
2.9	Target Classification Based Upon Acoustic Signatures	9
3	Generating Synthesized Multiple Target Scenarios	10
3.1	Autoregressive (AR)-Based Method	10
3.2	Interpolation-Based Method	10
4	High-Resolution Wideband DOA Estimation Methods	13
4.1	Steered Covariance Matrix (STCM) Algorithm	14
4.2	Incoherent Wideband MUSIC (IWM) Algorithm	15
4.3	Weighted Subspace Fitting (WSF) Algorithm	16
4.4	Simulation Results of Wideband DOA Estimation Methods	17
5	Array Manifolds & DOA Estimation	25
5.1	Mathematical Model for the Subarray	26
5.2	MUSIC-based Ambiguity Resolution	28
5.3	ESPRIT-based DOA Detection	28
5.4	Simulation Results	29
6	Source Separation Methods	31
6.1	Natural Gradient Based IICA Algorithm	31
6.2	Convolutional ICA (CICA) Algorithm	32
6.3	Simulation Results of IICA Algorithm on Actual SAFE II Data	33
6.4	Fast ICA Algorithm	36
6.4.1	Preprocessing for ICA	43
6.4.2	Fast ICA for One Unit	44
6.4.3	Fast ICA for Several Units	45
6.5	Simulation Results of Fast ICA on Synthesized Data	45
6.6	Simulation Results of Fast ICA on SAFE II Data	48
7	Composite Beampattern	63
8	Conclusions & Future Plans for Phase II	66
8.1	Future Plans for Phase II	66

1 Introduction and Objectives of Phase I Research

The problem of detection, classification and localization of multiple ground targets, e.g. trucks and tanks, using arrays of unattended passive acoustic sensors is complicated due to various factors. These include: variability and nonstationarity of target acoustic signatures, signal attenuation, loss of coherence and fading effects as a function of range and doppler, effects of wind noise and weather/environmental conditions on the sensory data, competing clutter with similar spectral characteristics, and lack of *a priori* knowledge about the number of the targets in the battlefield. In addition, the presence of multiple closely spaced targets can significantly complicate the detection/classification, data association and localization processes, especially when the tracks of the targets are allowed to cross, split, or remain close together. As a result, new schemes are needed to provide fast and extremely accurate bearing angle estimation and subsequent classification and localization of different types of narrowband and wideband sources from their acoustic signatures. However, in developing bearing angle estimation and classification schemes for this particular problem one has to consider power consumption and size constraints, which in turn place severe constraints on the complexity of the DSP and communication systems for these arrays.

Unattended passive acoustic sensors [1]-[3] are among the widely used sensors for remote battlefield surveillance, situation awareness and monitoring applications. Together with dedicated digital signal processing (DSP), these small and cost effective sensors can provide real-time information about different types of ground and airborne targets. They are rugged and reliable and can be left in the field for a long period of time after deployment. The DSP associated with these sensors must be capable of performing various tasks including target detection and direction of arrival (DOA) estimation, tracking, classification and/or identification. Generally, there can be a wide variety of target types in battlefield depending on the specific mission, e.g. troops, ground targets (trucks, tanks, etc), airborne targets (helicopters, missiles, airplanes) with signatures that overlap both spectrally and temporally. In addition, optimum performance is highly dependent on terrain, weather, and background noise.

The work at the Army Research Laboratory (ARL) [2]-[3] involved development of array signal processing algorithms using small baseline acoustic arrays to estimate DOA's, track, and classify moving targets from their acoustic signatures. Since conventional beamforming schemes generally do not provide good results in these situations, owing to the structural limitations of the array and lack of spatial coherence, high-resolution DOA algorithms must be developed. Current efforts on incoherent and coherent wideband MUSIC (MUltiple SIgnal Classification) show some promise for detecting and tracking multiple ground vehicles. In [2] by exploiting the multi-spectral content of the targets, better results were reported using wideband signal subspace DOA algorithms. Experimental results using a circular array of six sensors, with a diameter of 8 ft indicated the advantages of the wideband MUSIC over the delay-sum algorithm. In [3] focused wideband adaptive array processing algorithms are employed for the high-resolution DOA estimation of ground vehicles. Several methods including steered covariance matrix (STCM) and spatial smoothing or interpolation using the array manifold interpolation are considered. In addition, this study provides experimental analysis of incoherent and coherent wideband MUSIC algorithms and narrowband MUSIC for a circular array of acoustic sensors in terms of accuracy and stability of DOA estimates. It was shown that for certain signal-to-noise ratio (SNR) conditions incoherent wideband methods yield more accurate DOA estimates than the coherent methods for highly peaked spectra while for sources with flat spectra the coherent wideband methods generate more accurate DOA estimates. The study are indicated that the coherent wideband methods are much more statistically stable than the incoherent ones. The price paid for this improved stability is high computational cost.

As far as we know, none of the existing algorithms demonstrated proven capability to detect, classify and track multiple closely spaced sources in tight formations especially in presence of clutter and wind noise. This is critical in realistic battlefield scenarios where an overwhelmingly large number of targets may be encountered under changing and difficult environmental/terrain conditions. In addition, most of the

existing methods apply to arrays with linear placement of sensors and uniform spatial sampling. The goal of this Phase I research effort was to study and develop new DOA estimation and target classification methods that can be used to isolate multiple sources and classify them based upon the spectral/temporal features in their acoustic signatures as well as their dynamical behavior. We have carefully studied the geometry of the arrays and the properties of data sets and developed two classes of algorithms for localizing and resolving multiple closely spaced targets. The first class of approaches is based upon high-resolution subspace-based DOA estimation methods that can be used for localizing and tracking the targets. The second class, however, is based upon source separation methods using independent component analysis (ICA) and its variants for determining the number of potential targets. The primary criterion was to develop algorithms that can potentially be implemented in battlefield operations. In addition, the methods should not rely on prior knowledge of the number of targets, target's dynamical information and initial conditions, and background interference and clutter. Of particular importance was to investigate how the detection and extraction of useful target information can be done in spatially aliased data due to sparse nature of the arrays employed for this problem. Testing of the algorithms have been done on the real data acquired from US Army TACOM-ARDEC in Picatinny Arsenal, NJ as well as on synthesized data containing multiple target scenarios for a circular array with a wagon-wheel pattern geometry [2]. The effectiveness of the different schemes were demonstrated and benchmarked on these multiple target scenarios.

The organization of this final report is as follows. Section 2 provides a review of all the existing methods for multiple wideband source separation and DOA estimation problems using passive acoustic arrays. The barrier issues in developing efficient algorithms for detection, classification and tracking of multiple closely spaced targets in realistic battlefield conditions are also introduced. Section 3 introduces two different methods for generating realistic synthesized multiple target cases with various tight formations e.g. staggered, abreast and single-file. Section 4 investigates and develops various efficient wideband DOA estimation methods that consider the geometry of the arrays for high-resolution and robust target bearing angle estimation and separation. In particular, we investigated how to resolve, with minimum ambiguity and high confidence, the DOA's associated with multiple closely spaced targets in spatially aliased data due to sparse nature of the arrays employed for this problem. The effectiveness of the algorithms are demonstrated on both real and synthesized data. The algorithms are then benchmarked in terms of their accuracy, resolution and robustness in estimating DOA's and separating multiple closely spaced targets. In Section 5 we present some preliminary results of a dual-size array manifold that consists of a rectangular array grid to be spaced much greater than a half-wavelength, but at each grid has a circular array geometry. Simulation results on a narrowband case are also presented. Section 6 studies and develops various source separation algorithms that exploit ICA methods using higher order statistical properties of the sources. Different ICA algorithms are extended and applied to this problem. Results on several target scenarios are also presented. The performance of all the methods considered in this Phase I research in terms of accuracy, robustness and computational efficiency are compared and the promising methods for future investigation have been identified. Section 7 proposes a new algorithm for combining and associating the DOA estimates from multiple nodes in order to localize and identify all the sources in the formation. Finally, Section 8 gives the concluding remarks and important topics for Phase II research.

2 Identification of Barrier Issues & Review of Existing Methods

In this section the main barrier issues in the development of robust, high-resolution and real-time algorithms for tracking and classifying multiple targets in realistic environment operating conditions using unattended passive acoustic arrays are briefly presented. Below we provide a review of some of the existing methods and present the most critical issues, based on the state-of-art knowledge in the literature, that are considered worthwhile for further investigation. It is our opinion that the issues indicated below present some of the most challenging directions to be researched in the next stages of this project and in the future.

2.1 Narrowband Direction-of-Arrival (DOA) Estimation

The problem of DOA estimation from a sensor array has received much attention in recent years. This problem has been extensively studied, especially for narrowband sources, a large body of literature exists. The most basic configuration for a uniform linear array (ULA) consists of M identical and omnidirectional sensors that receive ($N < M$) narrow-band signals from the sources with unknown DOA's $\theta_1, \dots, \theta_N$. If the signals are transformed to baseband, the received signal vector for the n^{th} source can be written as

$$y(t) = a(\theta_n)s(t) + v(t), \quad t = 1, \dots, L$$

where $a(\theta_n)$ is the steering vector given by

$$a(\theta_n) \triangleq [1 \ e^{-j\omega_c\tau_{2n}} \ \dots \ e^{-j\omega_c\tau_{Mn}}]^T$$

where τ_{kn} is the time delay associated with the k^{th} sensor given by $\tau_{kn} = \frac{d_k \sin \theta_n}{c}$ with c being the velocity of sound propagation in air, θ_n is the DOA of the n^{th} source, and d_k is the distance between the k^{th} sensor and the 1^{st} sensor (reference). Note that it is assumed that $d_1 = 0$. Furthermore, for ULA we have $d_k = (k - 1)d$. For N sources, the above equation becomes

$$Y(t) = A(\underline{\theta})S(t) + \Upsilon(t)$$

where $Y(t)$, $S(t)$ and $\Upsilon(t)$ are the vectors of received signals, source signals and additive noise, respectively and $A(\underline{\theta})$ is the composite steering matrix of size $M \times N$ given by

$$A(\underline{\theta}) \triangleq [a(\theta_1), \dots, a(\theta_N)]$$

where $\underline{\theta} \triangleq [\theta_1, \dots, \theta_N]^T$ is the DOA vector. If the additive noise is assumed to be zero-mean spatially and temporally white Gaussian process with the unknown diagonal correlation matrix $Q = \text{diag}\{\sigma_1^2, \dots, \sigma_M^2\}$, the correlation matrix of the received signal vector, $Y(t)$, can be written as

$$R_Y = AR_S A^H + Q$$

where $R_S = E\{S(t)S^H(t)\}$ is the source correlation matrix and H denotes the Hermitian transpose.

The correlation matrix R_Y can be computed from the baseband data using $R_Y = \frac{1}{L} \sum_{t=1}^L Y(t)Y^H(t)$ where L is the number of snapshots in one measurement. Assuming that the sources are uncorrelated (incoherent) and the $\text{Rank}(AR_S A^H) = N$, then the eigenvalues of matrix R_Y can be arranged in decreasing order i.e. $\lambda_1 > \lambda_2 > \dots > \lambda_N \gg \lambda_{N+1} > \dots > \lambda_M$. The orthonormal eigenvectors associated with $\{\lambda_1, \lambda_2, \dots, \lambda_N\}$, and $\{\lambda_{N+1}, \lambda_{N+2}, \dots, \lambda_M\}$ form the signal and noise subspaces. If we denote these subspaces by $G_s = \{e_1, e_2, \dots, e_N\}$, and $G_n = \{e_{N+1}, e_{N+2}, \dots, e_M\}$, respectively, where e_i is the eigenvector associated with eigenvalue λ_i , then we can easily show that $A^H G_n = 0$ i.e. the columns of G_n belong to the null space of A^H . This leads to the important result that the DOA's, θ_n 's are the only solutions of the equation

$$a^H(\theta_n)G_n G_n^H a(\theta_n) = 0$$

Using the MUSIC algorithm, DOA's can be determined as the locations of the N highest peaks of the function, for $\theta_n \in [-\pi, \pi]$, of the function

$$P(\theta_n) = \frac{1}{a^H(\theta_n)G_n G_n^H a(\theta_n)}$$

To avoid ambiguity in estimating the DOA's in MUSIC, the Nyquist criterion is imposed, which gives $|\omega_c \tau_{max}| < \pi$. Clearly, this limits the use of MUSIC for wideband sources using a sparse array as spatial aliasing will be inevitable in such cases.

Given that the elements of a sensor array are commonly organized in a very regular and structured geometry such as linear, circular, and rectangular shapes, many researchers have exploited these geometrical structures to develop computationally efficient algorithms for the DOA estimation. For instance, Root-MUSIC, MODE, and IQML [4] are among some of the well-known techniques that take advantage of a uniform structure in the array field. ESPRIT is an alternative algorithm that requires an array consisting of two identical, translated sub-arrays to determine the DOA estimates. Of particular interest to this project is the so-called MI-ESPRIT [5] algorithm that attempts to generalize the standard ESPRIT algorithm to arrays that are composed of multiple identical sub-arrays arranged by translations of sub-arrays with arbitrary but known spacings. More details are provided in the subsequent subsection.

2.2 Wideband DOA Estimation

For wideband sources, however, the literature is somewhat limited. Some of the earlier work in this domain are due to Wax *et al.* [6], Wang and Kaveh [7], Buckley and Griffiths [8], and Su and Morf [9]. Both incoherent aggregation technique suggested in [6] and coherent signal subspace technique proposed in (Wang & Kaveh; [7]) represent in some way transition of narrowband processing techniques to the wideband cases. Furthermore, Bienvenu [10] and Buckley and Griffiths [8] have shown how to divide the spatio-temporal observation space into signal and noise subspaces and have suggested search functions to estimate the DOA's. Grenier [11] has generalized this notion to a so-called filter-spatial domain. Su and Morf [9] have suggested a modal decomposition of the signal subspace for estimating the DOA's.

The problem of wideband DOA estimation based on maximum likelihood principle is also investigated in [12]. The authors in [12] have proposed several search functions to obtain the ML estimate of DOA for wideband sources. Due to its extensive and time-consuming nature this approach is computationally expensive and impractical for real-time applications. The approach that is proposed by Bresler and Macovski [13] for the narrowband case, and a uniform linear array (ULA), formulates the problem as an iterative method known as the "iterative quadratic maximum likelihood" (IQML) for obtaining the ML solution. The IQML method involves the creation of a Toeplitz matrix that spans the subspace orthogonal to the signal subspace and can be parameterized by the coefficients of a prediction polynomial, whose roots yield the DOA estimates. In this case, the use of a parameterized model is equivalent to the problem of estimating the coefficients of this model from which DOA's can easily be calculated. In [14] the authors have developed, based on the ideas available for the parameter estimation of multiple narrowband sources in WGN, pseudo-maximum likelihood parameter estimators for the wideband sources by adapting the harmonic model of Kay *et al.* [15]. They have shown that the concept of an ARMA model for the observed data vector used in the narrowband case [13] can be generalized to model the spatio-temporal samples. As in the narrowband case, it is shown that the coefficients of the resulting ARMA model can be used to represent the null subspace of the wideband array steering matrix. This has resulted in the formulation of an IQML-like procedure for the parameter estimation of wideband sources that is similar to that for the narrowband case as suggested in [13]. The proposed approach is applicable to both coherent and incoherent sources. The performance of the proposed method was also studied on simulated cases.

2.3 DOA Estimation for Non-uniform Arrays

The problem of DOA estimation for non-uniform linear array (NLA) has also been investigated in [16-22]. Non-uniformly spaced (or sparse) arrays are still the subject of active investigation for both theoretical and practical reasons. Theoretically, it has been known for many years that non-uniform spacing may lead to significantly improved DOA estimation performance [23]. Research on the design of "optimal" non-uniform geometry is still in progress. In addition to DOA estimation accuracy issues, the problems with identifiability and ambiguity are also under active investigation [24]. A crucial requirement for DOA estimation by subspace-based methods is the assumption of linear independence among the steering vectors. In [25] Schmidt has classified manifold ambiguities according to their "rank" based on the algebraic linear

dependence of these vectors. Consequently, most DOA estimation techniques based on subspace approach have avoided such manifold ambiguity scenarios. For example, the study of the unique localization of multiple sources by passive sensor arrays (identifiability) conducted by Wax and Ziskind [26] has been based on the assumption that “any subset of distinct steering vectors from the array manifold is linearly independent.” In this paper, identifiability conditions have been defined in terms of the number of sensors and the rank of the inter-source correlation matrix, under this basic assumption. As a consequence of Schmidt’s definition, the ambiguity problem has usually been associated with manifold ambiguity, i.e., with the rank of the array manifold matrix. According to Proukakis and Manikas [27], “any subsequent research to handle the ambiguity problem was mainly concerned with either the performance of specific arrays, or with the identification of array structures free of ambiguities up to a certain rank of ambiguity.”

The linear dependence among the NLA steering vectors does not necessarily imply nonidentifiability, i.e., even though the conventional subspace-based DOA estimation algorithms may fail to deliver unambiguous DOA estimates in such cases, there exists other techniques that could be developed or be complemented MUSIC, etc. that are capable of manifold ambiguity resolution. It appears that the failure of subspace-based (MUSIC-type) algorithms to correctly identify sources with linearly dependent steering vectors (i.e., to resolve manifold ambiguity) has evolved into the misunderstanding that “the use of arrays with linearly independent steering vectors is crucial to applications that involve estimation of the DOA’s of multiple sources” [28]. Critically important results in this regard were recently obtained by Proukakis and Manikas [27], where it was proven that practically all NLA geometries mentioned in the literature are manifoldly ambiguous. They demonstrated that a sufficient condition for the presence of manifold ambiguities in any linear array is that the antenna array’s aperture measured in half wavelengths. Moreover, in [27] the authors introduced an approach to calculate the “ambiguous generator sets” (AGS’s) of any NLA, i.e., the sets of DOA’s that correspond to linearly dependent steering vectors.

Clearly, it is important to note that even if a scenario is identifiable, any particular DOA estimation algorithm may or may not yield unambiguous DOA estimates. Conversely, if a particular algorithm (e.g., MUSIC) is applied to a theoretically identifiable scenario, it may have the potential to create ambiguity, which may well be avoided by some other algorithm. As a result, one needs to carefully specify identifiability and ambiguity aspects with respect to a DOA estimation problem and to clarify and specify the association between manifold ambiguity and nonidentifiability. In cases where manifold ambiguity does not result in nonidentifiability, one must attempt to find an appropriate technique that can properly resolve manifold ambiguity. Given that NLA’s are suitable for DOA estimation beyond the limit of the “conventional” number of independent sources (that is $1 \leq N < M$), one needs to be concerned with the issue of identifiability in the “superior case” (that is $N \geq M$), where manifold ambiguity loses its meaning.

In [24], an effective solution to the above problems has been proposed where they attempt to find a best fit among the set of estimated spatial covariance lags and source powers for each of the MUSIC DOA estimates, including the ambiguous ones. The proposed approach is computationally efficient as it uses a linear programming algorithm and has demonstrated a high probability of correct identification in manifoldly ambiguous scenarios exceeding the performance of “abnormal” MUSIC behavior that is well-known and caused by the presence of low SNR and/or number of data samples.

One of the NLA subclasses considered is the “fully augmentable” arrays, which have the property that all intermediate distances (lags) are available, that is there is no gaps in the set of $\frac{M(M-1)}{2}$ inter-sensor separations implying that the set of all distances is complete. The problem of DOA estimation for the fully augmentable sparse linear arrays when there are more uncorrelated sources than sensors in a NLA has been investigated in [29].

The above-mentioned algorithms apply almost exclusively to linear arrays; whereas in most of the real-life situations the physics of the problem dictates a non-linear, e.g. circular or even volumetric, array

geometry. Additionally, these cannot be used in cases where the array is sparse leading to spatially aliased data. At present, there are only a few DOA estimation approaches for volume arrays (Liu & Mendel; 1998 [30]), (Barthelemy & Willett; 1998 [31]) and for non-uniform spatial sampling (Zoltowski & Mathews; 1994 [32]) but their applicability to multiple target detection and tracking is doubtful. This is particularly true when the targets are spatially close together and in presence of heavy clutter and correlated noise.

In general, for a non-uniform volume array, the time delays can be related to the DOA of the source and the actual location of the sensors i.e.

$$\tau_{mn} = -\frac{1}{c}\kappa_n^T \chi_m$$

where $\kappa_n = [\sin\theta_n \cos\varphi_n, \sin\theta_n \sin\varphi_n, \cos\theta_n]^T$ is the DOA vector for the n^{th} source with θ_n and φ_n being the azimuth and elevation angles, respectively, $\chi_m = [x_{1m}, x_{2m}, x_{3m}]^T$ represents the coordinate vector of the m^{th} sensor. In this case, the steering matrix A becomes,

$$A(\underline{\theta}, \underline{\varphi}) = [a(\theta_1, \varphi_1), \dots, a(\theta_N, \varphi_N)]$$

with the steering vector $a(\theta_n, \varphi_n) = [1 \ e^{-j\omega_c \tau_{2n}}, \dots, e^{-j\omega_c \tau_{Mn}}]^T$.

Thus, in addition to the difficulties in resolving multiple closely spaced targets another challenge in this development is how to detect and extract useful target information in spatially aliased data due to sparse nature of most of the sensor arrays used for this problem. This is especially important in presence of array manifold ambiguity.

2.4 DOA Estimation for Multiple Invariance Arrays

The main limitation for the MI-ESPRIT is that it requires a multidimensional search for the DOA arrays, which is computationally very time-consuming. In (Swindlehurst, Stoica, & Jansson; 2001[4]) a new algorithm is proposed that attempts to generalize the MUSIC technique denoted as MI-MUSIC. Unlike MI-ESPRIT the DOA estimate is obtained only through a 1-D search as opposed to a multi-dimensional search, however unlike ESPRIT it does not enjoy the statistical optimality properties. Furthermore, the authors have also generalized the Root-MUSIC and MODE techniques to multiple invariance versions. The advantage of the above algorithms is that even the need for a 1-D search is eliminated. It has been shown that MI-MUSIC and MI-Root-MUSIC algorithms yield good performance and that MI-MUSIC may actually be more robust than MI-ESPRIT in difficult threshold scenarios. For highly correlated sources both MI-ESPRIT and MI-MODE perform better than MI-MUSIC and MI-Root-MUSIC. The details are briefly stated below.

In the multiple invariance array [4] it is assumed that we have p identical translated subarrays of m elements each that are arranged with arbitrary but known spacing. In order to describe the array formally one of the subarrays is considered as the reference and the known translational and angular displacements of the other subarrays are denoted by δ_k and α_k , for $k = 1, \dots, p-1$. The structure may now be expressed as

$$JA(\theta) \triangleq \tilde{A} = \begin{bmatrix} F \\ F\Phi_1^{\delta_1} \\ \vdots \\ F\Phi_{p-1}^{\delta_{p-1}} \end{bmatrix}$$

where J is a known $mp \times M$ selection matrix, F is the unknown response of the reference subarray, and Φ_k is a diagonal matrix defined by

$$\Phi_k = \text{diag}\{e^{j\pi \sin(\theta_1 + \alpha_k)}, \dots, e^{j\pi \sin(\theta_d + \alpha_k)}\}$$

where δ_k is measured in the half-wavelengths units. If the subarrays are non-overlapping then the rows of $A(\theta)$ may be arranged so that $J = I$. Although the condition $d < M$ is necessary for any DOA estimation algorithm based on the covariance matrix, it turns out that it may not be sufficient in our application given that there are additional parameters that need to be estimated in F . Briefly stated the MI-ESPRIT algorithm applied to our configuration amounts to the following procedure

$$\hat{F}, \hat{\theta}, \hat{T} = \arg \min_{F, \theta, T} \|J\hat{G}_s W^{\frac{1}{2}} - \tilde{A}T\|_F^2$$

where $\|\cdot\|_F$ denotes the Frobenius norm, and W is a suitably chosen weighting matrix, and T is a full-rank matrix of dimension $d \times d$ that satisfies $JG_s = \tilde{A}T$. The necessary condition for the multiple invariance array is that $d \leq \min\{M - 1, m(p - 1)\}$. Similarly, the extensions for the algorithm to MI-MUSIC and MI-Root-MUSIC may also be developed as in [33].

2.5 DOA Estimation for Non-Gaussian Sources

Various DOA estimation algorithms are developed based on the covariance matrix of the array output. The delay-and-sum method as well as Capon's minimum variance method use the sample covariance matrix to measure the power as a function of the DOA. The subspace methods (such as MUSIC, ESPRIT, minimum norm, etc.) estimate the signal and noise subspaces from the eigenvectors of the covariance matrix. Provided that the data is Gaussian distributed, the sample covariance matrix is an optimal estimator of the unknown covariance matrix. However, as it is the case in most real-life situations the data are generally non-Gaussian, which can result in poor performance and unreliable DOA estimate of these algorithms. In another class of the DOA algorithms that are based on the maximum likelihood (ML) principle, the estimates for the DOA's are derived by assuming that the noise is modeled as a Gaussian random process. Similar to the previous algorithms, under these circumstances the ML estimates are significantly under-performing and are highly unreliable. In other words, when the sensor noise is spatially non-uniform white process, neither the conventional ML methods nor the colored noise modeling ML techniques are expected to provide acceptable performance.

In the general case, the sensor noise must be treated as a colored, spatially dependent process. For example, the ambient noise and wind conditions have been observed to be clearly non-Gaussian. This obviously calls for and necessitates development of "robust" DOA estimation algorithms for these nonstandard circumstances. Current research in the literature attempting to address the above issues are reported in (Lee & Kashyap; 1992 [34]) using M -estimation. The problem of DOA estimation in heavy-tailed noise generated from an α -stable distribution have also been studied in (Tsakalides & Nikiyas; 1996 [35]). Some authors attempt to model the noise as a finite mixture of Gaussian random variables and use the SAGE algorithm as in (Kozick & Sadler; 2000 [36]).

The above-mentioned robust algorithms for the DOA estimation all suffer from the limitations that they rely on the knowledge of the pdf or the number of the mixtures. Furthermore, they also need user-specified parameters (such as thresholds and weight matrices) that have to be selected based on trial-and-error or heuristic methods, lending these algorithms somewhat sensitive to the initialization problems. Therefore, there is a strong interest in developing computationally practical and easy to implement DOA estimation algorithms in real-time for the non-uniform noise situation. In (Pesavento & Gershman; 2001 [37]) this problem is tackled by developing a deterministic ML DOA estimator based on a non-uniform noise model. The algorithm is implemented based on the so-called stepwise concentration of the log-likelihood function with respect to the signal and noise nuisance parameters and requires only a few iterations to converge. In (Visuri, Oja and Koivunen; 2001 [38]) a high-resolution DOA estimation algorithm is proposed that is based on estimating the signal and noise subspaces from spatial sign or rank covariance matrix. Convergent estimates of the non-parametric statistics are developed. Furthermore, they have shown that their proposed algorithms have comparable performance compared to the optimal methods in presence of Gaussian noise and are not dependent on user-specified parameters.

2.6 DOA Estimation Under Missing Data/Array Scenarios

The problem of estimating the DOA from incomplete or partially available measurements has recently been investigated by (Larsson & Stoica; 2001 [39]). There are many factors that could cause faults in arrays which could eventually lead to failed arrays, resulting in incomplete available information. In our particular problem such failure may be resulted from the environmental and natural conditions. The presently available DOA techniques are not designed to cope and deal with these uncertainties, i.e., they are not “fault-tolerant”. Specifically, the techniques that use the sample covariance matrix as an estimate of the array output covariance matrix could fail to yield accurate and reliable results as they are based on the assumption that the sample covariance matrix is an accurate representation of the array covariance matrix.

The model of the sensor array that was considered in [36] assumes that one or more sensors fail to work after a certain period of time. Specifically, assuming that the total number of sensors in the array is M_1 and that data were collected with all M_1 sensors for $t = 1, \dots, L_1$. After $t = L_1$, at least one sensor fails to work so that M_2 working sensors still remain. Using these sensors data is collected from $t = L_1 + 1, \dots, L_1 + L_2$. This process is repeated for $t > L_1 + L_2$. It is clear that $M_1 > M_2 > \dots > M_p$. It is assumed that $\{M_1, \dots, M_p\}$ and $\{L_1, \dots, L_p\}$ are known *a priori*. This is justified by the fact that failing sensors and the times when they stop functioning are typically easy to identify.

The contribution of the work by (Larsson & Stoica; [39]) is to enable the existing techniques such as MUSIC, ESPRIT, etc. with a reliable statistical estimate of the array covariance matrix to be used instead of the sample covariance matrix. Several techniques were considered. In the first approach, the ML estimate of the covariance matrix and its asymptotic accuracy were derived and discussed. It was shown that by using the Covariance Matching technique (COMET), as opposed to MUSIC, one can use information on the accuracy of the covariance matrix estimate, and that this information can improve the performance in estimating the DOA's from the incomplete data. It was concluded that the proposed COMET approach may be the preferred choice when treating parameter estimation from incomplete data.

2.7 DOA Estimation using Independent Component Analysis and Blind Source Separation

Blind source separation (BSS) is an approach used to estimate original source signals through only the information of the mixed signals observed in each input channel. Recently work has been conducted for the BSS based on the independent component analysis (ICA) [40]. There are several methods proposed in the literature in which the inverse of the complex mixing matrices are calculated in the frequency domain to deal with the arrival lags among each of the elements of the microphone array system [41,42]. However, this ICA-based approach has the disadvantage that there is difficulty with the low convergence of nonlinear optimization [43]. In [44] a new algorithm is proposed for BSS, in which ICA and beamforming are combined to resolve the low-convergence problem through optimization in ICA. The proposed method consists of the following three parts: (1) frequency-domain ICA with DOA estimation, (2) null beamforming based on the estimated DOA, and (3) integration of (1) and (2) based on the algorithm diversity in both iteration and frequency domain. The inverse of the mixing matrix obtained by ICA is temporally substituted by the matrix based on null beamforming through iterative optimization, and the temporal alternation between ICA and beamforming can realize fast- and high-convergence optimization. The results of the signal separation experiments have shown that the signal separation performance of the proposed algorithm is superior to that of the conventional ICA-based BSS method, even under reverberant conditions.

2.8 Multiple Target Tracking and DOA Estimation for Unattended Ground Sensors

The work at the Army Research Laboratory (ARL) (Pham & Fong; 1997 [2]), (Pham & Sadler; 1997 [3]) involved development of array signal processing algorithms using small baseline acoustic arrays to

estimate DOA's, track, and classify moving targets from their acoustic signatures. Since conventional beamforming schemes generally do not provide good results in these situations, owing to the structural limitations of the array and lack of spatial coherence, high-resolution DOA algorithms must be developed. Current efforts on incoherent and coherent wideband MUSIC show some promise for detecting and tracking multiple ground vehicles. In [2] by exploiting the multi-spectral content of the targets, better results were reported using wideband signal subspace DOA algorithms. Experimental results using a circular array of six sensors, with a diameter of 8 ft indicated the advantages of the wideband MUSIC over the delay-sum (DS) algorithm. In [3] focused wideband adaptive array processing algorithms are employed for the high-resolution DOA estimation of ground vehicles. Several methods including steered covariance matrix (STCM) [45] and spatial smoothing or interpolation using the array manifold interpolation (AMI) are considered. In addition, this study provides experimental analysis of incoherent and coherent wideband MUSIC algorithms and narrowband MUSIC for a circular array of acoustic sensors in terms of accuracy and stability of DOA estimates. It was shown that for certain SNR conditions incoherent wideband methods yield more accurate DOA estimates than the coherent methods for highly peaked spectra while for sources with flat spectra the coherent wideband methods generate more accurate DOA estimates. The study are indicated that the coherent wideband methods are much more statistically stable than the incoherent ones. The price paid for this improved stability is high computational cost.

More recently, (Boettcher, Sherman & Shaw; 2002, [46]) developed a simple time-difference of arrival (TDOA) estimation method for localization of targets using a network of acoustic sensor arrays. TDOA is performed using spectral peaks from the acoustic signatures to allow drastic reduction in the bandwidth required to collaboratively determine bearing angles. Although this scheme shares some of the advantages of the coherent and closest point of approach (CPA)-based algorithms, it cannot be used to estimate DOA's associated with multiple closely spaced targets or in difficult target scenarios. In [47], Kaplan, Le and Molnar (2001) used ML method to localize a moving target using a network of passive acoustic arrays where each node consists of an array of microphones configured in a "wagon wheel" pattern. Each node transmits a DOA estimate to a central processor. The central node processes the bearing information to localize and track targets of interest. A distributed sensor measurement strategy dynamically designates the active nodes and assigns nodes to central processing task.

2.9 Target Classification Based Upon Acoustic Signatures

Although there are a number of bearing angle estimation methods for detection and tracking of vehicles (wheeled and/or tracked) using UGS acoustic arrays, the literature on classification of these targets based upon their acoustic signature and other features is very limited. Wu, Siegel and Khosla [48] used Principal Component Analysis (PCA) of the windowed acoustic signatures in the frequency domain as features for classification. When a new windowed signal is applied, its spectrum vector is projected onto the principal eigenvectors. Results on discrimination of passenger cars against trucks are also presented.

We believe subband features as well as velocity, acceleration and curvature profiles of various detected targets can be used to discriminate between different types of targets. The subband features are expected to reveal subtle tonal features in different frequency bands and provide clues to classify different heavy and light vehicles of both wheeled and tracked types. Of particular importance is to determine how the subband features can aid in extracting information about light vehicles as they present a major challenge to both detection and classification systems. The developed classification system must be flexible in that other target clues from other types of sensors, e.g. seismic, which complements the decision making process, may easily be incorporated into the system. The subband acoustic features together with the targets dynamical features can be measured at every few sensor snapshots and then used as inputs to a target classification system. The sequential Bayes classification scheme [49] developed by the PI can be employed here. The results can be updated on-line as more data is becoming available.

3 Generating Synthesized Multiple Target Scenarios

Two data sets were received from the US Army TACOM-ARDEC in Picatinny Arsenal, NJ. The first data set (SAFE II) was collected using three nodes each consisting of a circular (wagon wheel-type pattern) array of five identical elements. The second data set (YUMA) was collected using four nodes with a similar array structure. Although these data sets contain multiple target scenarios, according to the technical point of contact (POC), Mr. Robert Wade, they are not representative of real battlefield scenarios where multiple closely spaced targets in abreast, staggered or single-file formation are encountered. Consequently, several methods for generating synthetic multiple target data sets were developed and investigated. These data sets are then used to develop and test high-resolution and high confidence DOA estimation and source separation algorithms that offer reduced confusion in separating multiple targets in difficult battlefield situations. The following subsections present two different methods for generating synthesized data sets.

3.1 Autoregressive (AR)-Based Method

In these simulations the number of snapshots is set to $N = 1024$ and the sampling frequency $f_s = 1024 \text{ Hz}$. The number of sensors is $L = 5$ and the number of sources is $P \geq 2$ unless otherwise specified. Two types of sources are used. The sources are generated using 1st order Autoregressive (AR) processes driven by mutually independent zero-mean white Gaussian noise with unit variances. That is for the i th source we can write

$$s_i(n) = a_i s_i(n-1) + v_i(n) \quad (1)$$

where $v_i(n)$ is a zero-mean white Gaussian noise with unit variance mutually independent of $v_j(n)$, $j \neq i$. Variance of each source is adjusted to unit before the formation of the array measurements. Some of the truth files associated with SAFE II data were used to generate the synthetic target tracks with various close formations. Ten (10) frequency bins ($h = 10$) are used in the wideband DOA estimation algorithms (As described in details in Section 4). Bandpass filters had to be used to achieve desired frequency bands for the sensor measurement in the STCM and WSF methods (refer to Section 4 for details). These are FIR type filters with 21 weights designed using the appropriate MATLAB function. The frequency range was selected within the interval $[f_L, f_H] = [200 \text{ Hz}, 300 \text{ Hz}]$. Simulations with and without the passband filter were conducted for 16 independent runs. In the case of the circular array geometry the sensor spacing d_x and d_y are set to be 2ft. ($\approx 0.6 \text{ (m)}$) as in the SAFE II data.

The number and selection of the frequency bins influence the performance of the algorithms to some extent, and its choice needs to be decided carefully. The selection of the frequency bins is an issue that would need further research to optimize the performance of the algorithms. In our simulations, the powers of all the sensors are put together at each frequency bin, and the frequency bins that indicate the largest values are selected one by one until the desired number is reached. If the bin number is too small, the frequency bins that contribute to the accurate DOA estimate may be missed. On the other hand, if the bin number is too large, the heavily noisy frequency bins may be included, leading to poor DOA estimates. This ad-hoc way of selection works rather well in the simulations, and the number $h = 10$ was found to be a good choice in these results.

3.2 Interpolation-Based Method

More realistic simulated data sets containing multiple targets in abreast, single-file and staggered formations can be generated using an interpolation-based method that accounts for Doppler effects off moving sources. This method generates substantially more accurate simulated data sets as it does not assume time delays are multiples of the sampling interval. The wagon-wheel circular array geometry with 4ft. radius was considered and tested on the generated data sets.

To understand the difference between the previous approach and this new method imagine two hypothetical scenarios. In first case, assume that the track that the vehicle traverses is known and a number of signal emitters are placed on the track at a fixed interval. These emitters emit the source signal and are turned on/off by a remote controller. Using the original position of the virtual target, and its velocity, one can compute the time instances at which the target passes those positions. Then, to synthesize the data, one can use the remote controller to turn on the emitters one by one at these instances and collect the source signals using the array of sensors/microphones. Most of the commonly used schemes, including the above- mentioned AR-based method, for generating simulated array data are based upon such simplified assumption. In the second hypothetical scenario, assume that instead of placing a large number of emitters along the track, only one signal emitter is placed on an ideally silent vehicle which will follow the track with the same velocity as the target. Clearly, comparing these two scenarios, one can see that the latter scheme has several advantages. The first scheme can only produce the data at some isolated time intervals, while using the second scheme accurate source signals are generated. Most importantly, the first scheme does not take into account for the Doppler effects, whereas in second scheme, this is built in the setup. In practice, what we can assume to know is the signal emitted from a stationary target that is sampled at certain sampling frequency.

In our simulations, we assume that the signals from different targets and noise are additive at the sensors. Under this assumption, we can first calculate the signals received by a sensor from different targets separately in a one-target one-sensor fashion. Then, all the signals from different targets are added together with some noise. Figure 1 illustrates this one-target-one-sensor scenario. The position of the moving target at time t_0 is denoted by $(x(t_0), y(t_0))$ and $x(t), y(t)$ at time t . The position of the stationary sensor is (x_s, y_s) . The velocity of the target is $(v_x(t), v_y(t))$, where $v_x(t)$ and $v_y(t)$ denote the velocity components along the x-axis and y-axis, respectively. The velocity of the target could be a time varying function.

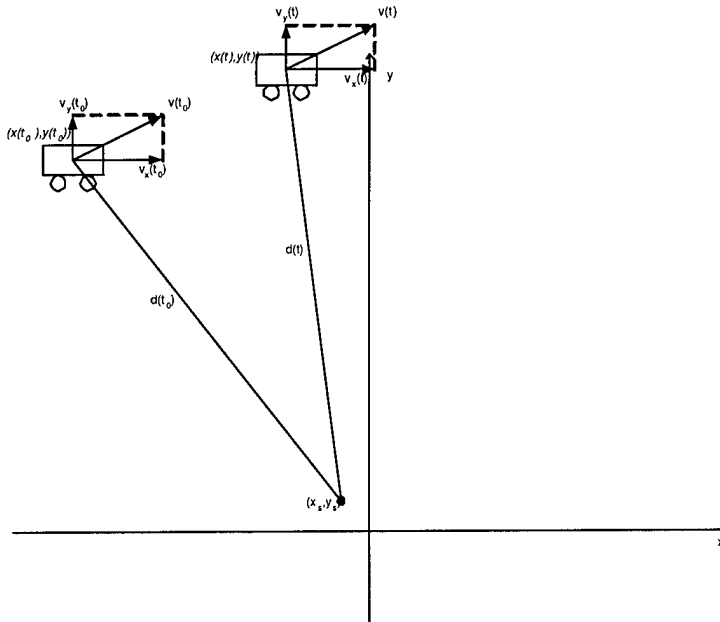


Figure 1: The scenario of one-target-one-sensor.

At time t , $t \geq t_0$, the position of the target is given by

$$x(t) = x(t_0) + \int_{t_0}^t v_x(t) dt \quad (2)$$

$$y(t) = y(t_0) + \int_{t_0}^t v_y(t) dt \quad (3)$$

Thus, the distance between the target and the sensor is $d(t) = \sqrt{[x(t) - x_s]^2 + [y^2(t) - y_s]^2}$. Let us assume that signal $S(t)$ emitted by the target is known in advance and let c be the speed of sound travelling in air. Then, the signal received by the sensor is $R(t) = S(t - d(t)/c)$. Note that this model actually takes into account the Doppler effects caused by the movement of the target. This will be more evident if we assume that the target is moving directly toward the sensor with a constant speed, the velocity in this case can be written as $(-\frac{x(t_0)-x_s}{T}, -\frac{y(t_0)-y_s}{T})$ where T is an arbitrary interval. Then the resultant signal received by the sensor is $R(t) = S((1 + \frac{d(t_0)}{Tc})t - \frac{d(t_0)}{c})$. It is obvious that the term $1 + \frac{d(t_0)}{Tc}$ multiplied by t indicates that $R(t)$ is a frequency shifted version of $S(t)$.

In practice, we assume that the sampled version of the wideband signal $S(t)$ emitted by the target, i.e. $s(n) = S(nT_0)$ where T_0 is the sampling interval, can be modelled by an autoregressive (AR) model. It is essential that when we simulate the signal $r(n)$ received by the sensor, we also use the same sampling interval T_0 . Then we have

$$\begin{aligned} r(n) &= R(nT_0) \\ &= S(nT_0 - d(nT_0)/c) = S(t_r) \end{aligned}$$

where $t_r := nT_0 - d(nT_0)/c$. The problem is that t_r is not always a multiple of T_0 , which precludes the direct use of values of $s(n)$. The solution is to use interpolation. In this case, let t_f and t_c be the floor and ceiling of t_r , respectively, i.e. $t_f = \lfloor t_r \rfloor$ and $t_c = \lceil t_r \rceil$. Note that $t_c - t_f = T_0$, then

$$r(n) = \frac{(S(t_c) - S(t_f))}{T_0}(t_r - t_f) + S(t_f)$$

To compute $d(nT_0)$, both $x(nT_0)$ and $y(nT_0)$ are needed. Equations (2),(3) can be approximated as follows:

$$\begin{aligned} x(nT_0) &= x(t_0) + \sum_{i=1}^n v_x((i-1)T_0)T_0 \\ y(nT_0) &= y(t_0) + \sum_{i=1}^n v_y((i-1)T_0)T_0 \end{aligned}$$

Figure 2 illustrates the positions of the array nodes and targets in the case where two abreast (side-by-side) targets are present. The two targets are moving with constant velocities and hence remain abreast in all observations. The signals received by the sensors are generated separately and packed into a database for later usage.

To generate realistic source signals, we devised a scheme where a 5th order AR model is fitted to the source signal in one of the real SAFE II data files that contained only one target. The AR model is found to be

$$x(n) = 1.627x(n-1) - 1.117x(n-2) + 0.6719x(n-3) - 0.4124x(n-4) + 0.1698x(n-5) + \eta(n)$$

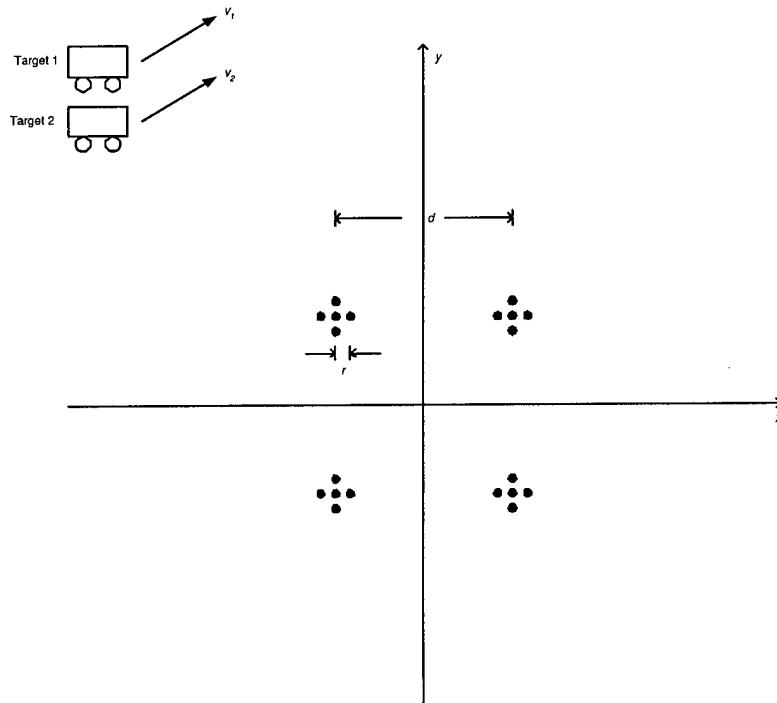


Figure 2: The setup of the case of two abreast targets.

where $\eta(n)$ is a zero-mean white Gaussian process with variance $\sigma_{\eta}^2 = 145.28$.

Figure 3(a) illustrates an example of two simulated target tracks generated using this scheme where the two targets are far apart. Figure 3(b) shows the detected tracks using the STCM method. This method is described in details in Section 4.1. Only one array is used in this DOA estimation. We can see that the two targets are perfectly detected, which suggests that the synthesized data is indeed useful.

4 High-Resolution Wideband DOA Estimation Methods

One of the main issues of paramount importance in this Phase I research project was the development of a high-resolution wideband DOA estimation scheme for separating multiple closely spaced targets. We investigated the applicability of several DOA estimation methods for the problem in hand. Three different wideband DOA estimation methods, namely incoherent weighted MUSIC (IWM) [33], coherent steered covariance matrix (STCM) [2],[45],[50] and weighted subspace fitting (WSF) [51] are considered. These algorithms are known in array signal processing, but many aspects of their performance are not completely understood and investigated, especially when applied to unattended passive acoustic arrays. First, these three algorithms are briefly introduced in a way that facilitates their implementation. More theoretical details can be found in the related references. Simulations on both real (SAFE II) and synthesized data are conducted to compare the performance of these algorithms, their strengths and weaknesses and to identify the issues that need to be carefully considered when these are applied to our problem. Extensive simulation results are presented for the uniform linear array (ULA) as well as the wagon-wheel array. Finally, some key observations are provided.

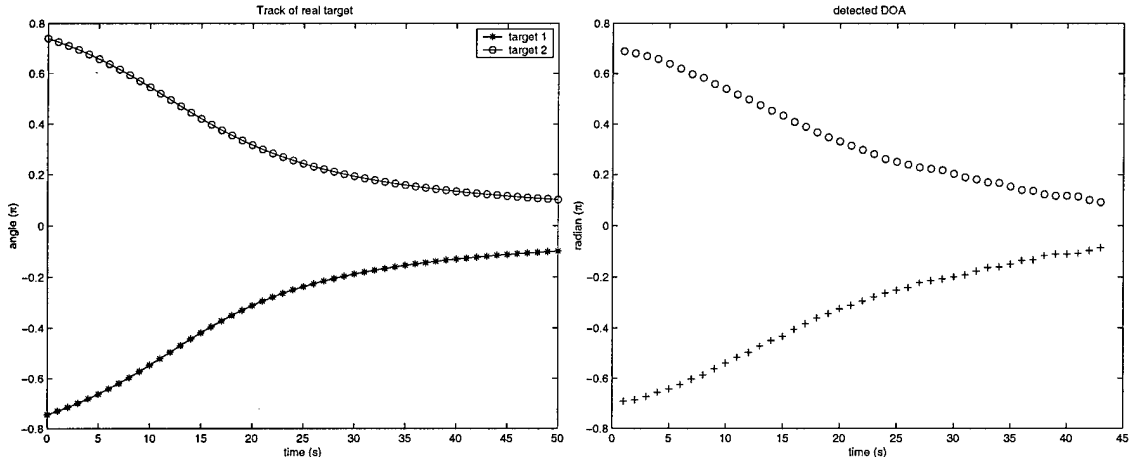


Figure 3: The real and detected tracks of two far-apart targets.

4.1 Steered Covariance Matrix (STCM) Algorithm

In this section we briefly review the STCM method and present some preliminary results on both the synthesized and real SAFE II data.

Let us denote the complex analytic signal of the output of a sensor at location x_m by $y(m, t)$, for $m = -K, \dots, K$, where the total number of sensors is $M = 2K + 1$. Then, $y(m, t)$, observed over a time interval of T seconds can be represented as,

$$y(m, t) = \sum_{i=1}^P s_i[t - \tau_m(\theta_i)] + v(m, t)$$

where $s_i(t), i = 1, \dots, P$ are stationary, zero-mean processes corresponding to the received source signals and $v(m, t)$ is the spatially and temporally stationary zero-mean noise process at the m th sensor. The second-order statistics of the field are completely specified by the cross-spectral density matrices, $R(\omega_k) = E[Y(\omega_k)Y(\omega_k)^*]$, for $k = l, \dots, h$, where $E[\cdot]$ denotes the expectation operator and $Y(\omega_k)$ is the frequency component at frequency ω_k . For the above model, we have

$$R(\omega_k) = A(\omega_k, \theta)P_s(\omega_k)A(\omega_k, \theta)^* + R_v(\omega_k)$$

where $A(\omega_k, \theta) = [a(\omega_k, \theta_1), a(\omega_k, \theta_2), \dots, a(\omega_k, \theta_P)]$ is the $M \times P$ source direction matrix, $a(\omega_k, \theta_i) = [e^{-j\omega_k\tau_{-K}(\theta_i)}, \dots, e^{-j\omega_k\tau_K(\theta_i)}]^T$ is the direction vector of the i th source, $P_s(\omega_k)$ is a $P \times P$ source spectral density matrix, $\theta = [\theta_1, \dots, \theta_P]$, and $R_v(\omega_k)$ represents the $M \times M$ noise covariance matrix. For wideband sources the problem is that the same source contributes a different rank-one component to $R_v(\omega_k)$ at the temporal frequency. To avoid this ambiguity problem, the basic idea behind the STCM [45],[50] is to preprocess the sensor outputs to ensure that arrivals from a particular direction have the same rank-one representation at all temporal frequencies. Letting θ to denote the direction of interest, we define $T_s(\theta, \omega_k)$ as

$$T_s(\theta, \omega_k) = \begin{bmatrix} e^{j\omega_k\tau_{-K}(\theta)} & 0 & \dots & 0 \\ 0 & e^{j\omega_k\tau_{-K+1}(\theta)} & \dots & 0 \\ \vdots & \vdots & \ddots & \vdots \\ 0 & 0 & \dots & e^{j\omega_k\tau_K(\theta)} \end{bmatrix} \quad (4)$$

Now, by multiplying $T_s(\theta, \omega_k)$ with $Y(\omega_k)$, we get

$$y_s(t, \theta) = \sum_{k=l}^h T_s(\theta, \omega_k) Y(\omega_k) e^{j\omega_k t} \quad (5)$$

Substituting (4) into (5) we get

$$y_s(t, \theta) = \{y[-K, t + \tau_{-K}(\theta)], y[-K + 1, t + \tau_{-K+1}(\theta)], \dots, y[K, t + \tau_K(\theta)]\}^T \quad (6)$$

The steered covariance matrix corresponding to direction θ is given by

$$R_s(\theta) = \sum_{k=l}^h T_s(\omega_k, \theta) R(\omega_k) T_s(\omega_k, \theta)^* \quad (7)$$

The structure of $R_s(\theta)$ can be used to motivate a variety of wideband spatial spectral estimation methods. For the circular array in our problem, the STCM is implemented as follows.

1. Form the estimated cross-spectral density matrices, $\hat{R}(\omega_k)$, over the frequency band of interest. A common method of forming $\hat{R}(\omega)$ from discrete-time sensor outputs is to divide the T second observation into N non-overlapping segments of ΔT seconds each, and then apply DFT to obtain uncorrelated frequency domain vectors, $\mathbf{Y}_n(\omega_k)$, for each segment $n = 1, \dots, N$. The cross-spectral density matrix at frequency ω_k is then estimated by taking

$$\hat{R}(\omega_k) = \frac{1}{N} \sum_{n=1}^N \mathbf{Y}_n(\omega_k) \mathbf{Y}_n(\omega_k)^*$$

2. For each steering direction, θ , of interest, compute the estimated steered covariance matrices,

$$\hat{R}_s(\theta) = \sum_{k=l}^h T_s(\omega_k, \theta) \hat{R}(\omega_k) T_s(\omega_k, \theta)^*$$

where $[\omega_l, \omega_h]$ are the frequency band of interest, and $T_s(\omega_k, \theta)$ for a circular array of five elements is $T_s(\omega_k, \theta) = \text{Diag}\{e^{-j\omega_k d_y \sin \theta/c}, e^{-j\omega_k d_x \cos \theta/c}, 1, e^{j\omega_k d_y \sin \theta/c}, e^{j\omega_k d_x \cos \theta/c}\}$.

3. Compute $\hat{R}_s(\theta)^{-1}$ and form the ‘‘Steered Minimum Variance’’ spectral estimator $\hat{Z}_{stmv}(\theta) = [\mathbf{1}^* \hat{R}_s(\theta)^{-1} \mathbf{1}]^{-1}$, where $\mathbf{1}$ is an $M \times 1$ vector of all ones, for each steering direction θ to obtain a broad-band spatial power spectral estimate. The estimation of the source locations is achieved by determining the peak positions of the spatial power spectral estimate $\hat{Z}_{stmv}(\theta)$.

4.2 Incoherent Wideband MUSIC (IWM) Algorithm

In the array considered here, we assume there are L sensors that measure signals impinging on the array from P wideband acoustic sources in presence of spatially uncorrelated additive noise. The sensor array can have an arbitrary known geometry. In this part of the report, both ULA and CSA geometries are considered in the simulations. The sensor measurement is denoted by $x_i(n)$, $i = 1, 2, \dots, L$, $n = 0, 1, \dots, N - 1$, and N is the number of snapshots that will be used in the DOA estimation. The sources are denoted by $s_i(n)$, $i = 1, 2, \dots, P$. The bandwidth of the sources is divided into h non-overlapping subbands or frequency bins of interest (the way to select the h subbands or frequency bins will be explained on later). Then, at each frequency bin with central frequency ω_k , $k = 1, 2, \dots, h$, we have the complex-valued measurements

$$\hat{\mathbf{X}}(\omega_k) = [\hat{\mathbf{X}}_1(\omega_k), \hat{\mathbf{X}}_2(\omega_k), \dots, \hat{\mathbf{X}}_L(\omega_k)], \quad k = 1, 2, \dots, h \quad (8)$$

The narrowband spatial correlation matrix (SCM) at each frequency bin is then computed using

$$\hat{\mathbf{R}}_X(\omega_k) = \hat{\mathbf{X}}(\omega_k)\hat{\mathbf{X}}^H(\omega_k), \quad k = 1, 2, \dots, h \quad (9)$$

In the next section, we present a brief review of another wideband DOA estimation scheme namely IWM [33], followed by the WSF algorithm [51],[52]. The steps in the IWM algorithm may be summarized as follows:

Step 1: Perform eigenvalue decomposition (e.g. Singular Value Decomposition (SVD)) for each spatial correlation matrix to obtain the noise subspace $\hat{\mathbf{U}}(\omega_k)$.

Step 2: For a bearing angle θ , evaluate

$$\hat{P}(\omega_k, \theta) = \frac{1}{\mathbf{a}^H(\omega_k, \theta)\hat{\mathbf{U}}(\omega_k)\hat{\mathbf{U}}^H(\omega_k)\mathbf{a}(\omega_k, \theta)}, \quad k = 1, 2, \dots, h \quad (10)$$

where $\mathbf{a}(\omega_k, \theta)$ is the steering vector that depends on the array manifold.

Step 3: Average the power over all the selected frequency bins for the bearing angle θ

$$\hat{P}(\theta) = \frac{1}{h} \sum_{k=1}^h \hat{P}(\omega_k) \quad (11)$$

Step 4: Calculate $\hat{P}(\theta)$ for all θ of interest, by repeating steps 2 and 3, and pick those for which $\hat{P}(\cdot)$ has a peak above certain level, as the DOA estimate(s).

4.3 Weighted Subspace Fitting (WSF) Algorithm

The steps in this algorithm can be summarized as follows:

Step 1: Perform SVD for each $\hat{\mathbf{R}}_X(\omega_k)$ to obtain the respective signal subspace $\hat{\mathbf{U}}_s(\omega_k)$. Then calculate the diagonal weighting matrices $\mathbf{P}(\omega_k)$ ($\eta_k \times \eta_k$, η_k :the number of signal components contained in $\hat{\mathbf{R}}_X(\omega_k)$)

$$\mathbf{P}(\omega_k)_{[k,k]} = \frac{\lambda_k(\omega_k) - \sigma_n^2}{\sqrt{\lambda_k(\omega_k)\sigma_n^2}} \rightarrow \sqrt{\lambda_k(\omega_k)} \quad (12)$$

for relatively small noise variance σ_n^2 . λ_k 's are the eigenvalues of $\hat{\mathbf{R}}_X(\omega_k)$. If the subband width is zero or for a frequency bin, one has $\eta_k = 1$ and $P(\omega_k)$ will be a scalar.

Step 2: Using the steering vector $\Theta = [\theta_1, \theta_2, \dots, \theta_P]^T$, compute

$$\hat{\mathbf{C}}(\Theta) = \mathbf{A}^\dagger(\omega_k, \Theta)\hat{\mathbf{U}}_s(\omega_k)\mathbf{P}(\omega_k) \quad (13)$$

where

$$\mathbf{A}^\dagger(\omega_k, \Theta) = (\mathbf{A}^H(\omega_k, \Theta)\mathbf{A}(\omega_k, \Theta))^{-1} \mathbf{A}^H(\omega_k, \Theta) \quad (14)$$

$$\mathbf{A}(\omega_k, \Theta) = [\mathbf{a}(\omega_k, \theta_1), \mathbf{a}(\omega_k, \theta_2), \dots, \mathbf{a}(\omega_k, \theta_P)]^T \quad (15)$$

Step 3: Calculate the following criterion for all the steering vectors Θ of interest, by repeating the steps 1 and 2, and taking the one that minimizes the criterion as the estimate of the DOA vector

$$\hat{\Theta}_{WSF} = \min_{\Theta} \sum_{k=1}^h \left\| \mathbf{A}(\omega_k, \Theta)\hat{\mathbf{C}}(\omega_k, \Theta) - \hat{\mathbf{U}}_s(\omega_k)\mathbf{P}(\omega_k) \right\|_F^2 \quad (16)$$

4.4 Simulation Results of Wideband DOA Estimation Methods

In this section we first present the results of the AR-based method for generating synthesized data. Figure 4 shows the results of applying IWM, STCM and WSF algorithms using a uniform linear array (ULA) to a synthetic data with $SNR = 0$ dB generated based upon the truth file associated with *newr1502* in SAFE II data set. Figure 5 gives the results of the three DOA estimation methods on the same data but using a circular (wagon-wheel) array geometry (CSA). Several intriguing observations can be made from these results. Comparing the results of IWM and WSF with those of STCM one can observe that the number of false peaks in the STCM is much higher than the other two algorithms. Clearly, WSF algorithm is the superior algorithm as it provided almost perfect DOA estimation and tracking ability for both array configurations (ULA and CSA) and in this very low SNR condition. Additionally, the results for the circular array has much smaller mean squared error (MSE) as compared to those of the ULA. This is particularly evident by comparing Figures 4(c) and 5(c) for WSF algorithm.

To show the power of the WSF algorithm for resolving closely spaced targets, a similar experiment was repeated using a synthetically generated data from the SAFE II data set associated with *newr1507* with $SNR = 5$ dB. This particular case presents a more challenging scenario with two closely spaced targets that move in abreast formation. Figures 6 and 7 show the results of IWM, STCM and WSF algorithms for a ULA and a CSA, respectively. Once again the results indicate the superiority of the WSF method for DOA estimation and tracking of closely spaced targets. To demonstrate the real usefulness of this algorithm in situations where more than two abreast targets may be encountered, we repeated the same experiment on a synthesized data set with three closely spaced targets in an abreast formation ($SNR = 10$ dB). Figures 8 and 9 show the results of these algorithms for a ULA and a CSA geometry, respectively. These results clearly demonstrate the superiority of WSF algorithm for DOA estimation in difficult target formations and SNR conditions. We can also conclude that the superiority of the WSF algorithm is not dependent on the number of the targets under consideration, as we have consistently achieved very good results in various multiple (≥ 2) closely spaced target scenarios.

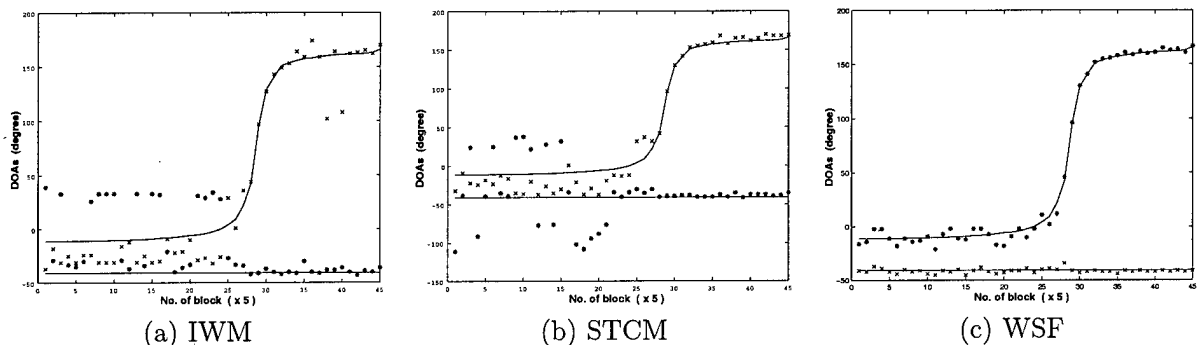


Figure 4: Uniform Linear Array (ULA) applied to synthetically generated SAFE II data set *newr1502* with $SNR = 0$ dB. The x -axis represents *time* in s. The number of blocks denotes the number of samples plotted in each interval of 5s.

Next, the second method for generating realistic synthesized multiple target formations is applied. We generated three cases of abreast, single-file and staggered targets. In all these cases, the radius of the array was 4 ft. and the center was located at (-5m,5m). For the abreast case, the two targets are originally at (-300m,-300m) and (-300m,-350m). For the single-file case, the two targets are originally at (-300m,100m) and (-250m,100m). In the staggered formation there are three targets at initial positions

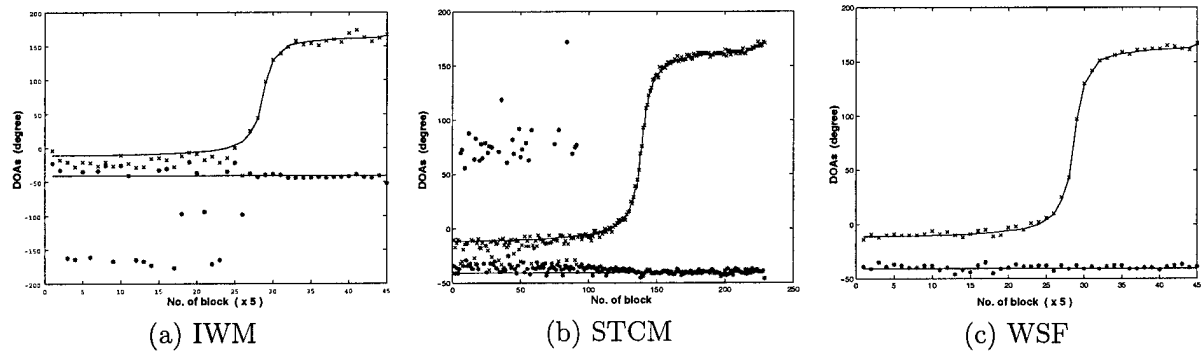


Figure 5: Cross Shaped Array (CSA) applied to synthetically generated SAFE II data set newr1502 with SNR = 0 dB. The x -axis represents $time$ in s . The number of blocks denotes the number of samples plotted in each interval of 5s.

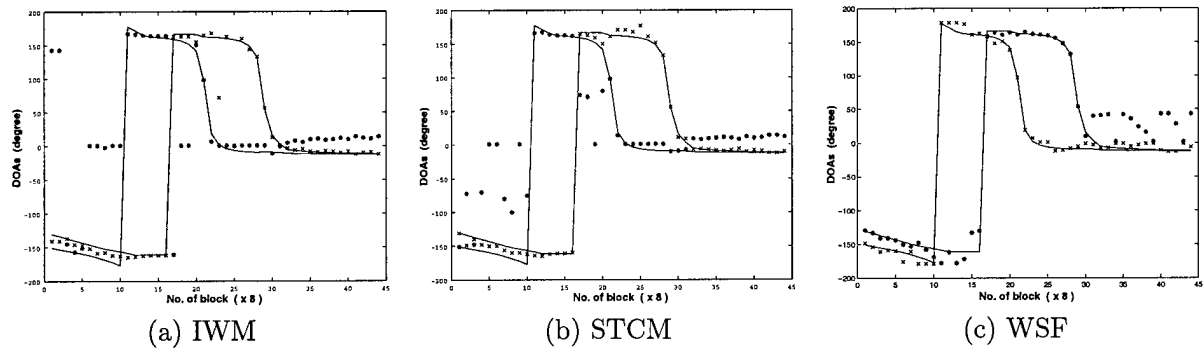


Figure 6: Uniform Linear Array (ULA) applied to synthetically generated SAFE II data set newr1507 using two targets with SNR = 5 dB. The x -axis represents $time$ in s . The number of blocks denotes the number of samples plotted in each interval of 5s.

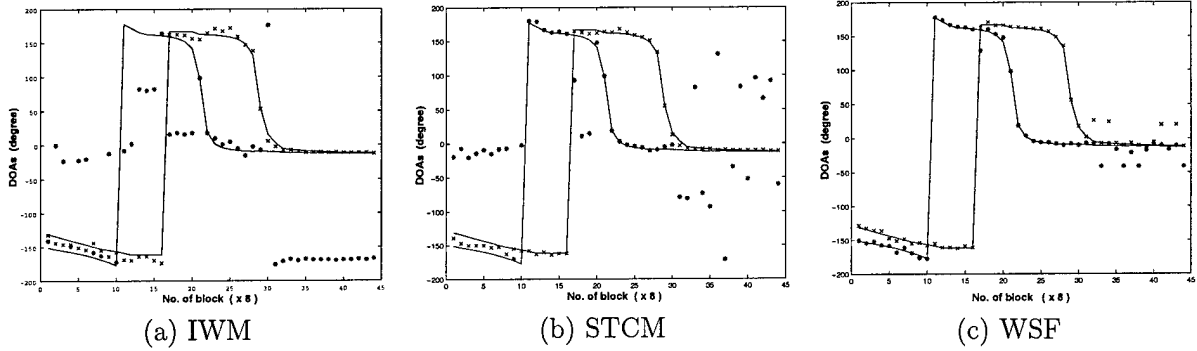


Figure 7: Cross Shaped Array (CSA) applied to synthetically generated SAFE II data set newr1507 using *two* targets with SNR = 5 dB. The x -axis represents *time* in s . The number of blocks denotes the number of samples plotted in each interval of 5s.

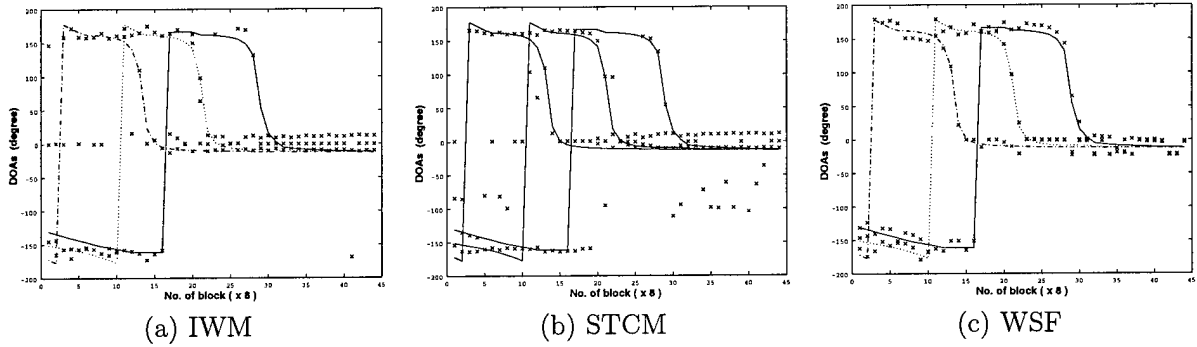


Figure 8: Uniform Linear Array (ULA) applied to synthetically generated SAFE II data set newr1507 using *three* targets with SNR = 10 dB. The x -axis represents *time* in s . The number of blocks denotes the number of samples plotted in each interval of 5s.

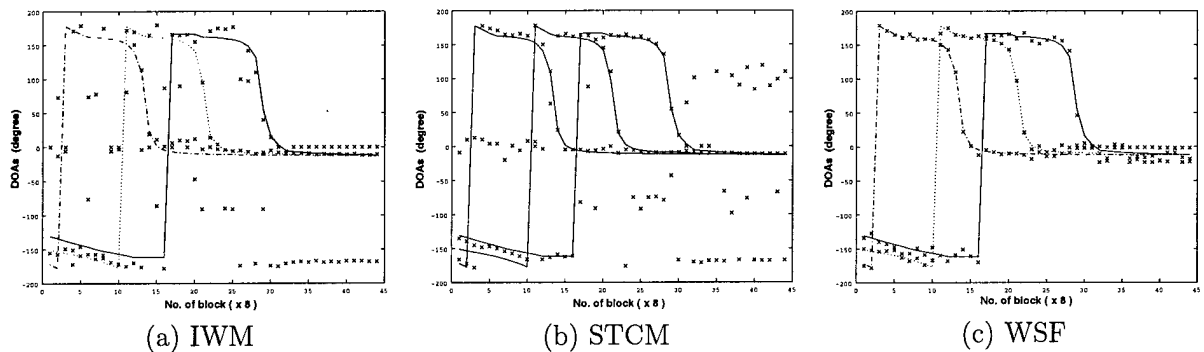


Figure 9: Cross Shaped Array (CSA) applied to synthetically generated SAFE II data set newr1507 using *three* targets with SNR =10 dB. The *x*-axis represents *time* in *s*. The number of blocks denotes the number of samples plotted in each interval of 5*s*.

(-300m,100m), (-250m,100m), (-275m,150m). In all these cases, the targets move to East with a constant speed of 25m/sec. The signal-to-noise ratio (SNR) was 10dB for these cases, which represents a nominal operating condition. In the following, only the results of the STCM and WSF algorithms are presented here as the IWM algorithm did not produce reliable results.

The STCM method was first applied to these cases. The results are shown Figures (10), (11), and (12) respectively. Figure (10)(a) shows the truth tracks of the two abreast targets. Figure (10)(b) gives the detected DOA's for this case using the STCM method. To investigate the resolution of this method in separating the two tracks, we generated the entire response of the STCM before peak picking operation. Figure (10)(c) shows this 3-D response pattern of the STCM versus time. In a sense this plot reflects the beam resolution of the STCM method. The frequency range used for the detection is $50Hz \leq f \leq 150Hz$. As can be seen, although the STCM method correctly detects the track of the two targets, it could not resolve them into two individual targets. Note that unlike the subband MUSIC algorithm which generates a large number of false peaks, the STCM method does not have this problem as evident from both Figures (10)(a) and (b). Nonetheless, if we expand the frequency range to $80Hz \leq f \leq 250Hz$, we start seeing some false peaks even though they are not larger than those of the targets in amplitude.

Figures (11)(a)-(c) show the results of the single-file case. Figures (12)(a)-(c), on the other hand, show the corresponding plots for the staggered formation. Again as we can see, the STCM detects the track of the two targets but could not resolve them well. *The important observation of this study is that the STCM method can indeed detect the DOA's of groups of closely spaced targets. This implies that this method may be a very useful pre-detection tool that provides approximate location or DOA of the formation. Once this information is determined, other methods, e.g. WSF, maybe used to resolve the formation into several targets.*

In contrast to the STCM that is unable to discriminate between the number of targets, the WSF algorithm is capable of separating the targets even in very tight formations. To demonstrate this, the same synthetic data for three rather difficult scenarios, namely single-file, staggered, and abreast formations are used. The results shown in Figures 10, 11, and 12 for the abreast, single-file and staggered formations, respectively are to serve as reference for comparison with the results of the WSF algorithm. As we have stated before, Figures 10 and 11 showed that although the STCM method correctly detects the track of the two targets, it is unable to resolve them into two individual targets. Similar observation can be drawn from

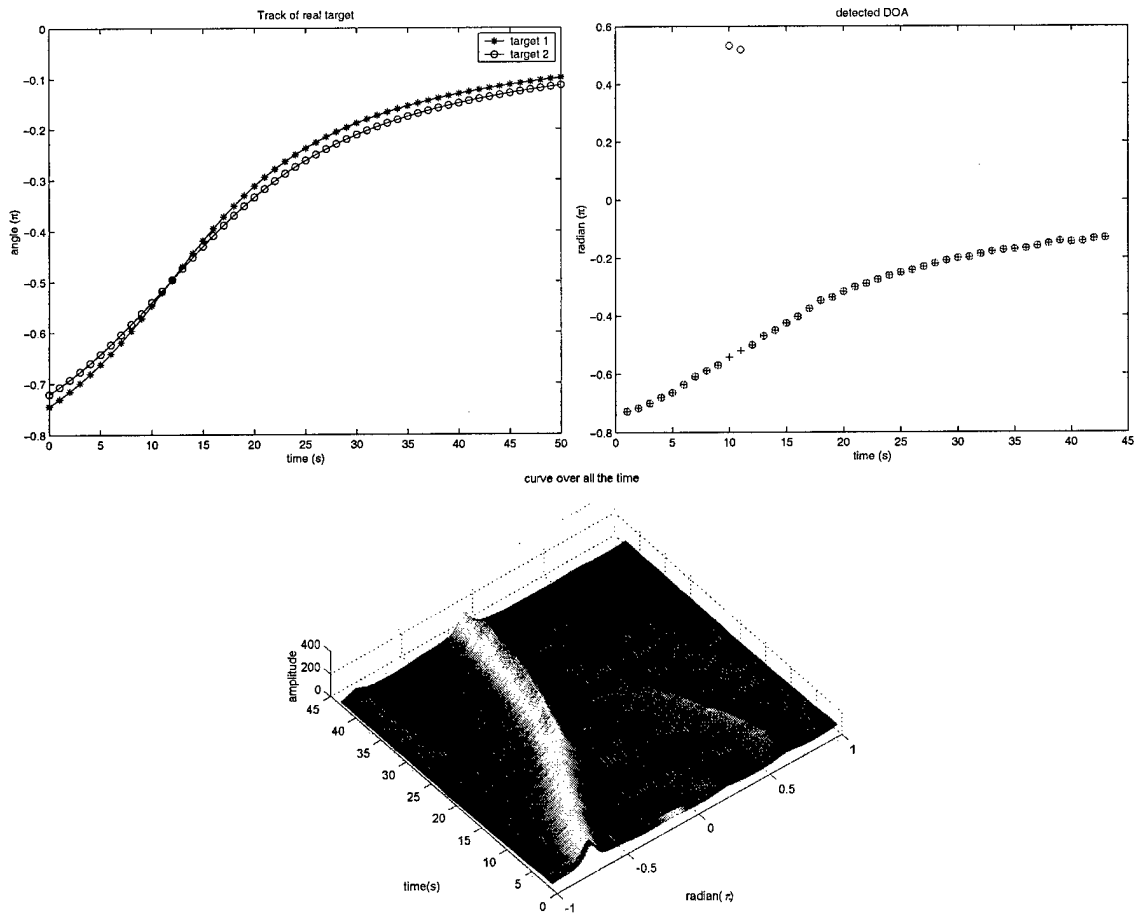


Figure 10: The real and detected tracks of two abreast targets.

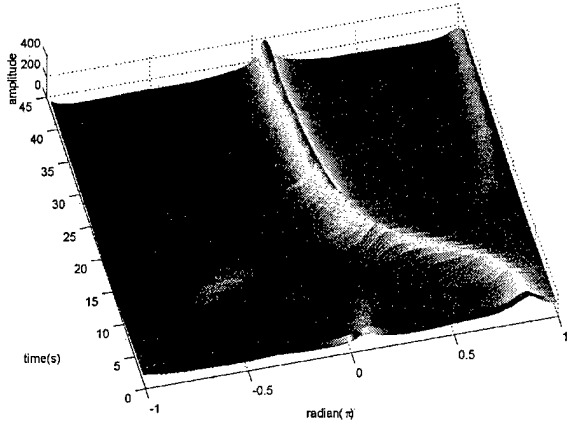
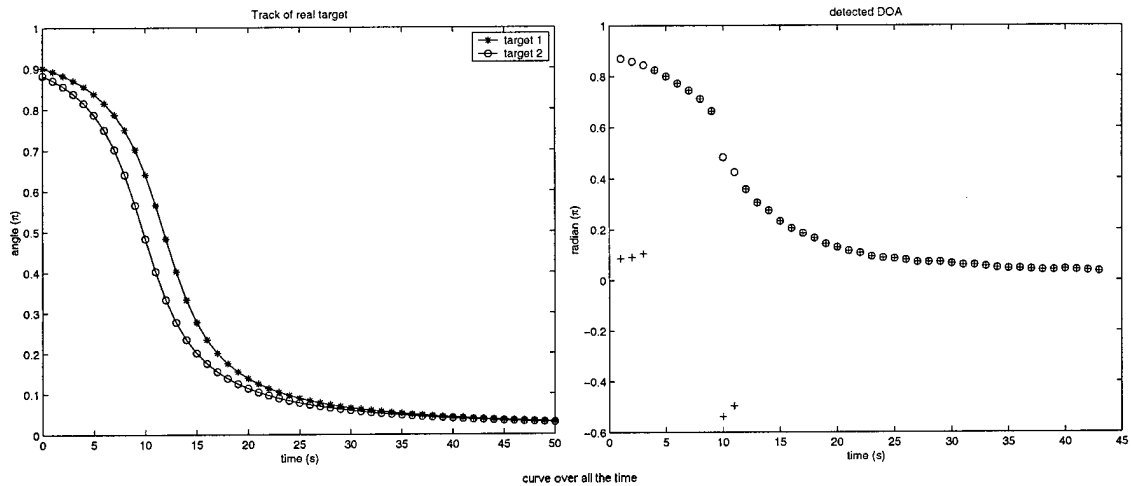


Figure 11: The real and detected track of two single-file targets.

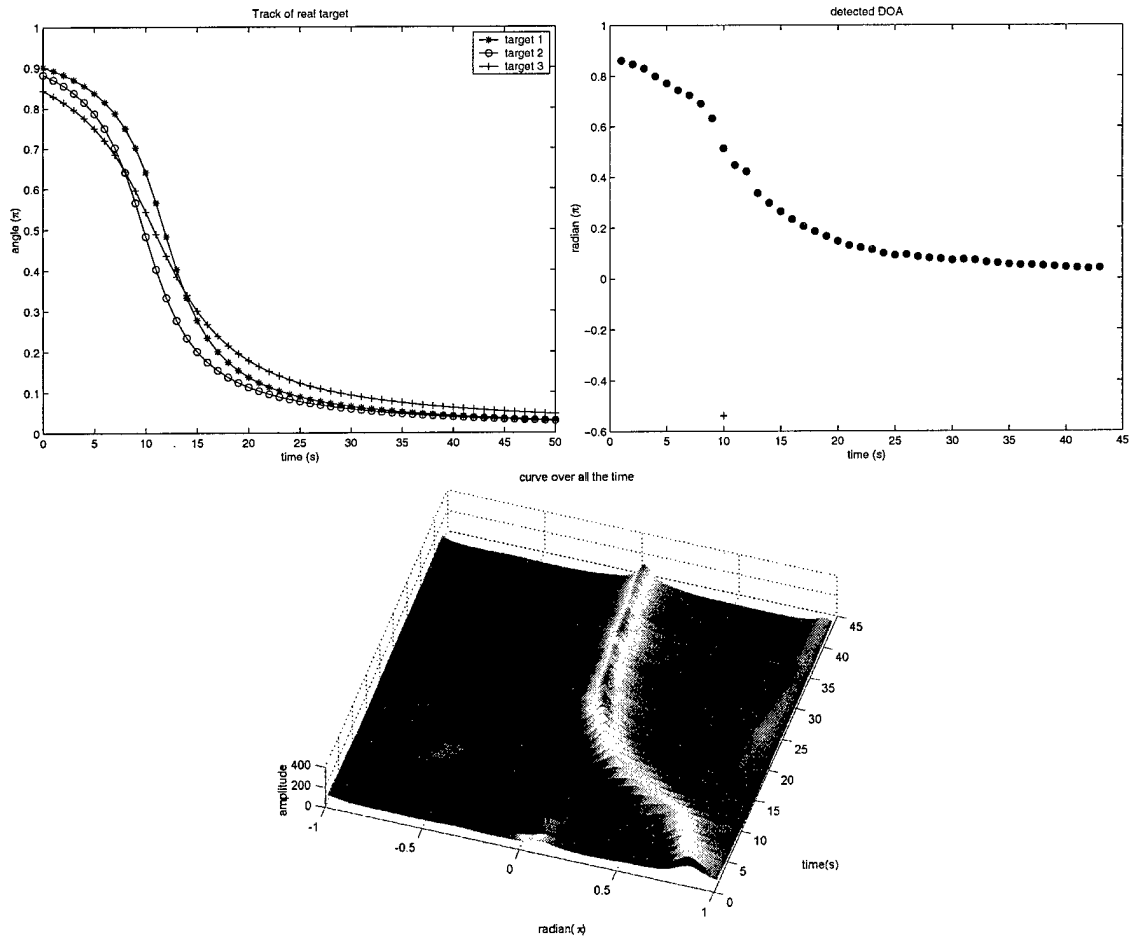


Figure 12: The real and detected track of three staggered targets.

the results of the staggered case, Figure 12, with three closely spaced targets. Since the STCM algorithm is computationally more efficient comparing to the WSF algorithm and further the STCM has shown good capabilities in identifying the target tracks, we propose to use the STCM algorithm as a pre-processor for the WSF algorithm. In this way, the search space for the WSF can be reduced significantly, yielding a computationally tractable algorithm with very good resolution capability for closely spaced targets. This is demonstrated in the results that follow.

Figures 13-15 depict the truth tracks of the abreast, single-file and staggered formations, respectively together with the detected tracks using the WSF algorithm. Note that the actual tracks are shown by solid, dotted and dashed lines in these figures while the results of the WSF algorithm are shown by *, x and o in these plots. Comparing these results with those of the STCM method clearly show the advantages of the WSF algorithm in resolving closely spaced targets. Among future research topics in Phase II is the design and development of a computationally efficient algorithm for implementing the WSF method.

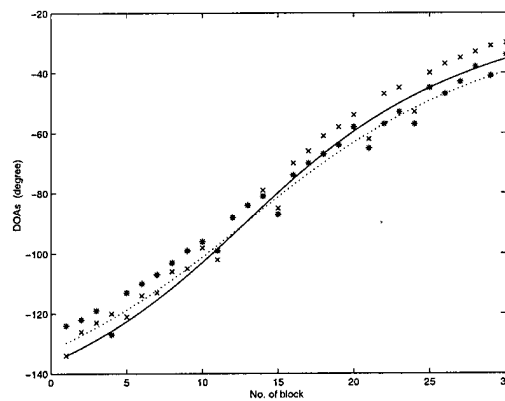


Figure 13: The WSF algorithm applied to the synthetically generated Abreast formation data. The number of blocks in the x -axis represents *time* in s .

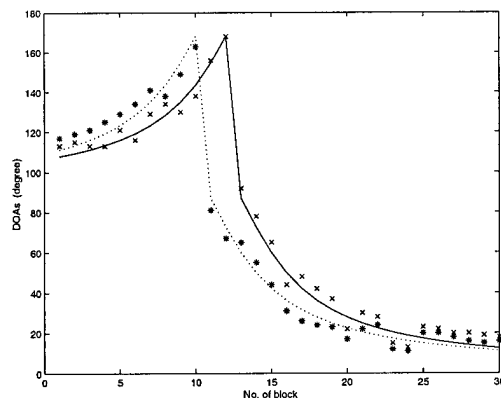


Figure 14: The WSF algorithm applied to the synthetically generated Single-File formation data. The number of blocks in the x -axis represents *time* in s .

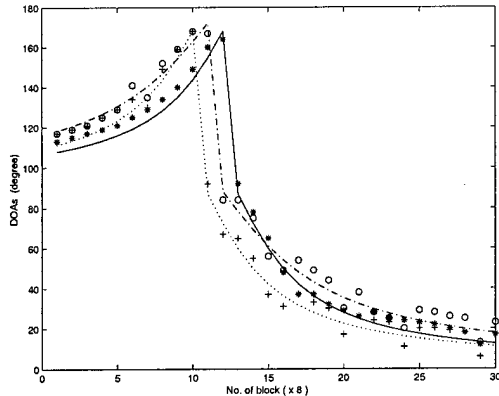


Figure 15: The WSF algorithm applied to the synthetically generated Staggered formation data. The number of blocks in the x -axis represents *time* in s .

5 Array Manifolds & DOA Estimation

In this part of the study we concentrate our efforts on a dual-size array geometry that consists of a rectangular array grid to be spaced much greater than a half-wavelength, but at each grid point a 5-element half-wavelength spaced cross-shaped subarray is utilized as shown in Figure 16. It is generally known that a larger array aperture will be able to produce a more accurate direction of arrival (DOA) estimate as compared to a smaller array aperture. The advantage of using a larger array aperture is also manifested in achieving a more robust resolution of very closely spaced target signatures. In order to formally extend the array aperture it is customary to employ sparse array configurations where the uniform intra-array spacing (denoted by Δ) is wider than the half-wavelength inter-subarray spacing (denoted by $\delta = \lambda/2$). Therefore, achieving the goal of more accurate estimate without using extra hardware. Unfortunately, this larger intra-array positioning will result in direction cosines u and v estimates (in the y and x axes, respectively) that are ambiguous. To resolve this ambiguity a sparse but regular array geometry embedded with a spatial invariance may be employed and MUSIC-based or ESPRIT-based DOA algorithms may be developed to exploit the specific geometry and to resolve the ambiguities [53]-[55].

The smaller spatial invariance $\delta = \lambda/2$ would result in an unambiguous but high-variance estimates of the DOAs whereas the larger spatial invariance $\Delta \gg \lambda/2$ would result in lower invariance at the expense of cyclically ambiguous estimates of the DOAs. Consequently, the proposed geometry would facilitate simultaneous development of less costly hardware architectures and computationally efficient algorithms that would take advantage of each spatial invariance.

For the sake of generality and completeness we consider a sparse rectangular array geometry as an $L \times M$ uniform grid consisting of five (5)-element identical subarrays. Consider P uncorrelated and narrowband signals that impinge on the 2-D grid. The k th signal may be characterized by a $5LM \times 1$ array manifold

$$\mathbf{a}(u_k, v_k) = \mathbf{q}_L(u_k, v_k) \otimes \mathbf{q}_s(u_k, v_k), \quad k = 1, \dots, P \quad (17)$$

where \otimes is the Kronecker multiplication operator, $\mathbf{q}_L(u_k, v_k)$ is a $LM \times 1$ vector consisting of the spatial phase factors associated with the sparse uniform array grid, $\mathbf{q}_s(u_k, v_k)$ is a 5×1 vector containing the subarray manifold, and $u_k = \sin\theta_k \cos\phi_k$, $v_k = \sin\theta_k \sin\phi_k$ represent the direction cosines along the y -axis and x -axis, respectively, and θ_k and ϕ_k represent the k^{th} source elevation (measured wrt the vertical z -axis)

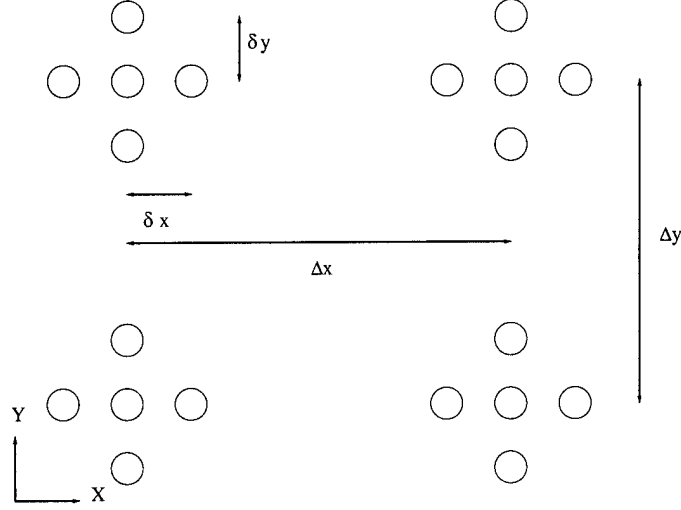


Figure 16: Extended aperture dual invariance sparse array with rectangular grid.

and azimuth angles (measured wrt the positive x -axis), respectively. For the rectangular grid geometry shown in Figure 16 we have the following relation

$$\mathbf{q}_L(u_k, v_k) = \begin{bmatrix} e^{j\frac{2\pi\Delta^y}{\lambda}0u_k} \\ \vdots \\ e^{j\frac{2\pi\Delta^y}{\lambda}(L-1)u_k} \end{bmatrix} \otimes \begin{bmatrix} e^{j\frac{2\pi\Delta^x}{\lambda}0v_k} \\ \vdots \\ e^{j\frac{2\pi\Delta^x}{\lambda}(M-1)v_k} \end{bmatrix} = \mathbf{q}_L^y(u_k) \otimes \mathbf{q}_L^x(v_k) \quad (18)$$

where $\Delta^x \gg \lambda/2$ and $\Delta^y \gg \lambda/2$, with Δ^x and Δ^y being the x -axis and y -axis intra-array distances between the grid points (nodes). The incident signal on the grid may now be represented as

$$\mathbf{z}(t) = \begin{bmatrix} z_1(t) \\ \vdots \\ z_{LM}(t) \end{bmatrix} = \underbrace{[\mathbf{a}(u_1, v_1), \dots, \mathbf{a}(u_P, v_P)]}_{:=\mathbf{A}(u_1, \dots, u_P, v_1, \dots, v_P)} \begin{bmatrix} s_1(t) \\ \vdots \\ s_P(t) \end{bmatrix} + \mathbf{n}(t) \quad (19)$$

where $z_i(t)$, $i = 1, \dots, LM$ is a 5×1 incident signal on the i^{th} subarray, $s_i(t)$ is the signal associated with source i , and $\mathbf{n}(t)$ refers to a complex valued zero-mean additive white noise. Using a total of N snapshots taken at distinct times $\{t_n, n = 1, \dots, N\}$, the DOA problem is then reduced to determining $\{\theta_k, \phi_k, k = 1, \dots, P\}$ from the $5LM \times N$ data set $\mathbf{Z} = [\mathbf{z}(t_1), \dots, \mathbf{z}(t_N)]$.

5.1 Mathematical Model for the Subarray

To complete the MUSIC-based algorithm that is developed here for the half-wavelength spaced subarray at each grid point we have

$$\mathbf{q}_s(u_k, v_k) = \left[e^{-j(2\pi\delta^x/\lambda)v_k}, e^{-j(2\pi\delta^y/\lambda)u_k}, 1, e^{j(2\pi\delta^y/\lambda)u_k}, e^{j(2\pi\delta^x/\lambda)v_k} \right]^T \quad (20)$$

and where $\delta^x \leq \lambda/2$ and $\delta^y \leq \lambda/2$ with δ^x and δ^y denoting the x -axis and y -axis distances of the elements within the subarrays.

The first step in the MUSIC-based algorithm is to compute the $5LM \times P$ signal-subspace eigenvector matrix \mathbf{E}_s from which the other matrix pencils are constructed corresponding to the P largest eigenvalues of the $5LM \times 5LM$ sample spatial correlation matrix. Namely, we have

$$\mathbf{R}_{zz} = \mathbf{Z}\mathbf{Z}^H = \sum_{n=1}^N \mathbf{z}(t_n)\mathbf{z}^H(t_n) = \mathbf{E}_s\mathbf{D}_s\mathbf{E}_s^H + \mathbf{E}_n\mathbf{D}_n\mathbf{E}_n^H \quad (21)$$

where \mathbf{E}_n is the $5LM \times (5LM - P)$ noise-subspace matrix corresponding to the $5LM - P$ smallest eigenvalues, \mathbf{D}_s is the $P \times P$ diagonal matrix whose diagonal entries are the largest P eigenvalues, and \mathbf{D}_n is a $(5LM - P) \times (5LM - P)$ diagonal matrix whose diagonal entries are the $5LM - P$ smallest eigenvalues. As the number of snapshots increase the value for \mathbf{E}_s may asymptotically be approximated by

$$\mathbf{E}_s = \mathbf{A}\mathbf{T} = [\mathbf{a}(u_1, v_1), \dots, \mathbf{a}(u_P, v_P)]\mathbf{T} \quad (22)$$

where \mathbf{T} denotes an unknown $P \times P$ nonsingular matrix to be determined. Two matrix pencils with spatial invariance are now constructed along the y -axis according to

$$\mathbf{A}_1^u = [I_{5(L-1)M \times 5(L-1)M} | 0_{5(L-1)M \times 5M}] \mathbf{A} \quad (23)$$

$$\mathbf{A}_2^u = [0_{5(L-1)M \times 5M} | I_{5(L-1)M \times 5(L-1)M}] \mathbf{A} = \mathbf{A}_1^u(\Phi^u)^\dagger \quad (24)$$

where Φ^u is a diagonal matrix with P diagonal elements and \dagger is the complex conjugate operation. The matrix pencils are now defined as

$$\mathbf{E}_1^u = [I_{5(L-1)M \times 5(L-1)M} | 0_{5(L-1)M \times 5M}] \mathbf{E}_s \quad (25)$$

$$\mathbf{E}_2^u = [0_{5(L-1)M \times 5M} | I_{5(L-1)M \times 5(L-1)M}] \mathbf{E}_s \quad (26)$$

The matrix pencils $\{\mathbf{E}_1^u, \mathbf{E}_2^u\}$ are formed along the y -axis by having all $(L-1)M$ subarrays at the top $L-1$ rows on the overall array's grid to contribute data to \mathbf{E}_1^u and by having all $(L-1)M$ subarrays at the bottom $L-1$ rows on the overall array's grid to contribute data to \mathbf{E}_2^u . The above two matrices are related to each other through the extended spatial invariance $\Delta^y \gg \lambda/2$ and can yield low variance but cyclically ambiguous DOA estimates along the y -axis. In the ideal case when there is no noise or the number of snapshots is sufficiently large we may write $\mathbf{E}_1^u \Phi^u = \mathbf{E}_2^u$, so that $\Phi^u = ((\mathbf{E}_1^u)^H \mathbf{E}_1^u)^{-1} ((\mathbf{E}_1^u)^H \mathbf{E}_2^u) = (\mathbf{T}^u)^{-1} \Psi^u \mathbf{T}^u$, where $[\Psi^u]_{ii}$ are the eigenvalues of Φ^u .

From the above discussion it now follows that a set of highly accurate but cyclically ambiguous estimates of the direction of cosines along the y -axis may be estimated as follows:

$$u_i := \frac{\angle[\Psi^u]_{ii}}{2\pi\Delta^y/\lambda}, \quad i = 1, \dots, P \quad (27)$$

where $\angle z$ refers to the principal argument of the complex number z in the range of $-\pi$ and π . Given that $\Delta^y \gg \lambda/2$ and $-1 \leq u_i \leq 1$, there exists a set of cyclically ambiguous estimates for u_i , that is

$$u_i^* = u_i + c_u \frac{\lambda}{\Delta^y} \quad (28)$$

$$\lceil \frac{-\Delta^y}{\lambda}(1 + u_i) \rceil \leq c_u \leq \lfloor \frac{\Delta^y}{\lambda}(1 - u_i) \rfloor \quad (29)$$

where $\lceil x \rceil$ and $\lfloor x \rfloor$ denote the ceiling and floor operators, respectively. Therefore, \mathbf{T} may be estimated to within an unknown permutation matrix \mathbf{P}^u as $\mathbf{T}^u = \mathbf{P}^u \mathbf{T}$.

Similar analysis may be carried out for the extended invariance along the x -axis, namely:

$\Phi^v = ((\mathbf{E}_1^v)^H \mathbf{E}_1^v)^{-1} ((\mathbf{E}_1^v)^H \mathbf{E}_2^v) = (\mathbf{T}^v)^{-1} \Psi^v \mathbf{T}^v$, where $[\Psi^v]_{ii}$ are the eigenvalues of Φ^v , and

$$v_i := \frac{\angle[\Psi^v]_{ii}}{2\pi\Delta x/\lambda}, \quad i = 1, \dots, P \quad (30)$$

$$v_i^* = v_i + c_v \frac{\lambda}{\Delta x} \quad (31)$$

$$\lceil \frac{-\Delta x}{\lambda}(1 + v_i) \rceil \leq c_v \leq \lfloor \frac{\Delta x}{\lambda}(1 - v_i) \rfloor \quad (32)$$

The pairs $\{u_i, v_i\}$ may be grouped together as in [53]-[55].

5.2 MUSIC-based Ambiguity Resolution

In order to overcome and remedy the cyclical ambiguity that was discussed in the previous section, a MUSIC-based approach is considered in this part of the project. Specifically, the above ambiguous estimates of (u_i, v_i) are substituted in the array manifold $\mathbf{a}(u_k, v_k)$. The best candidate is now selected as the one that minimizes a certain distance metric between \mathbf{E}_n and $\mathbf{a}(u_k, v_k)$. This disambiguation takes advantage of the superior accuracy of the MUSIC algorithm, but avoiding its computational complexity and cost. The specifics of the algorithm are as follows:

$$\{\hat{u}_k, \hat{v}_k\} = \arg \min_{\{u,v\}} \|\mathbf{E}_n^H (\mathbf{q}_L(u, v) \otimes \mathbf{a}(u, v))\|, \quad k = 1, \dots, P \quad (33)$$

The simulation results reported in [53]-[55] involving two closely spaced equal-power narrowband uncorrelated emitters and using a 3×3 sparse rectangular arrays have shown that the RMS standard deviation decreased by a factor of about 50 folds. Furthermore, the results in [54] using ESPRIT-based approach for a 9×9 sparse grid was compared with a 9×9 half-wavelength uniformly spaced square array. Although, in terms of the hardware and computational complexities the two array geometries are comparable, the DOA estimation performance of the sparse array configuration was shown to be surprisingly better than the uniform array, which also failed to resolve the two very closely spaced sources.

5.3 ESPRIT-based DOA Detection

There are two schemes for forming the subarrays when using ESPRIT-based method. In the first scheme we let all the sensors at the same position within the cross array be one subarray, e.g. all the sensors at the center of the cross array form one of these subarrays. In the second scheme we would include as many sensors into one subarray as possible [53]. Specifically, there are four possible subarrays in this case: (a) the one containing the top two sensors on each vertical leg of all the cross arrays, (b) the one containing the bottom two sensors on each vertical leg of all the cross arrays, (c) the one containing two leftmost sensors on each horizontal leg of all the cross arrays, and (d) the one containing two right most sensors on each horizontal leg of all the cross arrays.

The advantages of the first ESPRIT approach over the MUSIC-based approach are as follows:

1. In the first scheme, there are ML sensors in each subarray, thus the maximum number of targets that it can detect is $ML - 1$, while in the second scheme, this number is $2ML - 1$.
2. By including more sensors into the subarrays, the interference from noise is also reduced.

3. In the first scheme, there are 5 subarrays. Therefore, integration of the estimated DOA's becomes an issue, while in the second scheme, there exists an effective mechanism described in [53].

Due to the above reasons in our implementation, we only considered the ESPRIT-based scheme.

5.4 Simulation Results

Our objective here is to further investigate the use of the above techniques for development of ESPRIT-based algorithms that have specifically taken into consideration the sparse array geometry of our problem, and to benchmark their performance against the other standard geometries.

We have conducted several experiments to study and test the performance of the above method using the ESPRIT approach. The setup for all the experiments are $L = 2$, $M = 2$, $\delta_x = \delta_y = \lambda/2$, $\Delta_x = \Delta_y = 10\lambda$. In these simulations, we assumed the targets emit narrowband signals. The first experiment is designed to test the performance of the detection algorithm as a function of the variations in SNR. The result is shown in Figure 17. The x-axis measures the SNR in dBs and the y-axis denotes the Mean Square Error (MSE). In this experiment, two targets at $\theta_1 = \theta_2 = \pi/2$, $\phi_1 = 0.7\pi$, $\phi_2 = 0.9\pi$ are assumed. From the figure, we can observe that as expected, the MSE decreases when the SNR increases.

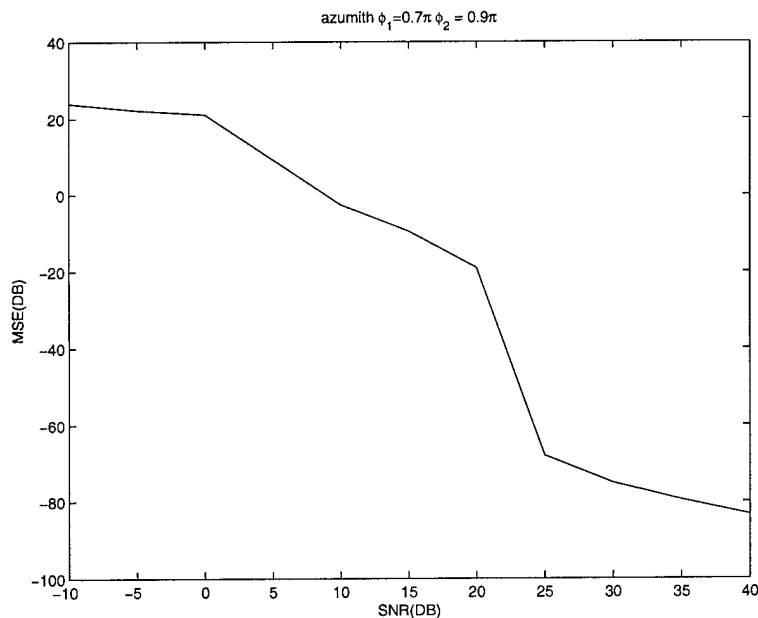


Figure 17: Performance of the ESPRIT-based algorithm with varying SNR.

The second experiment is designed to determine the DOA detectability of this method for resolving two very close targets. To achieve this, the DOA of the first target was fixed, and the DOA of the second target was continuously increased by 0.01π increments. The results in Figure 18 reveals an interesting behavior. That is, with an exception of several specific DOA differences (specifically at $0.04\pi, 0.09\pi$, etc.), this method exhibits very good performance in detecting two closely spaced targets.

To test the capability of the algorithm for detecting multiple (> 2) closely spaced targets, in the next experiment, a 4×4 grid was used. There are four targets with the corresponding DOA's that are

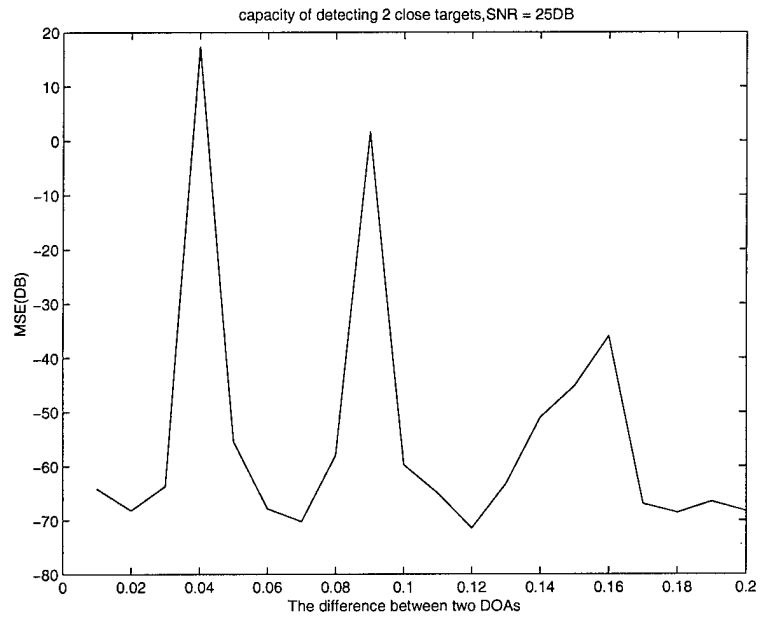


Figure 18: Performance of the 2-D planar array configuration on two close targets.

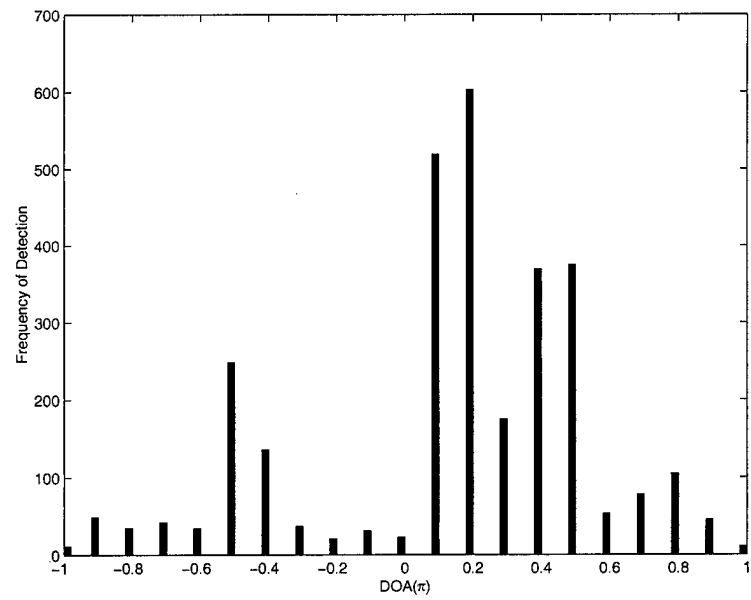


Figure 19: Performance of the 2-D planar array configuration on four close targets.

$0.1\pi, 0.2\pi, 0.3\pi, 0.4\pi$, respectively. The results were obtained by rounding the detected angle to multiples of 0.1π . From the results presented in Figure 19, it can easily be observed that this method can detect the true DOA's very frequently. Future work should include extending this approach to wideband sources.

6 Source Separation Methods

In this section we investigate various ICA algorithms and their applicability for blind source separation of multiple targets moving in closely spaced staggered and abreast formations. Among the researched algorithms are: instantaneous ICA (IICA) [56]-[61] and convolutive (CICA) [62]-[65]. We will also investigate neural network-based ICA methods, namely fast ICA in [66]. The actual data from SAFE II database as well as the synthesized data containing from 2-5 closely spaced targets are utilized to determine the performance of the IICA-based algorithm. It was observed that when the number of the targets for a given node is lower than the number of the microphones, the IICA algorithm may not be able to always correctly “de-confuse” or “discriminate” among the targets in certain situations. Consequently, our future research would involve modification or enhancement to the existing IICA algorithm to remedy and eliminate this “ambiguity” in determining the number of the targets. Furthermore, we shall investigate the applicability of CICA-based algorithms to the real (SAFE II data) as well as the synthetic data in order to determine the advantage and disadvantages of the two methods in terms of their “de-confusing” and “discriminatory” ability in resolving multiple closely spaced targets.

We first introduce one of the well-known instantaneous ICA (IICA) algorithms based on the natural gradient update of the demixing matrix. A number of nonlinear estimating functions that affect the performance of the algorithm are also given. Simulation results are then provided to demonstrate the performance of this algorithm. Finally, we present a convolutive ICA (CICA) algorithm that is obtained by extending the above-mentioned IICA, and also mention some other promising CICA algorithms developed in the literature.

6.1 Natural Gradient Based IICA Algorithm

The goal of ICA or blind source separation (BSS) is to estimate P statistically-independent source signals from L different measured mixtures of these signals. The linearly mixed measurements are obtained by a passive acoustic sensor array with L sensors, where $P \leq L$. For instantaneous mixing, a measured signal vector $\mathbf{x}(k) = [x_1(k), \dots, x_L(k)]^T$ is assumed to be linearly mixed from the unknown source signal vector $\mathbf{s}(k) = [s_1(k), \dots, s_P(k)]^T$, that is

$$\mathbf{x}(k) = \mathbf{A}\mathbf{s}(k) \quad (34)$$

where \mathbf{A} is an unknown $(L \times P)$ mixing matrix. The most important assumption is the source independence; i.e., all $s_i(k)$ are statistically-independent of each other. For the linear mixing, intuitively a linear demixing model may be applied for the source separation task, that is

$$\begin{aligned} \mathbf{y}(k) &= \mathbf{W}(k)\mathbf{x}(k), \quad k = 0, 1, \dots, N-1 \\ \mathbf{y}(k) &= [y_1(k), y_2(k), \dots, y_P(k)]^T \end{aligned} \quad (35)$$

where $\mathbf{W}(k)$ is a $P \times L$ demixing matrix with adjustable elements $w_{i,j}(k)$. We now seek for an algorithm to determine the demixing matrix $\mathbf{W}(k)$ such that the combined matrix $\mathbf{C}(k) = \mathbf{W}(k)\mathbf{A}$ is mapped to $\mathbf{\Phi}\mathbf{D}$, where $\mathbf{\Phi}$ is an $P \times P$ permutation matrix and \mathbf{D} is a diagonal nonsingular scaling matrix. Clearly, the output of the demixer $y_i(k)$ will be one of the scaled source signals. Ordering and/or identifying the recovered source signals $\mathbf{y}(k)$ is not possible without additional information about them.

Numerous techniques have been proposed to solve this problem (see [56]-[61]). A density-based ICA method known as *natural gradient* algorithm proposed by Amari [58] is of particular interest owing to its

good performance, robust stability properties, and low computational requirements in comparison with other similar algorithms. Specifically, it is given by

$$\mathbf{W}(k+1) = \mathbf{W}(k) + \mu(k) [\mathbf{I} - \mathbf{f}(\mathbf{y}(k))\mathbf{y}^T(k)] \mathbf{W}(k) \quad (36)$$

where $\mu(k)$ is a positive learning rate parameter, $\mathbf{f}(\cdot)$ is a vector of a scalar nonlinear function $f(\cdot)$ known as estimating function or scoring function. Several possible candidates for this function are listed below.

$$f(y) = \text{sgn}(y) \quad (\text{instantaneously - mixed speech sources}) \quad (37)$$

$$f(y) = \beta y + y^3, \beta \geq 0 \quad (\text{negative - kurtosis sources}) \quad (38)$$

$$f(y) = \beta y + \tanh(\alpha y), \beta > 0 \quad (\text{super - Gaussian sources}) \quad (39)$$

$$f(y) = \frac{29}{4}y^3 - \frac{47}{4}y^5 - \frac{14}{3}y^7 + \frac{25}{4}y^9 + \frac{3}{4}y^{11} \quad (\text{general}) \quad (40)$$

$$f(y) = \frac{1}{2}y^5 + \frac{2}{3}y^7 + \frac{15}{2}y^9 + \frac{2}{15}y^{11} - \frac{112}{3}y^{13} + 128y^{15} - \frac{125}{3}y^{17} \quad (\text{general}) \quad (41)$$

We have found that when applied to the above algorithm (36), the estimating function of higher order requires more snapshots or data to ensure convergence and stability. Generally, it is preferable to use a low-order function as long as the selected function has a good fit to the statistical properties of the sources.

Figure 20 shows the three independent sources and their estimates by the IICA algorithm (36) with estimating function (41). Clearly, the sources are well-separated after 300 batch iterations. In Figure 21, the rejection indices of the algorithm using three different estimating functions are also shown. It can be observed that the estimating functions (40) and (41) lead to the same convergence rate, but the latter yields smaller steady-state rejection index on average. However, (41) is more complicated and needs more computational time. Estimating function (38) is much simpler than (40) and (41). However, it takes longer (by about 50 iterations) to converge. Note that the use of the estimating functions (37) and (39) was not successful in our simulations for this example. Figure 22 shows one example of using the function (39). The corresponding convergence of the rejection index is given in Figure 21 (d), where the learning rate parameter was adjusted to 0.075 such that the convergence is similar to those using estimating functions (40) and (41). Other parameters β and α were set to 0.1 and 0.5, respectively. Adjusting these two parameters did not change the performance of the algorithm significantly. Estimating function (37) just simply failed in all the runs.

6.2 Convolutional ICA (CICA) Algorithm

In many applications, the use of convolutional mixing is more practical, since sources impinge on each sensor at different times. Clearly, if the source frequencies and the sensor spacings are much smaller than the travelling speed of source, the time lag or delay may be ignored, and the IICA may be approximately applied equally effectively. On the other hand, if this is not the case, we may need to consider using CICA-type algorithms. The convolutional mixing is more complicated than the instantaneous one. In convolutional mixing, we have

$$\mathbf{x}(k) = \sum_{j=-\infty}^{\infty} \mathbf{A}_j \mathbf{s}(k-j) \quad (42)$$

where the sequence of matrices \mathbf{A}_j ($L \times P$) is the multichannel impulse response of the unknown mixing system. The demixing system is assumed to be governed by

$$\mathbf{y}(k) = \sum_{j=0}^M \mathbf{W}_j(k) \mathbf{x}(k-j) \quad (43)$$

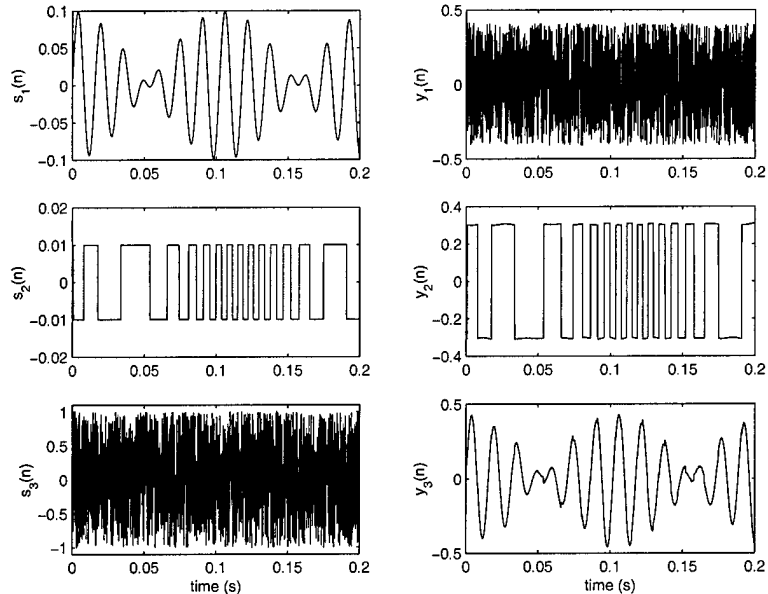


Figure 20: Three actual sources used (left column) and their estimates (right column) by algorithm (36) and estimating function (41).

The CICA algorithm is obtained by extending the spatial-only scheme of (36) to the spatio-temporal case and by introducing certain approximations, which may then be represented by

$$\mathbf{W}_j(k+1) = \mathbf{W}_j(k) + \mu(k) [\mathbf{W}_j(k) - \mathbf{f}(\mathbf{y}(k-M))\mathbf{u}^T(k-j)] \quad (44)$$

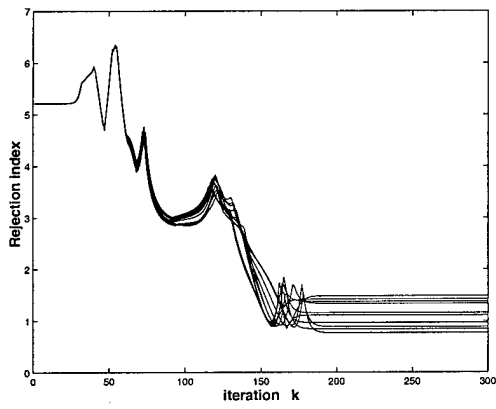
$$\mathbf{u}(k) = \sum_{q=0}^M \mathbf{W}_{M-q}^T(k)\mathbf{y}(k-q) \quad (45)$$

The above algorithm has an elegant form and is computationally efficient. However, some of the approximations made in order to derive it may degrade the performance. This is an area that needs much further research. Recently, several other promising techniques have been proposed in the literature. The geometric source separation method [62], [63] and the generalized sidelobe decorrelator [62], [64] based on the cross-power spectral minimization can resolve the ambiguities inherent in the CICA algorithm by introducing geometric constraints. A new CICA method has also been proposed in [65], which uses a forward FIR model to identify the multi-path channel and a backward FIR one to generate the independent sources. All these methods have been confirmed effective when applied to acoustic signals recorded in a reverberant environment. Their applicability and suitability to our problem is under investigation.

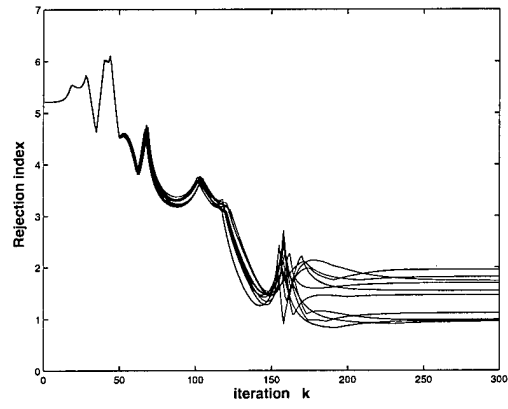
6.3 Simulation Results of IICA Algorithm on Actual SAFE II Data

Our preliminary results of the IICA algorithm on two sets of real SAFE II data are given below. In all the subsequent figures the plots on the left column correspond to the sensor array measurements x_i (except the last row), and the ones on the right column designate the demixer output y_i (except the last row). The plots in the last row show the convergence of the weights. Another performance indicator is the mutual (1st order) correlation coefficient matrix (CCM) evaluated at steady-state condition of the algorithm. The learning rate is set to be 0.075 and the number of snapshots is 2000.

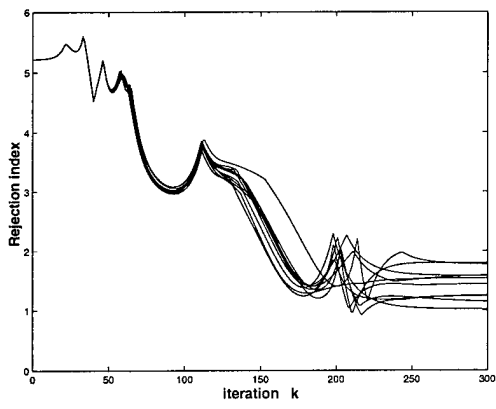
The results shown in Figures 23 to 28 are applied to the actual data for Node 1 (newr1502 in SAFE



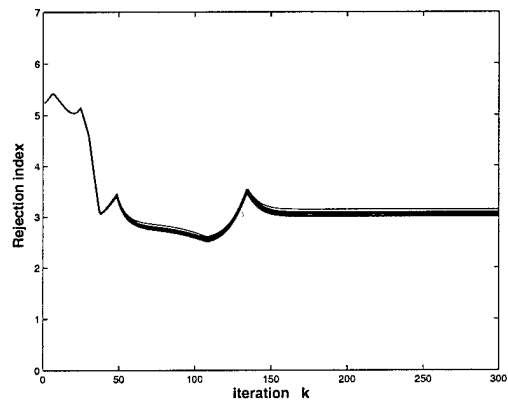
(a) The estimating function (41)



(b) The estimating function (40)



(c) The estimating function (38) with $\beta = 0.01$



(d) The estimating function (39)

Figure 21: Rejection indices corresponding to different estimating functions.

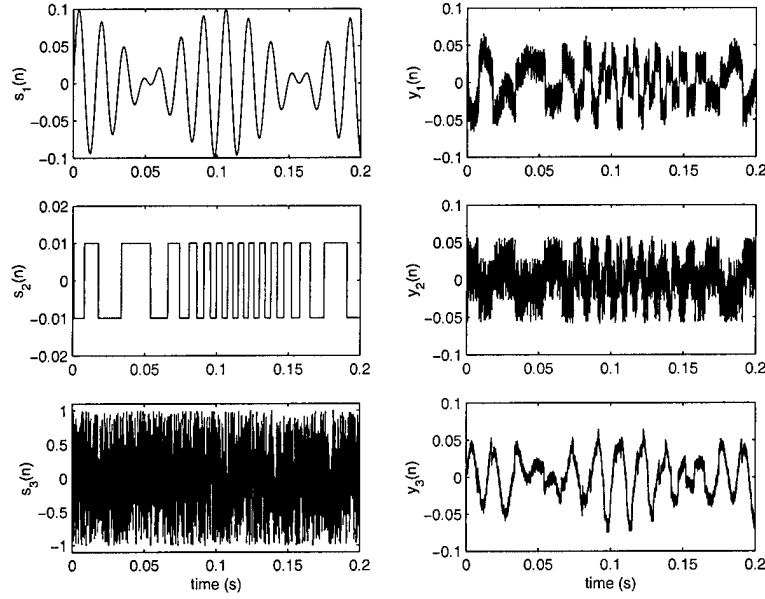


Figure 22: Three actual sources used (left column) and their estimates (right column) by algorithm (36) and estimating function (39).

II) containing two targets using the estimating functions (37)-(40). The corresponding CCM's for these functions are as follows, respectively

$$\begin{aligned}
 2 \text{ sensors} \rightarrow CCM_{13} &= \begin{bmatrix} 1.000 & -0.040 \\ & 1.000 \end{bmatrix}, & 3 \text{ sensors} \rightarrow CCM_{13} &= \begin{bmatrix} 1.000 & 0.010 & 0.167 \\ & 1.000 & -0.009 \\ & & 1.000 \end{bmatrix} \\
 2 \text{ sensors} \rightarrow CCM_{14} &= \begin{bmatrix} 1.000 & -0.535 \\ & 1.000 \end{bmatrix}, & 3 \text{ sensors} \rightarrow CCM_{14} &= \begin{bmatrix} 1.000 & -0.598 & -0.467 \\ & 1.000 & 0.471 \\ & & 1.000 \end{bmatrix} \\
 2 \text{ sensors} \rightarrow CCM_{15} &= \begin{bmatrix} 1.000 & 0.001 \\ & 1.000 \end{bmatrix}, & 3 \text{ sensors} \rightarrow CCM_{15} &= \begin{bmatrix} 1.000 & 0.0005 & 0.0004 \\ & 1.000 & 0.0005 \\ & & 1.000 \end{bmatrix} \\
 2 \text{ sensors} \rightarrow CCM_{16} &= \begin{bmatrix} 1.000 & -0.572 \\ & 1.000 \end{bmatrix}, & 3 \text{ sensors} \rightarrow CCM_{16} &= \begin{bmatrix} 1.000 & -0.613 & -0.504 \\ & 1.000 & 0.491 \\ & & 1.000 \end{bmatrix}
 \end{aligned}$$

The results for the estimating function (41) are not shown as the algorithm did not converge for this choice on the real SAFE II data. This could be due to low number of snapshots used during the training process. From the above results it can be observed that the algorithm using functions (37) and (39) is capable of identifying and separating the two targets. However, the performance is not as satisfactory using functions (38) and (40). These observations follow by noting the very small off-diagonal elements for the 2 sensors cases for (37) and (39), and relatively significant off-diagonal elements for the cases (38) and (40). On the other hand, separating the array signals into three distinct signals results in a relatively large off-diagonal elements in the 3 sensor case as seen from CCM matrices for the functions (37), (38), and (40). This may be viewed as an indication that the actual number of sources is two in these cases as opposed to three. However, this conclusion is weakened by noting that the CCM in case of 3 sensors for (39) suggests the presence of three targets contrary to the reality in this case. This clearly indicates that

further research is warranted to resolve this ambiguity in determining the true number of targets in the collected sensory data.

The results tested for the actual data for Node 1 (newr1536) from SAFE II containing five targets and using two to five sensors are shown in Figures 29 to 32, respectively. The CCM's for various choices of sensors and using the estimating function (38) are shown below. It can be observed that the algorithm is capable of identifying and perhaps separating the targets as indicated by the very small off-diagonal terms in the CCM's. The results for the other functions are not as good as these and in some cases the weights did not converge at all.

$$\begin{aligned}
 2 \text{ sensors} \rightarrow CCM_{14} &= \begin{bmatrix} 1.000 & -0.000 \\ & 1.000 \end{bmatrix}, \quad 3 \text{ sensors} \rightarrow CCM_{14} = \begin{bmatrix} 1.000 & 0.001 & -0.006 \\ & 1.000 & 0.008 \\ & & 1.000 \end{bmatrix}, \\
 4 \text{ sensors} \rightarrow CCM_{14} &= \begin{bmatrix} 1.000 & -0.015 & -0.006 & 0.001 \\ & 1.000 & 0.021 & -0.005 \\ & & 1.000 & 0.007 \\ & & & 1.000 \end{bmatrix}, \\
 5 \text{ sensors} \rightarrow CCM_{14} &= \begin{bmatrix} 1.000 & -0.014 & 0.004 & 0.013 & -0.005 \\ & 1.000 & -0.006 & 0.002 & 0.027 \\ & & 1.000 & -0.096 & 0.050 \\ & & & 1.000 & -0.001 \\ & & & & 1.000 \end{bmatrix}.
 \end{aligned}$$

Several interesting observations can be made from these preliminary results. These are given below.

1. When the number of independent sources, P , is larger than the number of sensors, L , i.e. $P > L$, the IICA algorithm under-estimates the number of sources and identifies a maximum of L sources. This is due to the fact that the algorithm may treat a particular grouping or lumping of independent sources as a single independent source. On the other hand, when $L > P$, the algorithm over-estimates the number of sources. In this case, in addition to the independent sources, linear combination of them may also be identified as potential sources. It is indeed possible to narrow down the choices by performing some type of postprocessing on the extracted sources. This is one aspect that would require further research and modifications for a successful implementation of the algorithm.
2. An objective performance evaluation of the results of this algorithm seems to be rather difficult, since the outcome of IICA is *highly* affected by several factors including: nature of the sources, choice of the estimating function used, and actual mixing situation at the array, i.e., instantaneous mixing or convolutive mixing. One of our objectives and goals for future (Phase II) is to conduct further and more thorough investigation of this scheme and provide a comprehensive benchmark with the other source separation and DOA estimation algorithms. Of great importance to this study is to determine how this method performs when scenarios with tight target formations are encountered.

6.4 Fast ICA Algorithm

In this part of the report we investigate, develop and test a Fast ICA-based algorithm [66]. Fast ICA algorithm is an algorithm that attempts to maximize the so-called contrast function (neg-entropy) required to implement ICA [66]. Below we follow a step-by-step process for developing and implementing this algorithm. This algorithm is then applied the synthetically generated data set as well as to the real SAFE II sets corresponding to series 503, 510 and 537 scenarios. Interesting results are obtained. Also other interesting research venues are identified and indicated. One aspect that we intend to investigate in Phase II will be the development of data association and fusion schemes that attempt to reduce the ambiguities that may arise from the application of Fast ICA algorithm to different nodes in the array configuration.

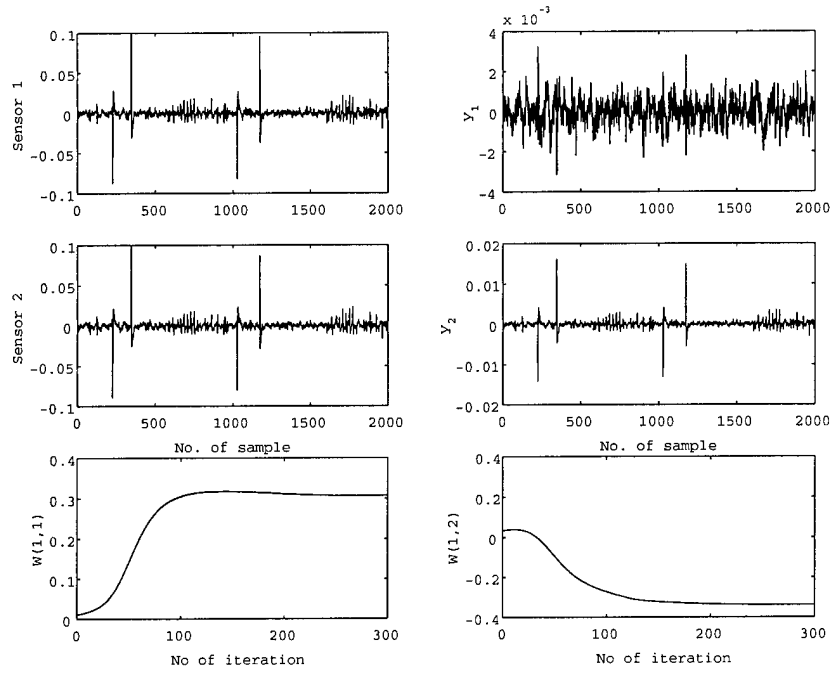


Figure 23: Two sensor array signals and two demixer outputs case using estimating function (37) for SAFE II real data newr1502.

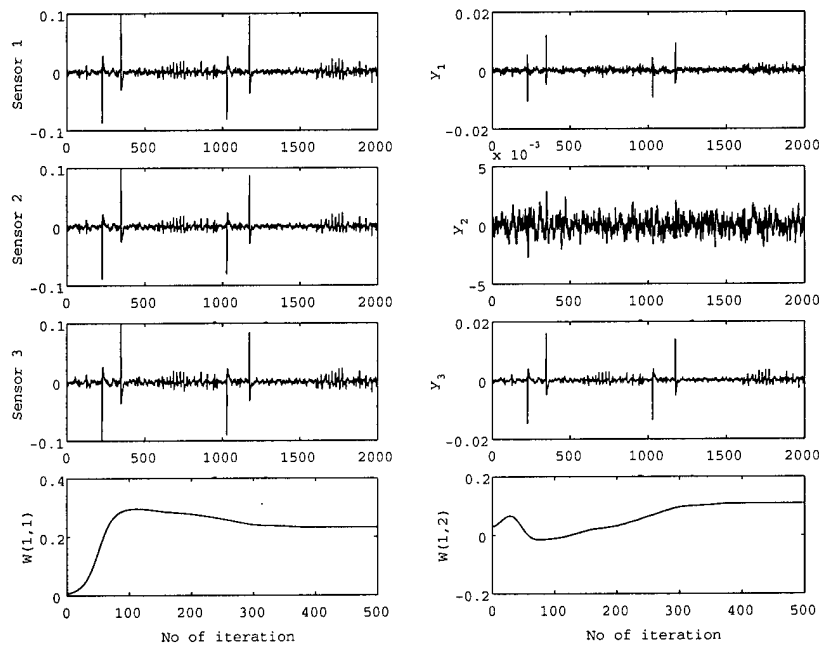


Figure 24: Three sensor array signals and three demixer outputs case using estimating function (37) for SAFE II real data newr1502.

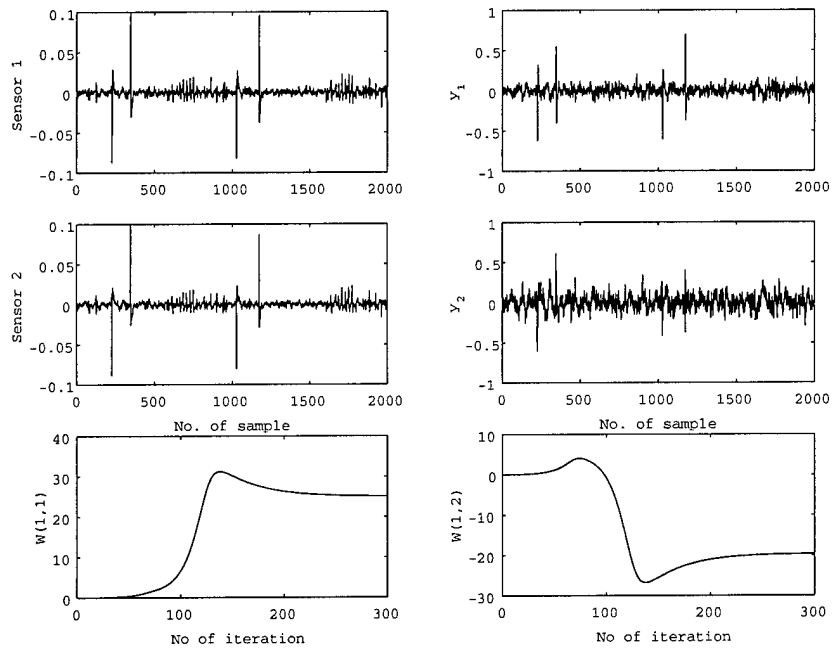


Figure 25: Two sensor array signals and two demixer outputs case using estimating function (38) for SAFE II real data newr1502.

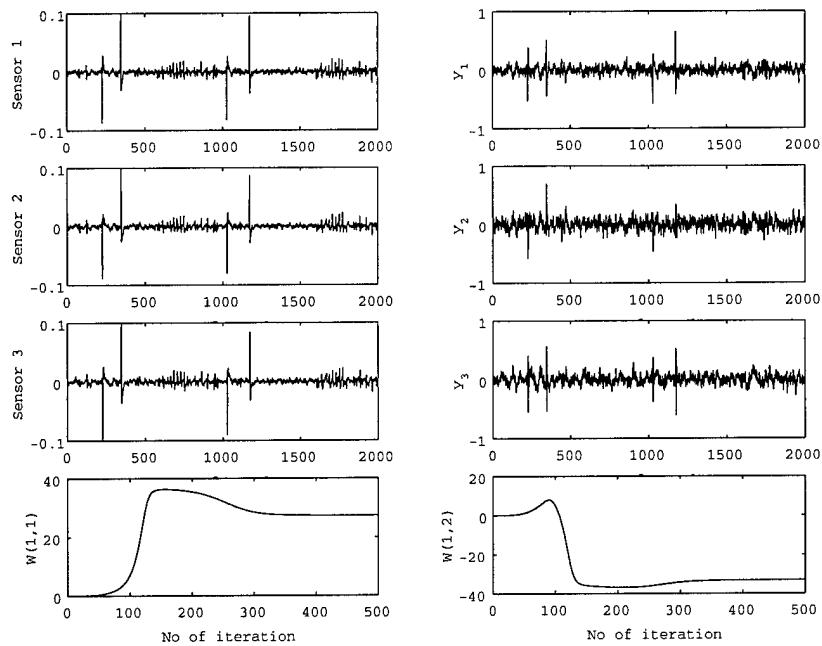


Figure 26: Three sensor array signals and three demixer outputs case using estimating function (38) for SAFE II real data newr1502.

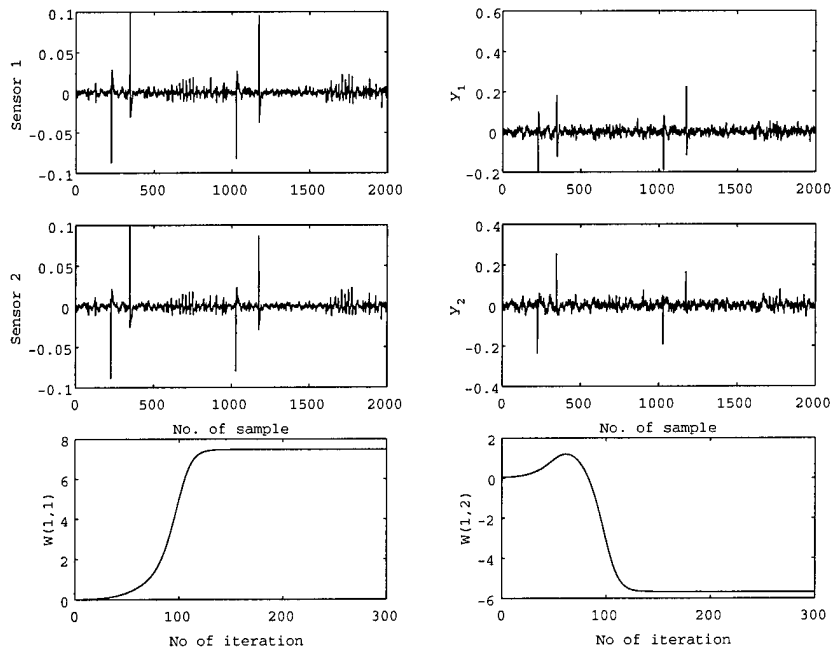


Figure 27: Two sensor array signals and two demixer outputs case using estimating function (39) for SAFE II real data newr1502.

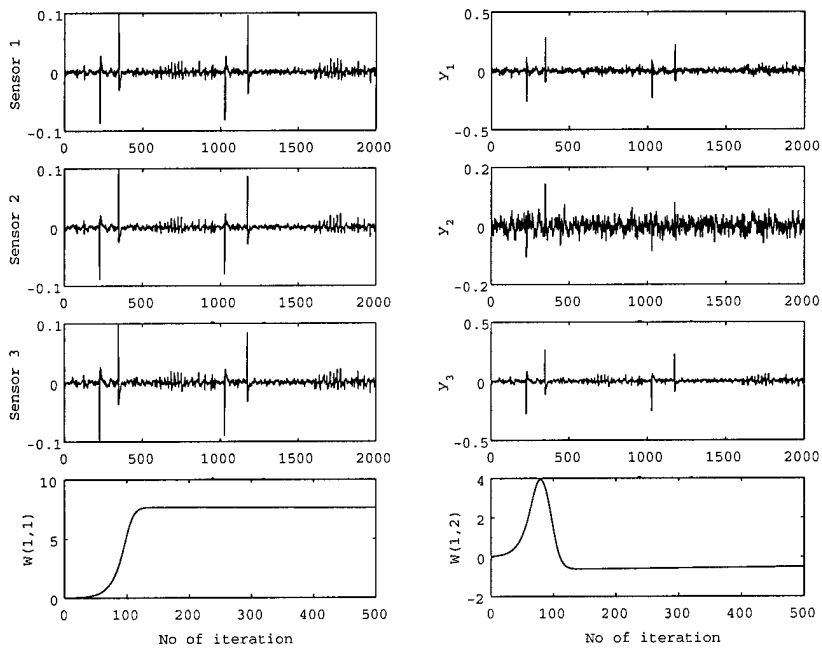


Figure 28: Three sensor array signals and three demixer outputs case using estimating function (39) for SAFE II real data newr1502.

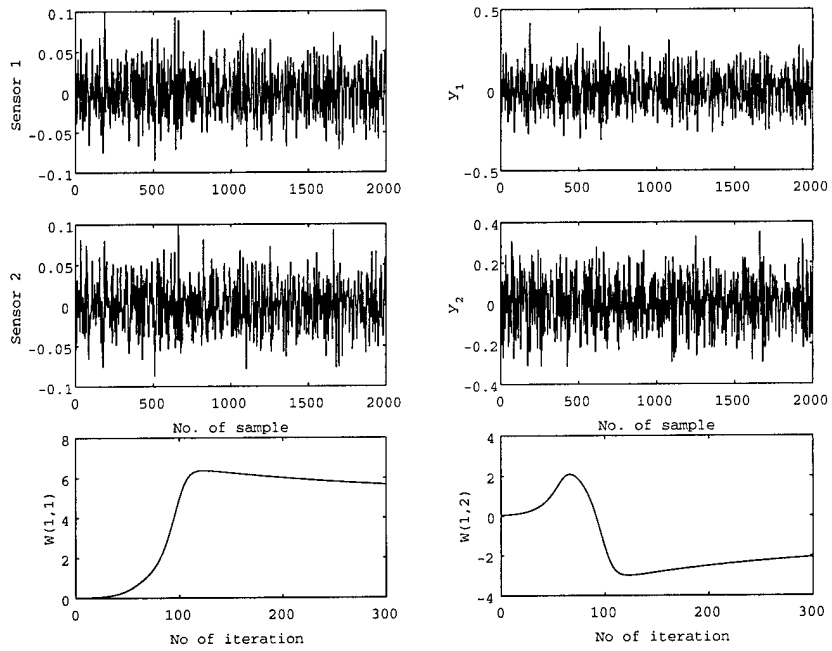


Figure 29: Two sensor array signals and two demixer outputs case using estimating function (38) for SAFE II real data newr1536.

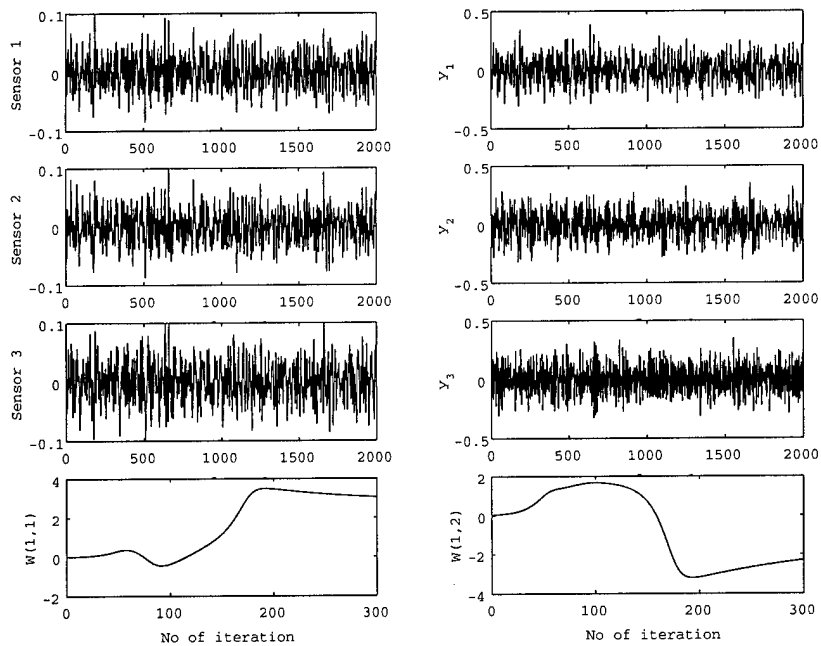


Figure 30: Three sensor array signals and three demixer outputs case using estimating function (38) for SAFE II real data newr1536.

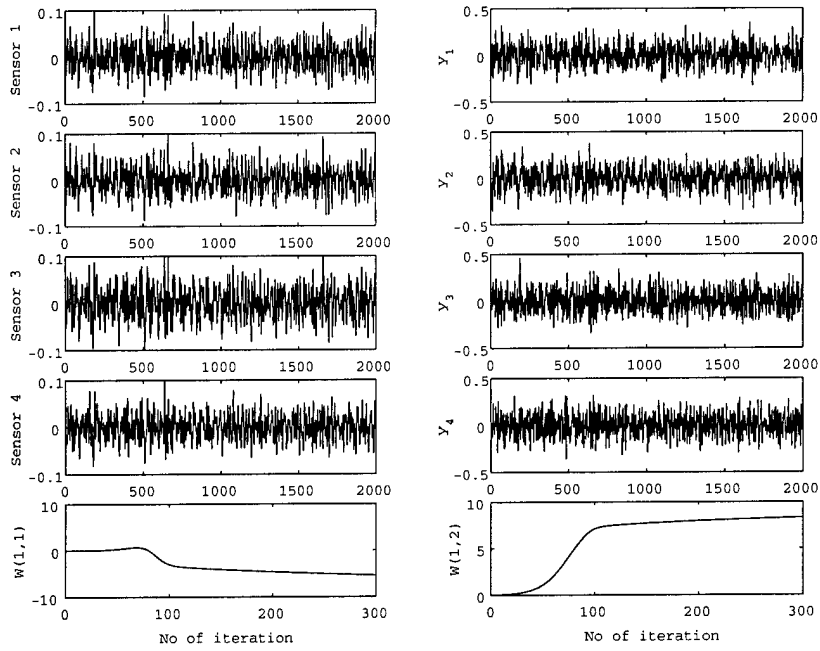


Figure 31: Four sensor array signals and Four demixer outputs case using estimating function (38) for SAFE II real data newr1536.

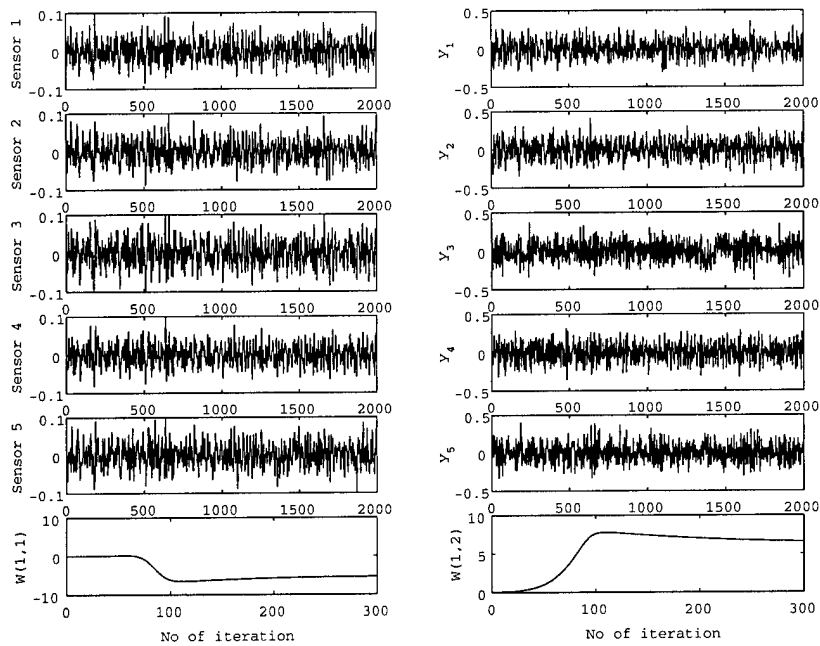


Figure 32: Five sensor array signals and Five demixer outputs case using estimating function (38) for SAFE II real data newr1536.

As mentioned before, the estimation of data model of ICA is usually performed by formulating an objective function and then minimizing or maximizing it. Often such a function is called a contrast function. An ICA method can be expressed as the combination of an objective function and its optimization algorithm. The statistical properties of the ICA method depend on the choice of the objective function, and the algorithmic properties depend on the optimization algorithm. These two classes of properties are independent in the sense that different optimization methods can be used to optimize a single objective function, and conversely a single optimization method may be used to optimize different objective functions [61]. The key to estimating the ICA model is non-Gaussian property. Two classes of contrast functions are available to estimate the data model in ICA, which are described below.

A: Multi-Unit Contrast Functions

Using these type of contrast functions the whole data model of ICA is estimated in one shot.

- *Likelihood and network entropy*: The likelihood in the noise-free ICA model is formulated and then the model is estimated by a maximum likelihood (ML) method [67]. From a neural network viewpoint this is equivalent to maximizing the output entropy (information flow) of a neural network with nonlinear outputs. Often this is termed as “infomax” [57],[60].
- *Mutual information and Kullback-Leibler divergence*: The mutual information is a natural measure of the dependence between random variables. It is always non-negative, and zero if and only if the variables are statistically independent. Finding a transform that minimizes the mutual information between the components s_i is a very natural way of estimating the ICA model [56].

Among other contrast functions considered in the literature are nonlinear cross correlation by Jutten and Herault [68], nonlinear PCA criteria [69], higher-order cumulant tensors [70] and weighted covariance matrix [71].

B: One-Unit Contrast Functions

These functions estimate single component at a time instead of the whole data model. This approach shows clearly the connection to neural networks and prior knowledge of the number of independent components is not needed. After estimating one independent component, one can use simple decorrelation to find a different independent component, since the independent components are by definition uncorrelated.

Negentropy: A most natural information-theoretic one-unit contrast function is negentropy. The independent components correspond to directions in which the differential entropy of $\mathbf{w}^T \mathbf{x}$ is minimized. However, a modification has to be made, since differential entropy is not invariant for scale transformations. In order to obtain a linearly invariant version of entropy, the negentropy J is defined as

$$J(\mathbf{y}) = H(\mathbf{y}_{gauss}) - H(\mathbf{y}) \quad (46)$$

where \mathbf{y}_{gauss} is a Gaussian random vector of the same covariance matrix as \mathbf{y} and H denotes the entropy. Negentropy is always negative, and zero if and only if \mathbf{y} has a Gaussian distribution [56]. The usefulness of this definition is prominent when mutual information is expressed using negentropy as

$$I(y_1, \dots, y_P) = J(\mathbf{y}) - \sum_i J(y_i) + \frac{1}{2} \log \frac{\prod C_{ii}^y}{\det C^y} \quad (47)$$

where C^y is the covariance matrix of \mathbf{y} , and the C_{ii}^y are its diagonal elements. If the y_i 's are uncorrelated, the third term is 0, and hence we get

$$I = J(\mathbf{y}) - \sum_i J(y_i) \quad (48)$$

As negentropy is invariant for linear transformation, it is obvious that finding maximum negentropy directions, i.e., directions where the elements of the sum $J(y_i)$ are maximized, is equivalent to finding a representation in which mutual information is minimized [56]. The estimation of negentropy is difficult, and therefore this contrast function remains a topic for theoretical investigation. Negentropy can be approximated by higher-order cumulants or by more accurate methods as shown below.

As in the multi-unit case, negentropy can be approximated by higher-order cumulants such as [72]:

$$J(\mathbf{y}) \approx \frac{1}{12}\kappa_3(\mathbf{y})^2 + \frac{1}{48}\kappa_4(\mathbf{y})^2 \quad (49)$$

where κ_i is the i -th order cumulant of \mathbf{y} . However, the validity of such approximation may be rather limited. In [72], it was argued that cumulant-based approximations of negentropy are inaccurate, and in many cases too sensitive to outliers. The new approximations are based on the maximum-entropy principle. In general, one may obtain an approximation of the form $J(\mathbf{y}) \approx \sum_{i=1}^q c_i [E\{G_i(\mathbf{y})\} - E\{G_i(\nu)\}]^2$ where c_i 's are some positive constants, ν is a Gaussian variable of zero mean and unit variance, and G_i 's are practically any non-quadratic functions. In the case where one uses only one function G , the approximation becomes of the form:

$$J(\mathbf{y}) \approx c[E\{G(\mathbf{y})\} - E\{G(\nu)\}]^2 \quad (50)$$

The result is a generalization of the cumulant-based approximation of (51) where \mathbf{y} is symmetric. For instance, using $G(\mathbf{y}) = \mathbf{y}^4$, one then obtains (51) from (52). This one-unit contrast function will be used later for the development of Fast ICA algorithm.

6.4.1 Preprocessing for ICA

Before applying an ICA algorithm on the observed data, it is usually very useful to do some preprocessing. The steps involved are given below.

1. *Centering*: The mean vector of \mathbf{x} , denoted by $\mathbf{m} = E[\mathbf{x}]$, is subtracted from \mathbf{x} to make it a zero-mean variable. This preprocessing is done to simplify the ICA algorithm. After estimating the mixing matrix \mathbf{A} with centered data, the estimation can be completed by adding the mean vector of \mathbf{s} back to the centered estimates of \mathbf{s} . The mean vector of \mathbf{s} is given by $\mathbf{A}^{-1}\mathbf{m}$.
2. *Whitening*: After centering the observed vector $\tilde{\mathbf{x}}$, it is transformed linearly so that the new vector is white i.e., its components are uncorrelated and their variances equal to unity. In other words, the covariance matrix of $\tilde{\mathbf{x}}$ equals the identity matrix:

$$E[\tilde{\mathbf{y}}\tilde{\mathbf{y}}^T] = I \quad (51)$$

The popular method of whitening is to use the eigenvalue decomposition (EVD) of the covariance matrix $E[\tilde{\mathbf{x}}\tilde{\mathbf{x}}^T] = \mathbf{H}\mathbf{D}\mathbf{H}^T$, where \mathbf{H} is the orthogonal matrix of eigenvectors of $E[\mathbf{x}\mathbf{x}^T]$ and \mathbf{D} is the diagonal matrix of its eigenvalues, $\mathbf{D} = \text{Diag}(d_1, \dots, d_P)$. Now

$$\tilde{\mathbf{x}} = \mathbf{E}\mathbf{H}^{-\frac{1}{2}}\mathbf{E}^T\mathbf{x} \quad (52)$$

Whitening reduces the number of parameters to be estimated and it transforms the mixing matrix into a new one, $\tilde{\mathbf{A}}$. From equations (34) and (52)

$$\tilde{\mathbf{x}} = \mathbf{E}\mathbf{H}^{-\frac{1}{2}}\mathbf{E}^T\mathbf{A}\mathbf{s} = \tilde{\mathbf{A}}\mathbf{s} \quad (53)$$

6.4.2 Fast ICA for One Unit

By “unit” we imply an artificial neuron having a weight vector \mathbf{w} where the neuron is allowed to update its weight through a learning rule. The Fast ICA learning rule finds a direction, i.e., a unit vector \mathbf{w} such that the projection $\mathbf{w}^T \mathbf{x}$ maximizes nongaussianity. Nongaussianity here is measured by the approximation of negentropy $J(\mathbf{w}^T \mathbf{x})$ given as $J(\mathbf{y}) = c\{E[G(\mathbf{y})] - E[G(\nu)]\}^2$. G is practically any non-quadratic function, c is any constant. The algorithm is now based on a fixed-point iterative scheme for finding a maximum of the nongaussianity of $\mathbf{w}^T \mathbf{x}$. Let g denote the derivative of the nonquadratic function G used above. The basic form of the Fast ICA algorithm can be expressed as follows [66]:

1. Choose an initial (e.g. random) weight vector $\mathbf{w}(0)$,
2. Define $\mathbf{w}^+ = E[\mathbf{x}g(\mathbf{w}^T \mathbf{x})] - E[\mathbf{x}g(\mathbf{w}^T \mathbf{x})]\mathbf{w}$, and
3. Let $\mathbf{w} = \mathbf{w}^+ / \|\mathbf{w}^+\|$, denote the normalized \mathbf{w}^+
4. If there is no convergence, then go back to step 2.

Here by convergence we imply that the old and the new values of \mathbf{w} point in the same direction, i.e. their dot-product is (or almost) equal to 1. In the derivation of the Fast ICA, first the maxima of the approximation of the negentropy of $\mathbf{w}^T \mathbf{x}$ are obtained at certain optima of $E[G(\mathbf{w}^T \mathbf{x})]$. According to the Kuhn-Tucker conditions, the optima of $E[G(\mathbf{w}^T \mathbf{x})]$ under the constraint $E[(\mathbf{w}^T \mathbf{x})^2] = \|\mathbf{w}\|^2 = 1$ are obtained at points where

$$E[\mathbf{x}g(\mathbf{w}^T \mathbf{x})] - \beta \mathbf{w} = 0 \quad (54)$$

Denoting the function on the left side of (54) by F , its Jacobian matrix becomes

$$JF(\mathbf{w}) = E[\mathbf{x}\mathbf{x}^T g'(\mathbf{w}^T \mathbf{x})] - \beta I \quad (55)$$

Since the data is whitened, a reasonable approximation seems to be

$$E[\mathbf{x}\mathbf{x}^T g'(\mathbf{w}^T \mathbf{x})] = E[\mathbf{x}\mathbf{x}^T]E[g'(\mathbf{w}^T \mathbf{x})] = E[g'(\mathbf{w}^T \mathbf{x})]I \quad (56)$$

Thus, the Jacobian matrix becomes diagonal and can easily be inverted. The following Newton's iteration is approximated:

$$\mathbf{w}^+ = \mathbf{w} - |E[\mathbf{x}g(\mathbf{w}^T \mathbf{x})] - \beta \mathbf{w}| / |E[g'(\mathbf{w}^T \mathbf{x})] - \beta| \quad (57)$$

This again can be simplified by multiplying both sides of (57) by $\beta - E[g'(\mathbf{w}^T \mathbf{x})]$. This gives after some algebraic manipulation, the Fast ICA iteration. In practice, the expectations in Fast ICA must be replaced by their estimates. The natural estimates are clearly the corresponding sample means. The averages can be estimated using a smaller sample, whose size may have a considerable effect on the accuracy of the final estimates. The sample points should be chosen separately at every iteration. If the convergence is not satisfactory, an increment of the sample size may be required.

6.4.3 Fast ICA for Several Units

To estimate several independent components the one-unit Fast ICA need to be run using several units with weight vectors $\mathbf{w}_1, \dots, \mathbf{w}_P$. To prevent different vectors from converging to the same maxima the outputs $\mathbf{w}_1^T \mathbf{x}, \dots, \mathbf{w}_P^T \mathbf{x}$ must be decorrelated after every iteration. A simple way of achieving decorrelation is a deflation scheme based on a Gram-Schmidt like decorrelation. After estimating q independent components, or q vectors $\mathbf{w}_1, \dots, \mathbf{w}_q$, the one-unit fixed-point algorithm is run for \mathbf{w}_{q+1} and after every iteration step the "projections" $\mathbf{w}_{q+1}^T \mathbf{w}_j \mathbf{w}_j$, $j = 1, \dots, q$ of the previously estimated q vectors are subtracted from \mathbf{w}_{q+1} , and the result is then normalized as follows:

1. Define $\mathbf{w}_{q+1} = \mathbf{w}_{q+1} - \sum_{j=1}^q \mathbf{w}_{q+1}^T \mathbf{w}_j \mathbf{C} \mathbf{w}_j$, and then normalize it according to
2. $\mathbf{w}_{q+1} = \mathbf{w}_{q+1} / [\mathbf{w}_{q+1}^T \mathbf{C} \mathbf{w}_{q+1}]^{1/2}$

where \mathbf{C} is the Covariance of the data. Since the data is sphered, therefore \mathbf{C} is replaced by an identity matrix \mathbf{I} .

Properties of Fast ICA Algorithm

The Fast ICA algorithm and its contrast functions have a number of desirable properties:

- The convergence is cubic or at least quadratic. This is in contrast to other ICA-based schemes that are derived based on stochastic gradient descent methods, where the convergence is only linear. This means a very fast convergence.
- The algorithm is easy to use as there is no step size to choose.
- It finds directly independent components of any non-Gaussian distribution using any nonlinearity.
- The performance of the method can be optimized by choosing a suitable nonlinearity.
- The independent components can be estimated one-by-one. This is useful in exploratory data analysis, and decreases the computational load of the method in cases where only some of the independent components need to be estimated.
- The Fast ICA algorithm enjoys many advantages of neural networks algorithms such as: parallel and distributed processing, simplicity, and requiring little memory space.

6.5 Simulation Results of Fast ICA on Synthesized Data

The ICA is performed for each window of 1 second duration. We have generated three cases of Abreast, Single-file and Staggered target formations. In all these cases the radius of the array was 4 ft. For the Abreast case, the two targets are originally at (-300m,-300m) and (-300m,-350m). For the Single-file case, the two targets are originally at (-300m,100m) and (-250m,100m). In Staggered formation there are three targets at initial positions (-300m,100m), (-250m,100m), (-275m,150m). In all these cases, the targets move to East with a constant speed of 25m/s. The signal-to-noise ratio (SNR) was 10db for these cases. The results for these three cases are described in details below.

- **Single-file case:** The ground truth plot associated with the two targets is shown in Figure 33. The set of the principal components (PC's) based on the eigenvalue decomposition algorithm for the "window" index 5 are also shown in this figure. In all the figures shown below the left column depicts the raw data from the five sensors, the middle column depicts the centered data as discussed in the preprocessing Section 6.4.1, and the right column represents the independent components that are estimated by the Fast ICA algorithm. The ICA is performed in two stages where in the first stage the algorithm is allowed to estimate all the independent components available in the data set. In

the second stage the algorithm is imposed to estimate two or three independent components based on the dominant PCA singular values as shown in Figure 33. Figure 34 shows the ICA of the data set for the window index 5 with estimation of five components. It can be observed from this figure that there are clearly two source signals and the other three are noise sources. In the next set of simulations instead of estimating five components, the Fast ICA algorithm is asked to generate only two components. These results are **also** shown in Figure 34 due to space limitations. Specifically, the 1st and the 2nd signals from the top in the right column is the response of the Fast ICA that is limited to generating *two* independent components. This should confirm clearly the presence of only two targets.

- **Abreast case:** The ground truth plot associated with the two targets is shown in Figure 35. The set of the principal components based on the eigenvalue decomposition algorithm for the the window index 14 are also shown in this figure. Figure 36 shows the ICA of the data set for the window index 14 with estimation of five components. It can be observed from these figures that there are clearly two source signals and the other three are noise sources. In the next set of simulations instead of estimating five components the Fast ICA algorithm is asked to generate only two components. These results are **also** shown in Figure 36 (the 4th and the 5th independent signals in the right column) which should again confirm the presence of only two targets.

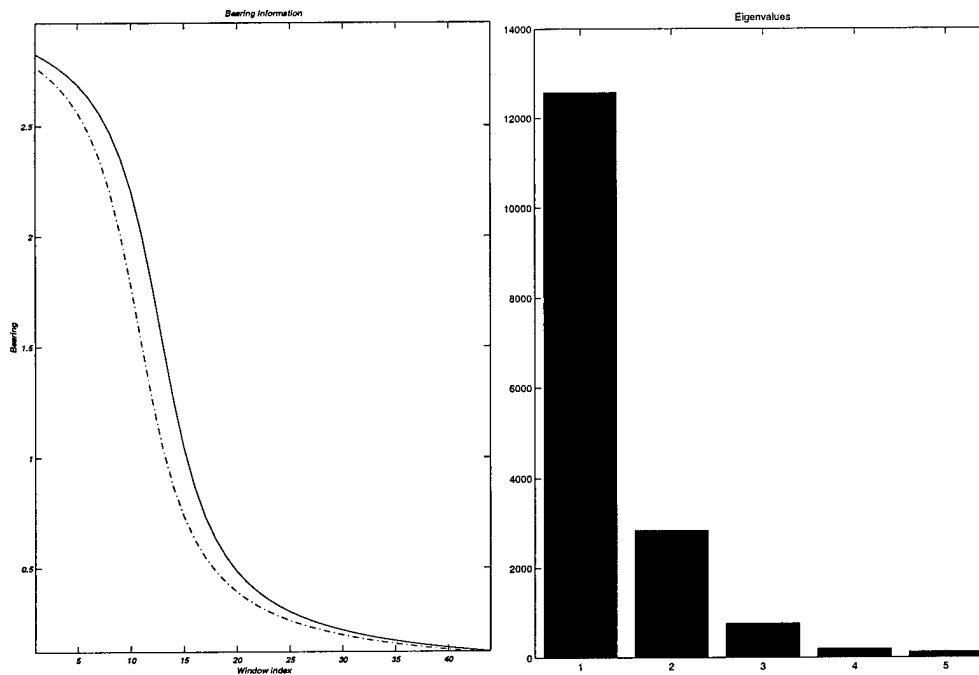


Figure 33: Ground truth and Principal components (PCA) based on Eigenvalue Decomposition (EVD) algorithm for the Single-File formation case and for the window index 5.

- **Staggered case:** The above results are now repeated for the Staggered synthetic data. The ground truth plot associated with the three targets is shown in Figure 37. The set of the principal components based on the eigenvalue decomposition algorithm for the window index 40 are also shown in this figure. Figures 38 show the ICA of the data set for the window index 40 with estimation of five components. It can be observed from this figure that there are clearly three source signals and

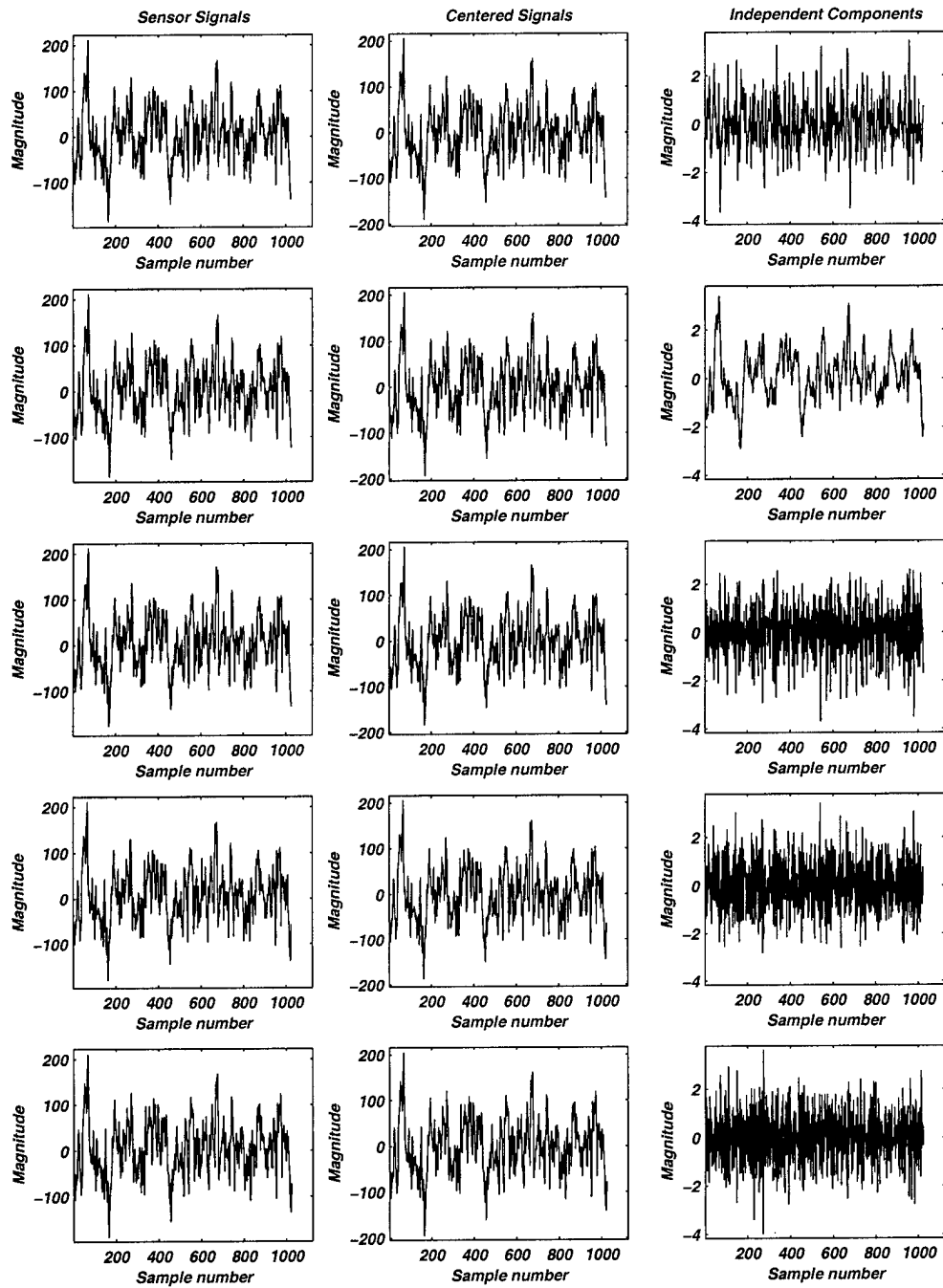


Figure 34: Fast ICA algorithm applied to Single-File formation data. The right column indicates the independent components using five components for window index 5. Limiting the algorithm to *two* independent components results in the 1st and 2nd signals from the top right column as the independent components.

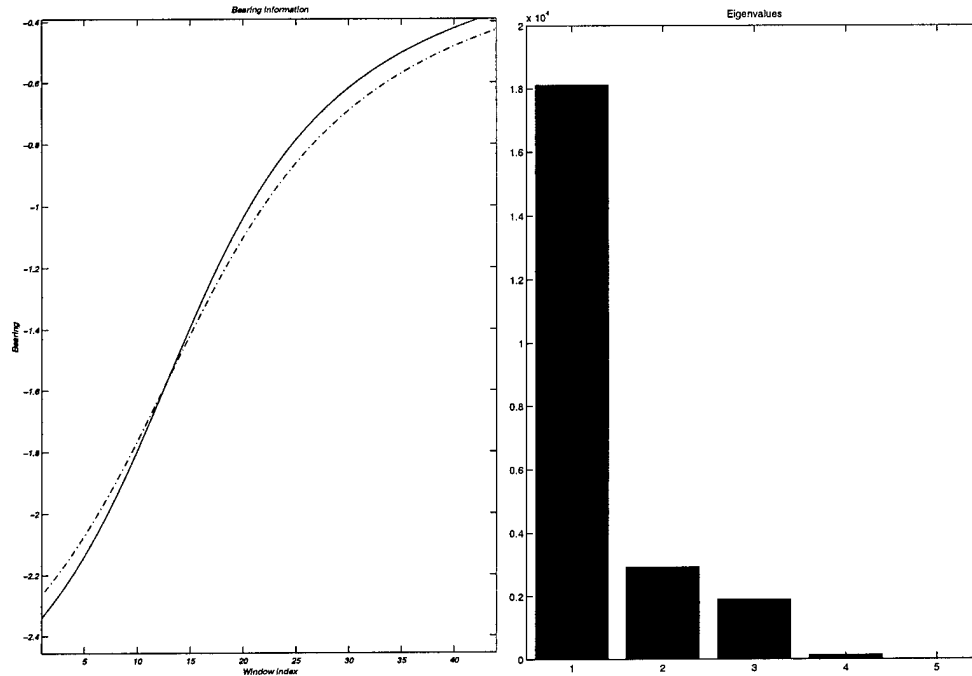


Figure 35: Ground truth and Principal components (PCA) based on Eigenvalue Decomposition (EVD) algorithm for the Abreast formation case and the window index 14.

the other two are noise sources. In the next set of simulations instead of estimating five components the Fast ICA algorithm is asked to generate only three components. These results are also shown in Figure 38 (the 2nd, 3rd and the 5th independent components in the right column) which should again confirm the presence of only three targets.

6.6 Simulation Results of Fast ICA on SAFE II Data

The ICA is performed for each window of 1 second duration and for each three (3) nodes consisting of five (5) sensors. The first data set (503 series) chosen here has two independent sources. The ground truth plots associated with the three nodes are shown in Figure 39. As in the previous set of results, the horizontal axes in this figure represents the "window" index. The fast ICA is performed on this data set in two stages where in the first stage the algorithm is allowed to estimate all the independent components available in the data set. In the second stage the algorithm is imposed to estimate the independent components based on the *dominant* PCA singular values (see Figure 40). In all the figures shown below related to the Fast ICA independent components the left column depicts the raw data from the five sensors, the middle column depicts the centered data as discussed in the preprocessing Section 6.4.1, and the right column represents the independent components that are estimated. Figure 41 shows the ICA of data set for node 1 with estimation of five components, where our goal was to initially estimate five components. From this figure the presence of two source signals and three noisy signals is rather evident. To substantiate this, the Fast ICA algorithm is run by requiring it to generate *only* two independent components (source signals). The results are shown directly in Figure 41 (due to space limitations) corresponding to the 1st and the 3rd signals from the top in the right column subfigure, which demonstrates the independence of the two sources for this case. Very similar results for nodes 2 and 3 are also obtained, however due to space limitations are not shown here.

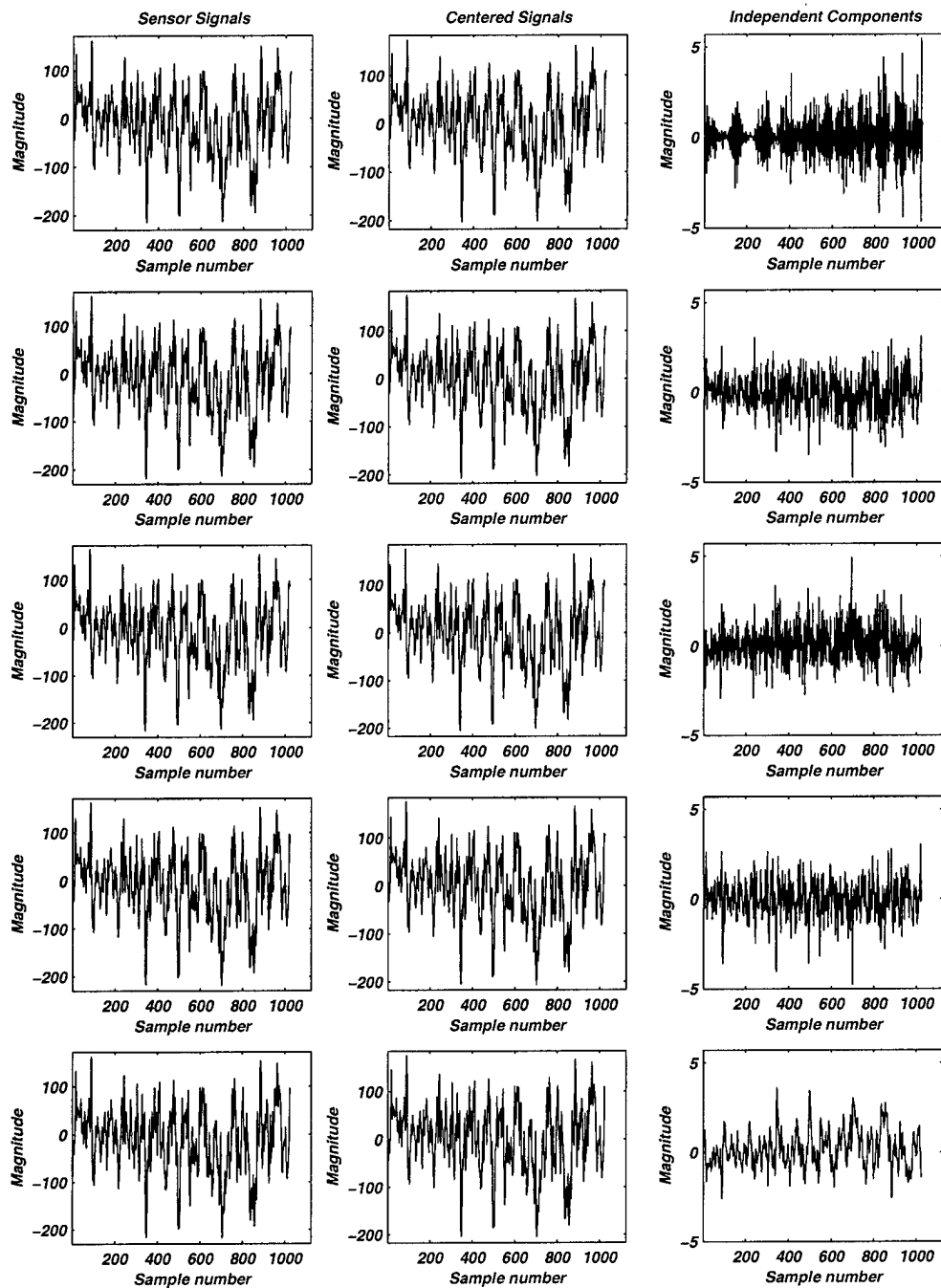


Figure 36: Fast ICA algorithm applied to Abreast formation data. The right column indicates the independent components using five components for window index 14. Limiting the algorithm to *two* independent components results in the 4th and 5th signals from the top right column as the independent components.

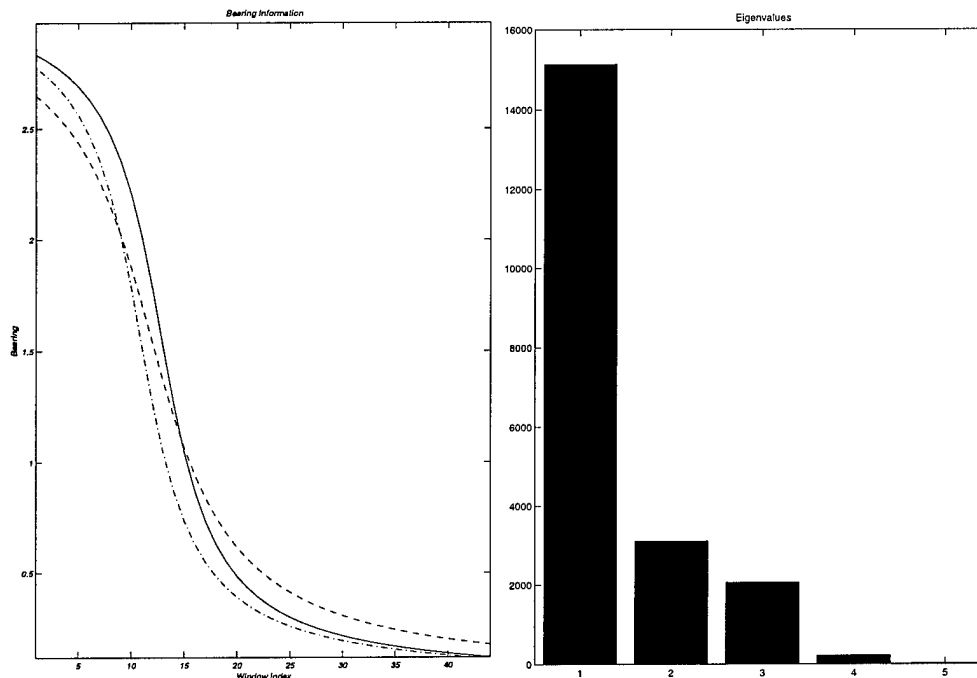


Figure 37: Ground truth and Principal components (PCA) based on Eigenvalue Decomposition (EVD) algorithm for the Staggered formation case and the window index 40.

Next, in Figures 42 we have repeated the above experiments by using the window index 130 for nodes 2 & 3 and index 90 for node 1 (refer to Figure 39 for detailed references). As can be seen from Figure 39 the above window indexes correspond to the situation where the moving target is at its closest proximity to the sensors. We are particularly interested in this situation in order to determine the performance of the Fast ICA algorithm with respect to its dependence to the distance of targets to sensors. It can be shown from Figure 42 that the dominance of two targets is more profoundly indicated for data newr2503 and newr3503 as compared to the results that we obtained in Figure 40 for data newr2503 to newr3503 for window indexes 20 and 30, respectively. These results translate further into better resolution of source signals from noisy signals as shown in Figure 43. The results using two independent sources demonstrate (the 1st and the 3rd signals from the top right column) the fact that there are indeed two source signals in this case. Very similar results are also obtained for node 2 but due to space limitations are not included here. However, the results for data newr1503 (node 1) for the window index 130 is inaccurate, as the Fast ICA algorithm is suggesting the presence of five independent sources. This unexpected behavior is an issue that we need to further investigate in Phase II.

The next data set chosen is from the 510 series where one distinctive source signal is present. Figure 44 depicts the ground truth plots corresponding to nodes 1 to 3. Based on the PCAs obtained associated with the window index 20 for all three nodes, one can infer for node 1 the presence of *two* sources, whereas nodes 2 & 3 confirm the presence of one source signal. To see this Figure 45 shows the separated signals for node 2 using five components. This figure shows components that are very similar to those obtained in node 3 (not shown due to space limitations). A careful analysis of the results for node 1 does suggest consistency with PCA results. In other words, there are possibly two independent source signals. However, this conclusion is not supported by the results seen from Figure 45 and those obtained from node 3 where there is an indication of only one independent source signal. Limiting the Fast ICA to generate only one

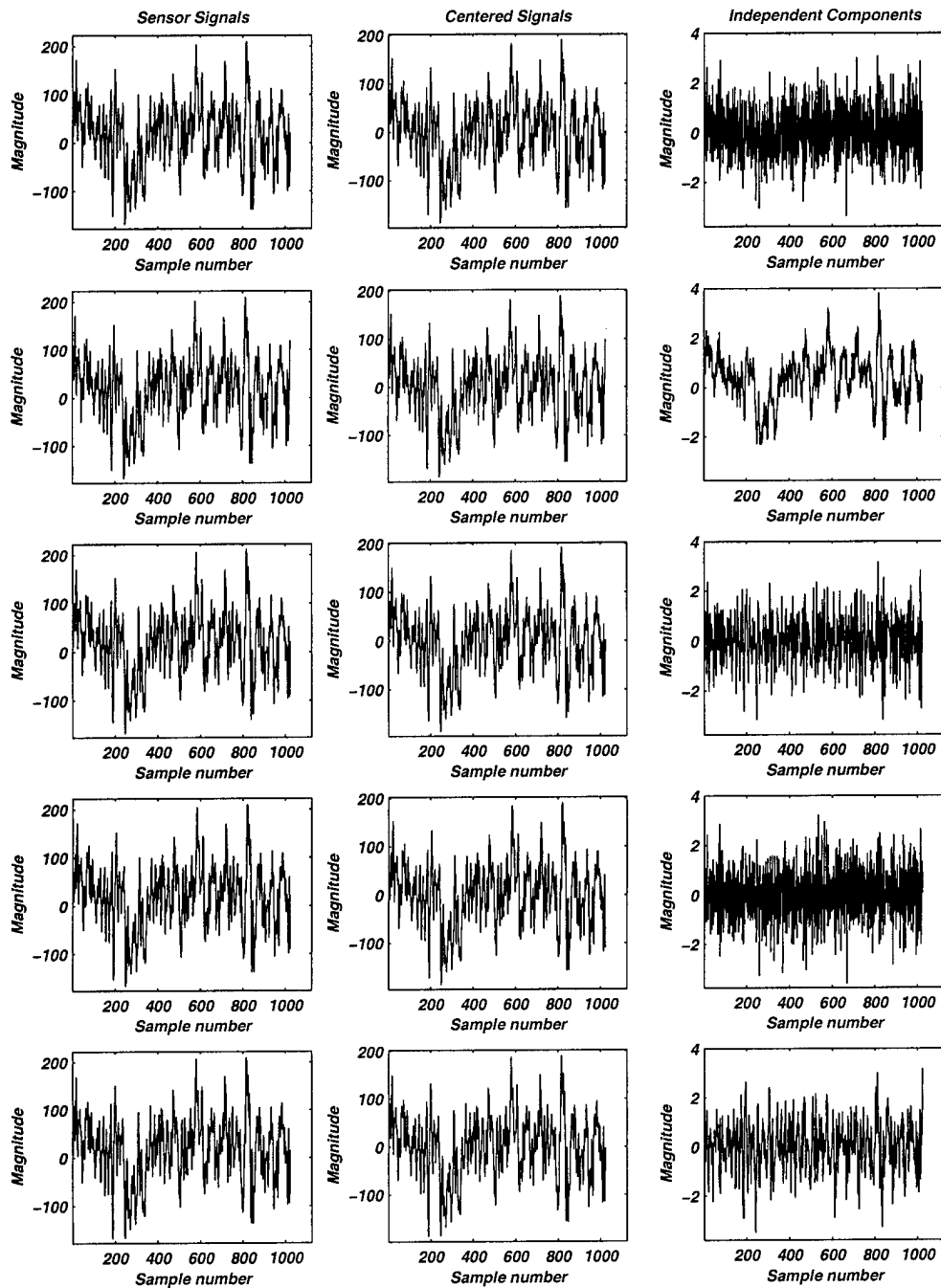


Figure 38: Fast ICA algorithm applied to Staggered formation data. The right column indicates the independent components using five components for window index 40. Limiting the algorithm to *three* independent components results in the 2^{nd} , 3^{rd} and the 5^{th} signals from the top right column as the independent components.

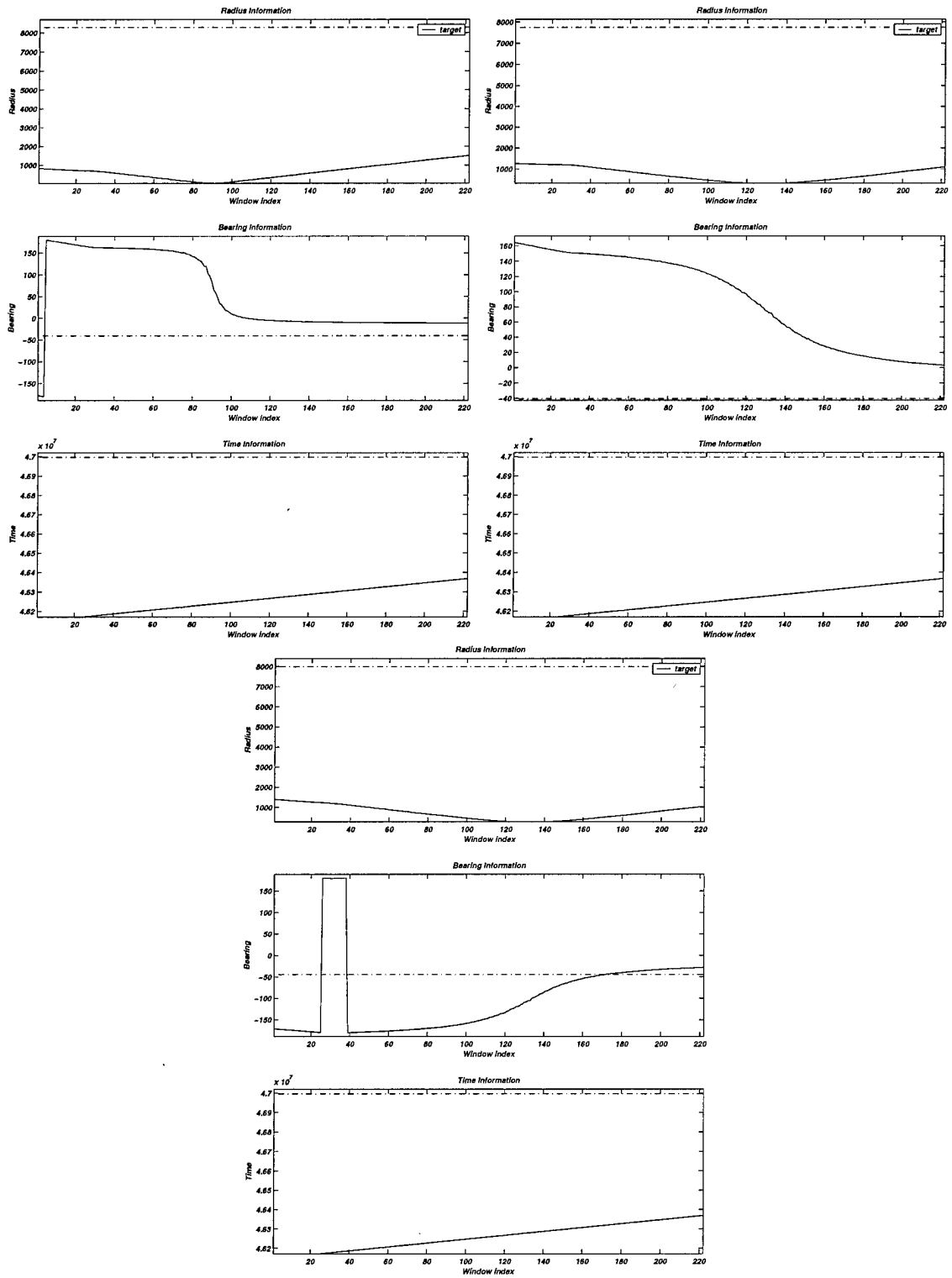


Figure 39: Ground truth diagrams for SAFE II real data newr1503 to newr3503.

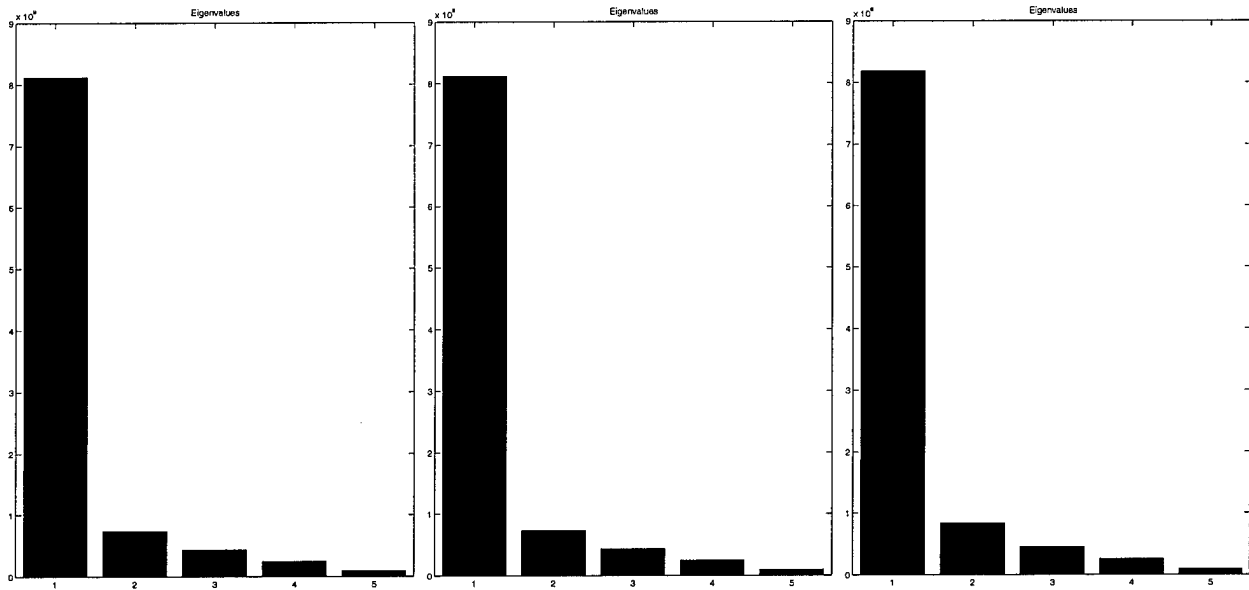


Figure 40: Principal components (PCA) based on Eigenvalue Decomposition (EVD) algorithm applied to SAFE II real data newr1503 to newr3503 for the window indexes 20, 20, and 30, respectively.

independent component results in the 4th signal from the top in the right column of Figure 45 as being the source signal.

The final data set chosen is from the 537 series where five distinctive source signals are present. Results in Figure 46 depicts the ground truth associated with nodes 1 to 3 and the definitions corresponding to the window indexes. Figure 47 depicts the PCA estimates for window index 125 for nodes 2 & 3 and index 100 for node 1. Although node 3 clearly indicates the presence of five dominant signals, this is to a lesser extent confirmed by node 2 and even to a lesser degree by node 1. Figures 48 depicts the five independent components that are generated by the Fast ICA algorithm for node 2, which does suggest the presence of only two source signals as opposed to five components. The reasons for this discrepancy and error will be investigated in more details in Phase II.

The next data set chosen from the 537 series are from the window index 200 for node 1 and index 250 for nodes 2 & 3. By plotting the PCA values in this case it can be seen (deleted due to space limitations) that nodes 1 & 3 clearly indicate the presence of five dominant signals, however this is to a lesser extent confirmed by node 2. Figures 49 depicts the five independent components that are generated by the Fast ICA algorithm for node 2. Finally, from the result of the PCA estimates for the window index 400 for all the three nodes, it follows that nodes 2 & 3 indicate the presence of five independent source signals, whereas node 1 does only suggest the presence of one independent source signal. The corresponding Fast ICA generated independent components for node 1 are shown in Figure 50, again indicating an error in source separation. In contrast the results in nodes 2 & 3 both indicate the presence of 5 source signals, but these plots are omitted due to space limitations.)

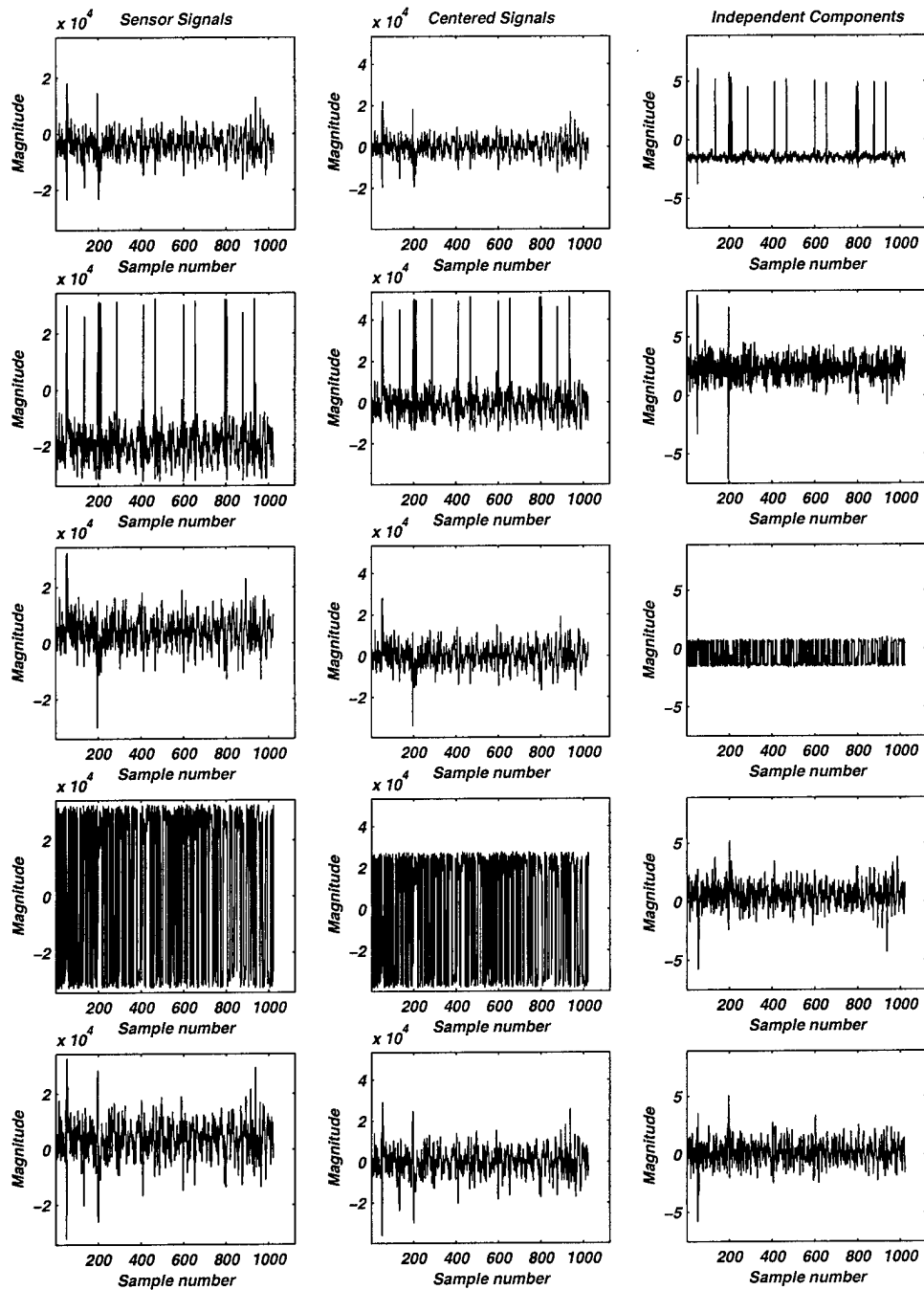


Figure 41: Fast ICA algorithm applied to SAFE II real data newr1503. The right column indicates the independent components using five components for window index 20. Limiting the algorithm to *two* independent components results in the 1st and 3rd signals from the top right column as the independent components.

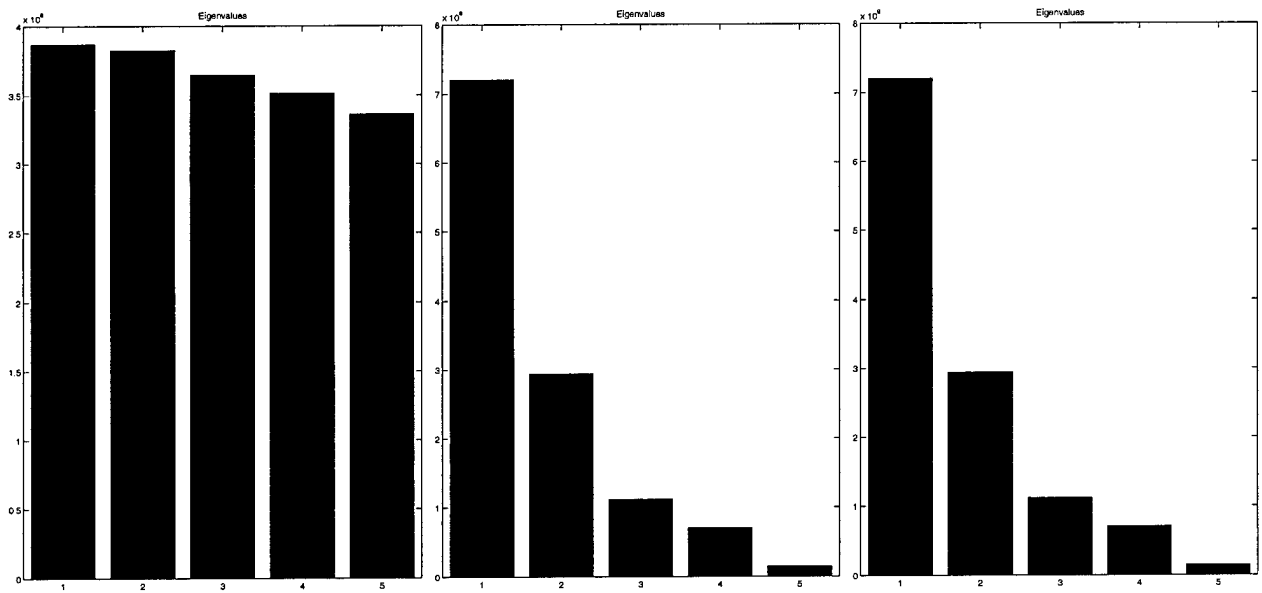


Figure 42: Principal components (PCA) based on Eigenvalue Decomposition (EVD) algorithm applied to SAFE II real data newr1503 to newr3503 for the window indexes 130, 130, and 90, respectively.

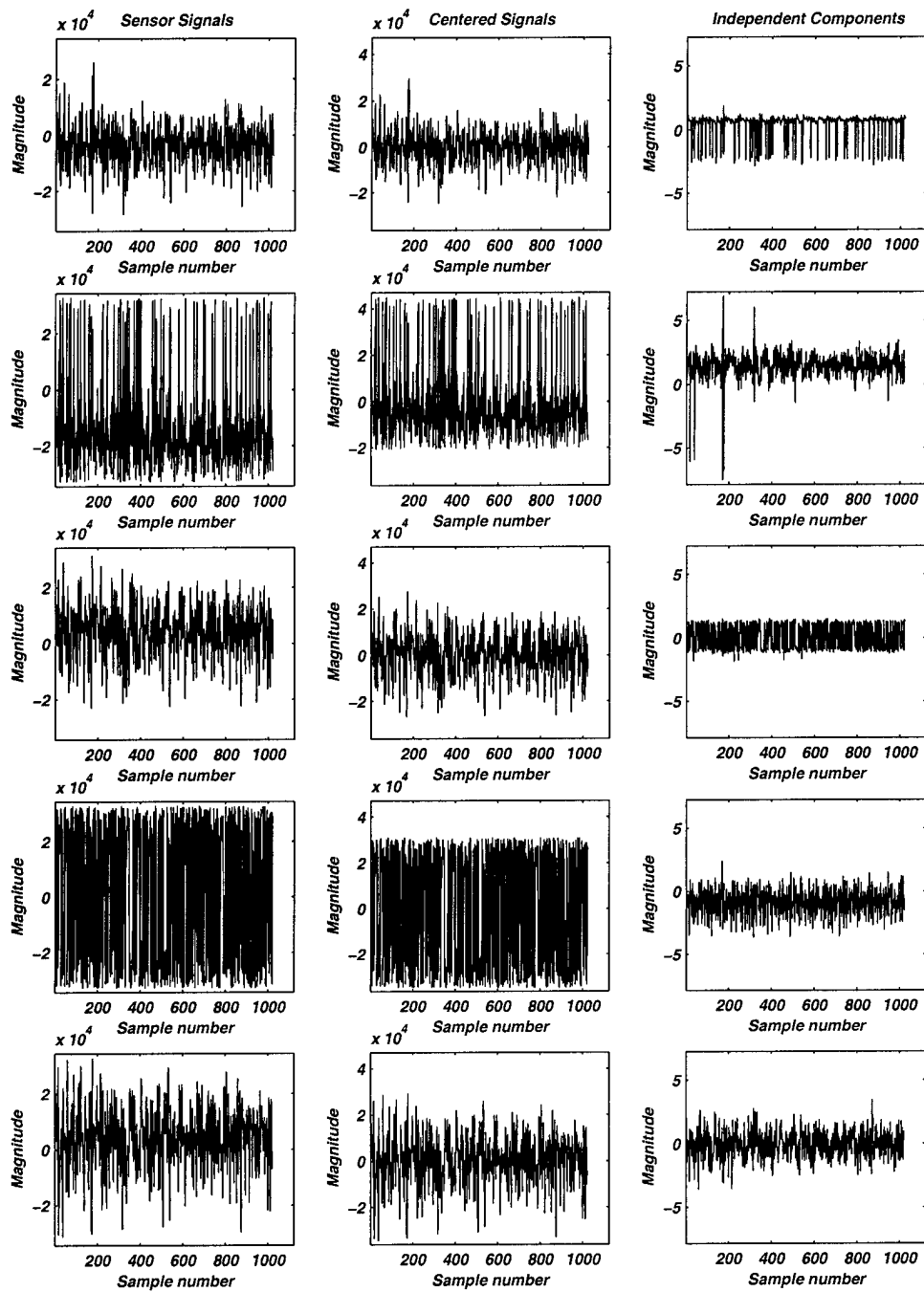


Figure 43: Fast ICA algorithm applied to SAFE II real data newr2503. The right column indicates the independent components using five components for window index 130. Limiting the algorithm to *two* independent components results in the 1st and 3rd signals from the top right column as the independent components.

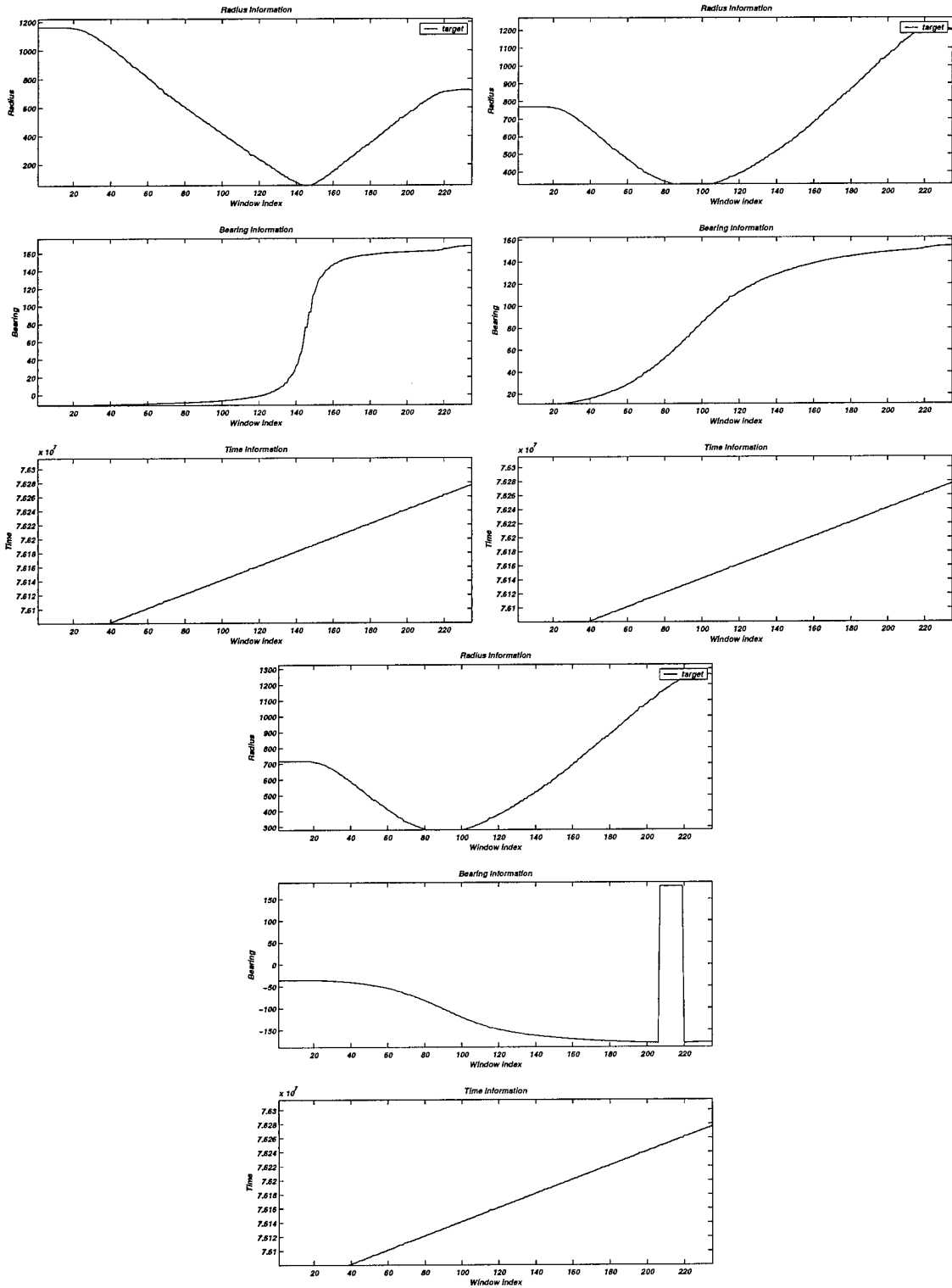


Figure 44: Ground truth diagrams for SAFE II real data newr1510 to newr3510.

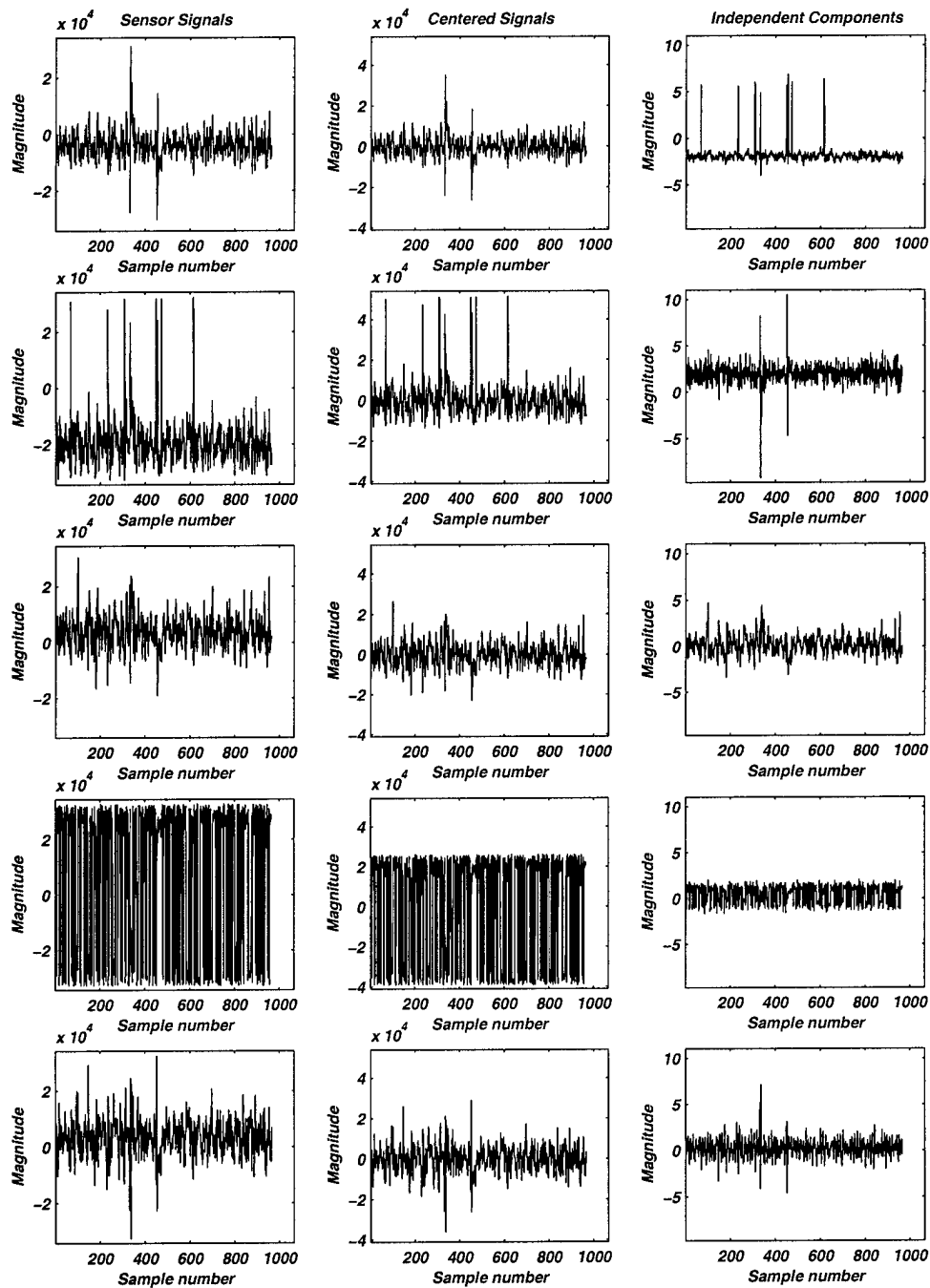


Figure 45: Fast ICA algorithm applied to SAFE II real data newr2510. The right column indicates the independent components using five components for window index 20. Limiting the algorithm to *one* independent component results in the 4th signal from the top right column as the independent component.

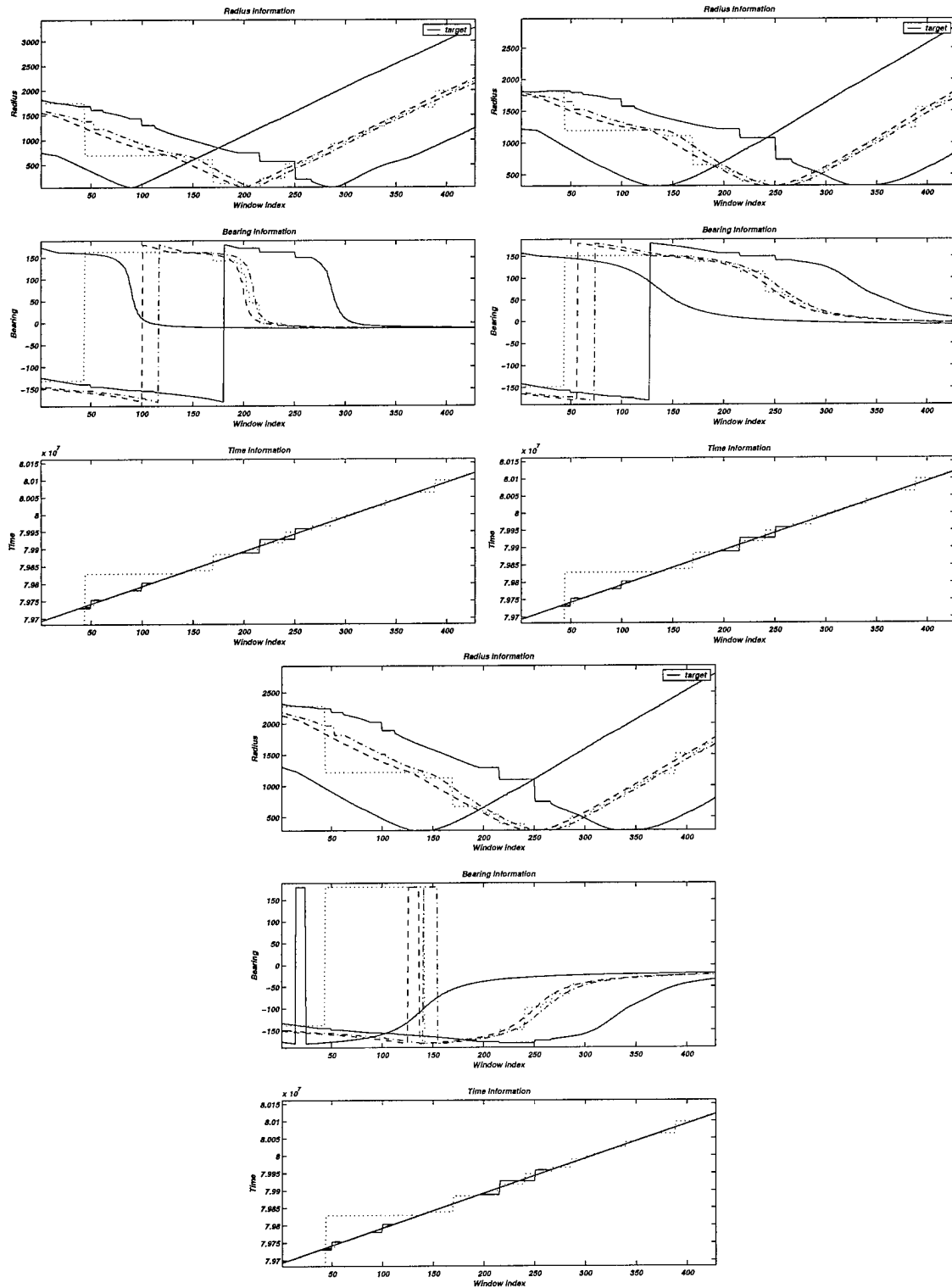


Figure 46: Ground truth diagrams for SAFE II real data newr1537 to newr3537.

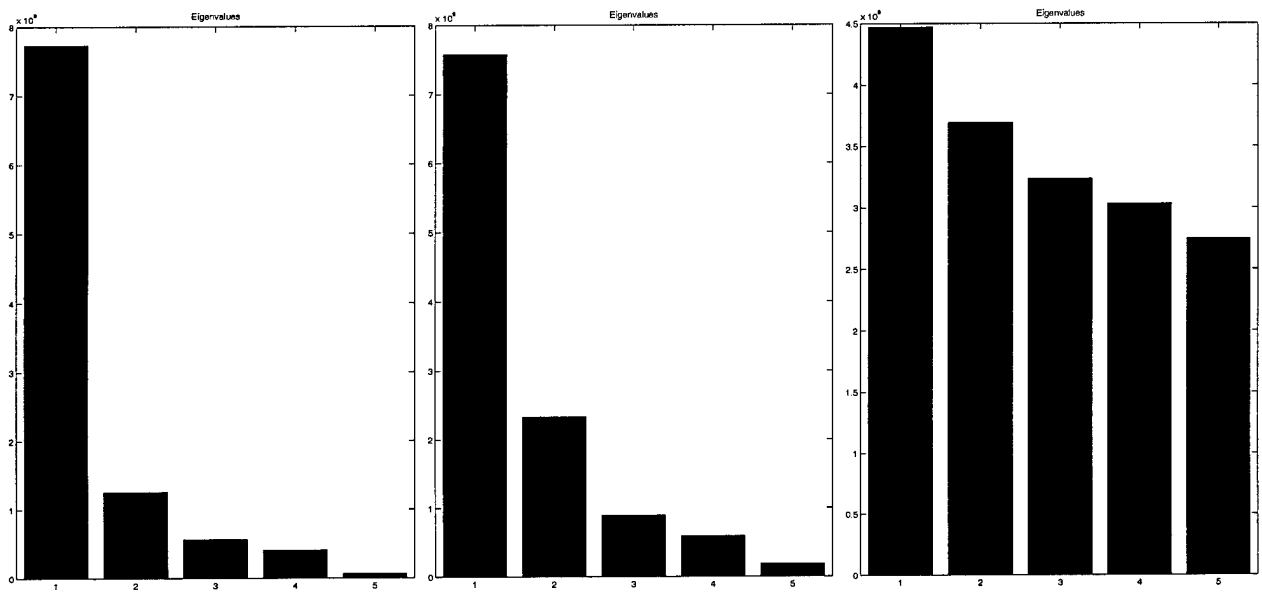


Figure 47: Principal components (PCA) based on Eigenvalue Decomposition (EVD) algorithm applied to SAFE II real data newr1537 to newr3537 for window indexes 100, 125, and 125, respectively.

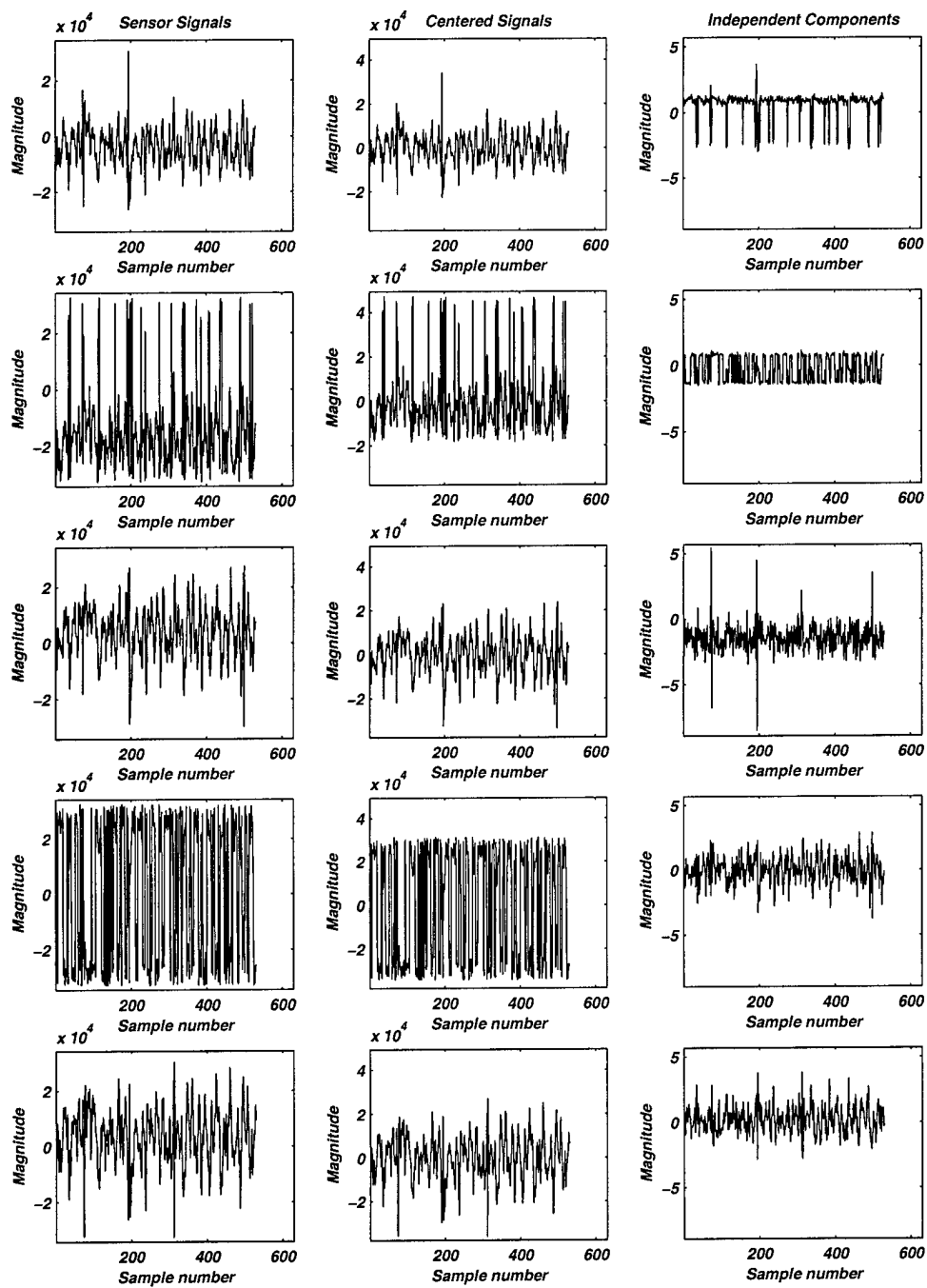


Figure 48: Fast ICA algorithm applied to SAFE II real data newr2537. The right column indicates the independent components using five components for window index 125.

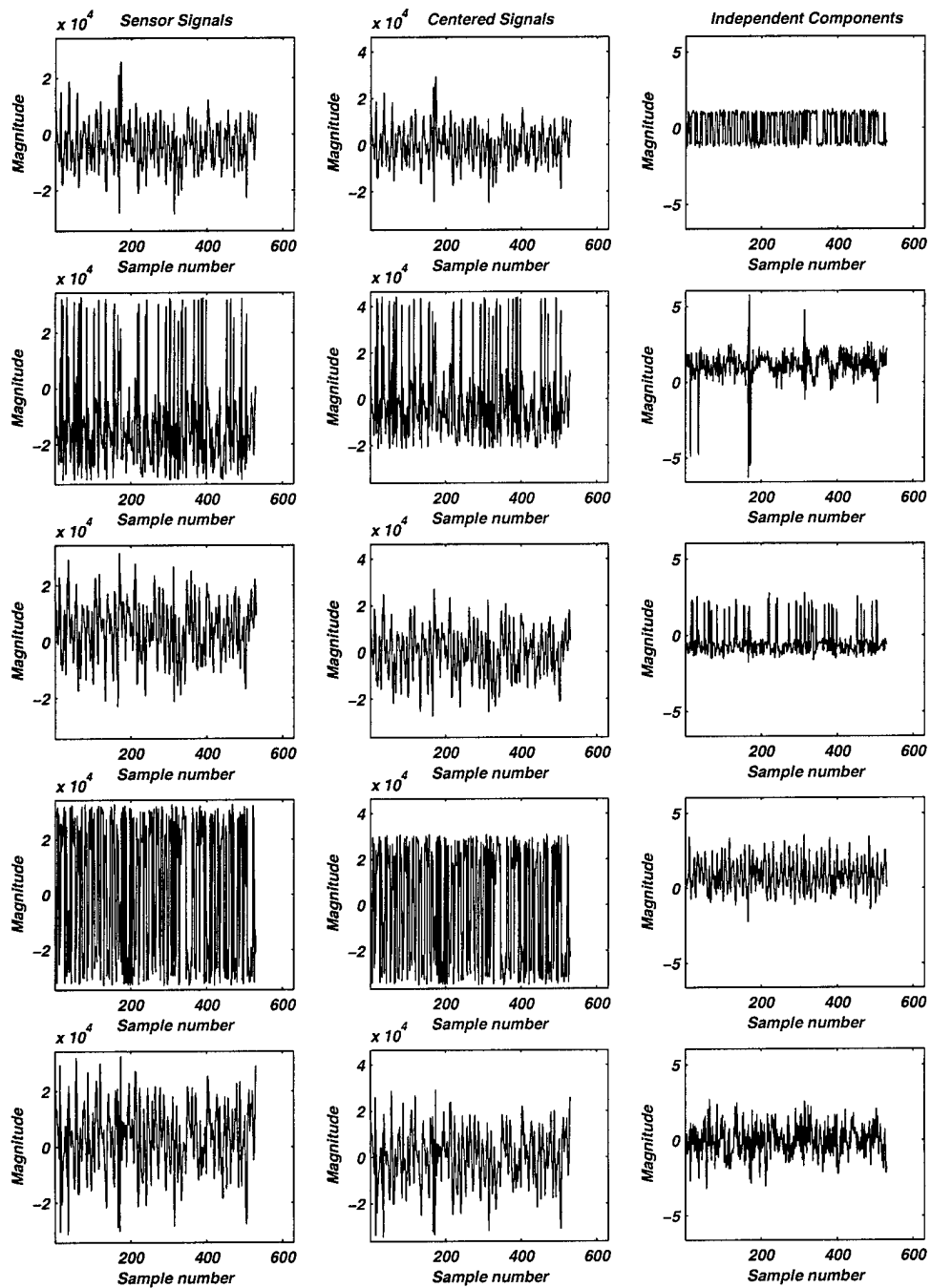


Figure 49: Fast ICA algorithm applied to SAFE II real data newr2537 using five components.

Observations:

- The PCA analysis conducted shows that the degree of dominant features could be different depending on the particular node and the location of the targets to sensors that one considers. Specifically, for the 510 series data it can be argued that the sets newr2510 and newr3510 may be approximated by one independent component whereas the newr1510 data suggested *two* strongly dominant source signals. This is interesting, as we clearly know that there is only one target in this case, therefore it would be interesting to determine the nature of the second feature present in this node, as well as to use a data fusion algorithm to integrate these results to generate valid, verifiable, and reliable conclusions.
- The above observation also applies to series 537 where in nodes 1 & 2 in window indexes 100 and 125 there seem to exist less than five independent source signals. This is interesting as we know that there are five independent source signals. Integration and fusion of these specific nodes with the other nodes should be able to remove this ambiguity and inconsistency. This is a topic of future research and investigation in Phase II.
- In all the simulation results conducted above it is interesting to note that the uniformly “flat” component signal is the most dominant pattern in all the cases and for all the nodes. We are speculating (without having any further information) that this should correspond to a “feature” that is very common for all the vehicles present in real data.

7 Composite Beampattern

In practice, the arrays are normally deployed hundreds of meters apart. However, the farther the arrays are, the less coherent the signals received from the arrays. As we know, most of DOA detectors rely on coherence of the signals received from different sensors. As a consequence, the original version of the ESPRIT algorithm described in the previous section that uses the signals from all the arrays in the DOA estimation process will not directly apply to this case.

To deal with this problem, an alternative method that relies on forming the “composite beampattern” is proposed here. The motivation behind this method is that even though one array may not resolve two closely spaced targets, the two targets might look different in different arrays. Additionally, even if one array cannot detect all the targets, the other arrays will pick up these missed detected targets. For example, assume that the arrays are linear and the two targets form a vertical line with respect to one array. Now, if the second array is placed perpendicular to the previous array, it will see a parallel line formed by the targets. This property, in turn, will result in a slight difference in the peaks of the beampatterns formed by different arrays. Thus, the composite beampattern of all the arrays would exhibit peaks corresponding to all the detected targets. The proposed procedure is as follows:

Let $b_1(\theta)$, $b_2(\theta)$, $b_3(\theta)$ and $b_4(\theta)$ be the individual beampatterns of arrays 1, 2, 3 and 4, respectively. Suppose that for a target $\theta_1, \theta_2, \theta_3$ and θ_4 are the DOA's relative to the center of each array, as shown in Figure 5. Let us denote the composite beampattern by $b_x(\alpha)$ where α is the DOA with respect to the origin and take the DOA, θ_1 , detected by array 1 as the reference. The known position of the center of array 1 is assumed to be at (x_1, y_1) . Now, if the target has a DOA of θ_1 relative to the center of array 1 and a DOA of α relative to the origin, by knowing the position of array 1 (denoted by (x_1, y_1)), we could represent the position of the target, (u, v) , as,

$$\begin{aligned} u &= \frac{y_1 - x_1 \tan \theta_1}{\tan \alpha - \tan \theta_1} \\ v &= u \tan \alpha \end{aligned}$$

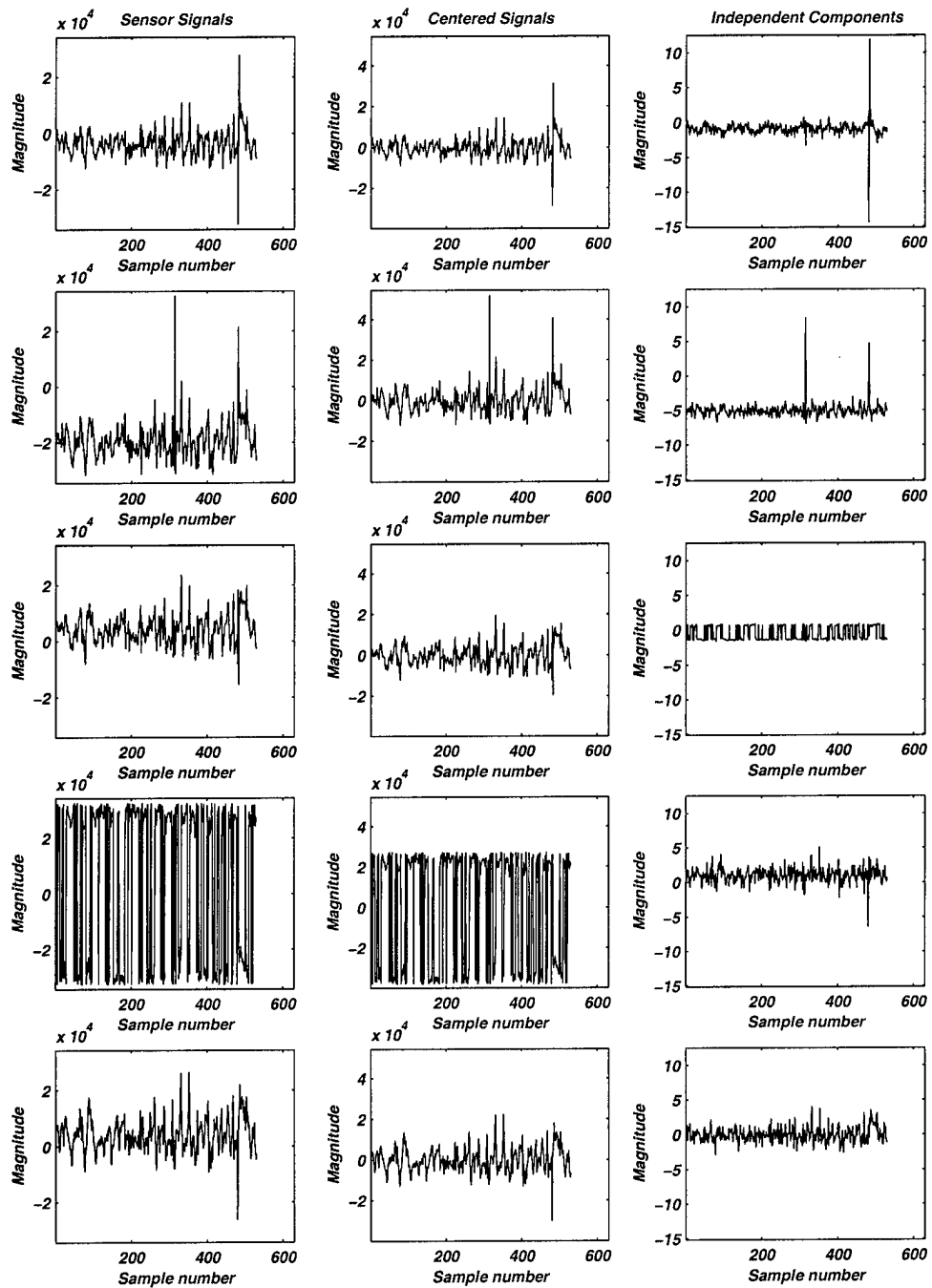


Figure 50: Fast ICA algorithm applied to SAFE II real data newr1537 using five components.

for $\theta_1 < \alpha < \tan^{-1} \frac{y_1}{x_1}$. After (u, v) is obtained, one can easily represent the corresponding DOA's θ_2 , θ_3 and θ_4 , relative to the center of arrays 2,3 and 4, respectively, i.e.

$$\theta_i = \tan^{-1} \frac{v - y_i}{u - x_i} \quad i = 2, 3, 4$$

Then, the composite beampattern at DOA α is $b_x(\alpha) = b_2(\theta_2) + b_3(\theta_3) + b_4(\theta_4)$. Note that since we used beampattern 1 as the reference, θ_1 is actually fixed (i.e. the peak of beampattern 1) and hence $b_1(\theta_1)$ is also fixed. Thus, it does not make any difference whether or not we add $b_1(\theta_1)$ to the composite beampattern.

The procedure involves incrementing α within the range $\theta_1 < \alpha < \tan^{-1} \frac{y_1}{x_1}$, and forming the composite beampattern. The peaks of the composite beampattern correspond to the DOA's of all the targets. It must be pointed out that α is incremented with the same resolution as that used to form the individual beampattern for each array. This due to the fact that the resolution of the composite beampattern is determined by the individual resolutions.

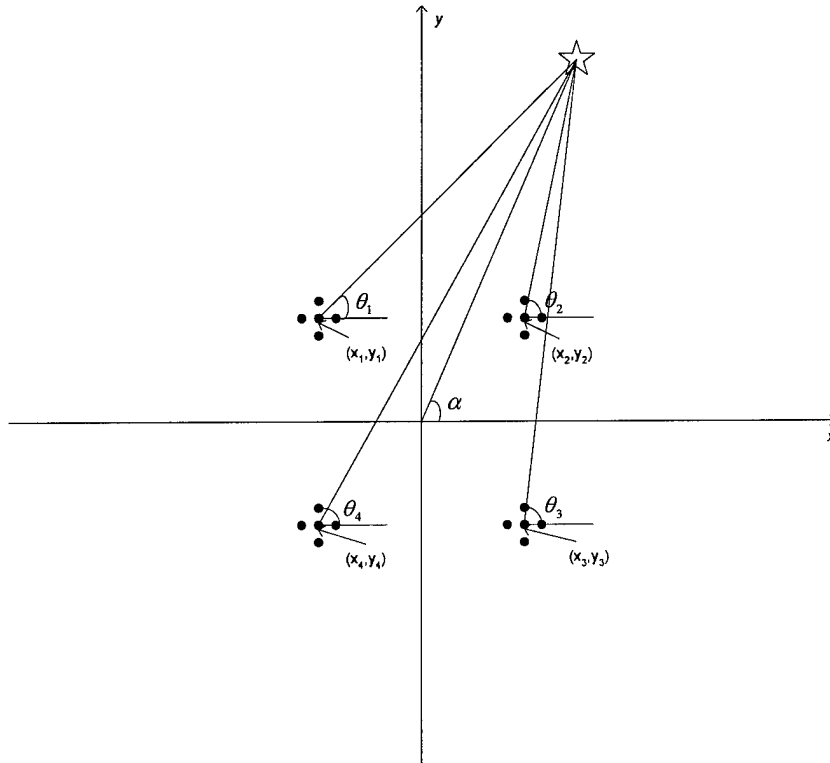


Figure 51: Forming Composite Beampattern.

One of the main goals to pursue for the next phase of this research effort is to experimentally implement and test the above algorithms for both a real (e.g. SAFE II) data set as well as our synthetically generated data sets consisting of several closely spaced targets in single-file, staggered and abreast formations. In particular, our Phase II efforts should address the following problems of the above-mentioned algorithm.

- The spatial invariance approach using ESPRIT relies on coherence of the signals arriving at the sparse arrays. However, this assumption is not valid when the spacing Δ is very large or in presence of wind noise and cluttered environment. Thus, this method needs to be extended to address the very issue in our specific application.

- Presently, the spatial invariance approach using ESPRIT is applied to narrowband sources. We plan to develop a subband version of this algorithm for wideband sources,
- Implementation, testing and bench marking of the composite beampattern algorithm on both real and synthetic data, and
- Comparison of the performance, robustness and accuracy of the approaches presented above for several spatially invariant subarray configurations.

8 Conclusions & Future Plans for Phase II

The problem of detection, localization and tracking of multiple closely spaced targets from several arrays of unattended acoustic sensors was considered in this Phase I project. The research activities in this phase were concentrated on the development of various high-resolution and robust algorithms for detecting and resolving multiple targets in tight formations. Barrier issues critical to the development of a realistic acoustic signature analysis system were also investigated. Several wideband DOA estimation methods, namely incoherent wideband MUSIC (IWM), coherent steered covariance matrix (STCM), and weighted subspace fitting (WSF) methods, were carefully studied (Section 4) and benchmarked on both synthesized as well as some limited real data (SAFE II). Our studies indicated that the STCM is an efficient method for locating and tracking target formations though it may not be very effective in resolving the individual targets, especially when they are very close together. On the other hand, WSF method exhibited very good resolution in separating different targets in a formation. The results on abreast, staggered and single-file formations revealed the excellent resolution of this method. However, this algorithm requires an exhaustive and laborious search through the entire space in order to reduce the ambiguity in estimating the DOA's. Our simulation results also demonstrated an interesting observation that if STCM is first applied as a preprocessor to detect and locate the target formations, then WSF could efficiently be implemented on a reduced search space to resolve the individual targets. This is one of the items that we intend to research further in Phase II. Another methodology for separating the targets (sources) was also extensively studied. This approach is based upon blind source separation using ICA methods. Two different ICA algorithms namely IICA and Fast ICA were investigated and applied to this problem. Our results revealed that from both computational simplicity and performance Fast ICA is a preferred algorithm for source separation. This algorithm is very simple and easy to use comparing to other ICA methods. One of the objectives in Phase II will be to investigate and develop "nonlinear" version of the Fast ICA and investigate its performance as compared to the linear ICA algorithms investigated in Phase I. The sensitivity of both the linear ICA and the nonlinear ICA algorithms to the variations in the nature of the sources, choice of the contrast functions employed, noise and other complicating attributes will be fully investigated in Phase II.

Additionally, we investigated the applicability of the spatial invariance scheme using a rectangular array consisting of subarrays/elements of the nodes that are sparsely distributed in the field. The expected benefit of this approach is wider aperture and hence better resolution. Preliminary results of this narrowband algorithm demonstrated the potential of the method for our problem. Finally, we proposed a new algorithm for combining the estimated DOA's from different arrays in order to yield unambiguous target detection and tracking.

8.1 Future Plans for Phase II

We shall continue our current research activities in Phase I toward developing dedicated high-resolution and robust DOA estimation methods for detection, separation and subsequent classification and tracking of multiple closely spaced targets. Various barrier issues and major impediments to the development of practical and real-life systems have been identified in Phase I of this project. Among the major issues that

we have identified for further investigation and research are: (a) solutions to the above-mentioned problems under non-uniform and arbitrary geometries, taking into account the advantages and disadvantages of multiple invariance geometries such as the planar geometry that is currently being utilized by the US Army Labs, (b) robustness and sensitivity analysis of the proposed as well as standard methods to the correlated and non-Gaussian noise sources, wind, heat/cold and environmental effects and competing clutter, as well as possible losses in data and failure in the array elements and/or array nodes due to unexpected circumstances, (c) multiple target tracking and classification for unattended ground sensors, and (d) ICA and blind source separation techniques for determining the number of sources from their convolutive mixture. In particular, Phase II research involves development of algorithms that address all the above-mentioned requirements and can be integrated as part of the Government acoustic data acquisition and analysis system. The testing, performance evaluation and benchmarking of the algorithms will be performed on a large number of multiple closely spaced target scenarios under various realistic operating conditions. The specific research objectives of the Phase II research study are listed below.

1. Considering the geometry of the arrays and the nodes (typically nonuniform) commonly used in battlefield scenarios, our goal is to develop efficient dedicated DOA estimation, source separation and classification algorithms for high-resolution and robust target bearing angle estimation and separation. The purpose here is to develop novel ideas for optimally combining different elements of the nodes in order to substantially improve spatial resolution for distinguishing targets in abreast, staggered or single-file formations. The proposed methods use spatial invariance by taking a rectangular array consisting of subarrays/elements of the nodes that are sparsely distributed in the field. The benefit is certainly wider aperture and much finer resolution. To avoid cyclical ambiguity due to spatial aliasing, we propose a new way of combining the sparse arrays and using subband processing. Furthermore, by developing MUSIC and ESPRIT-based approaches for this architecture it is our goal to improve on these standard techniques. We are also interested in considering the advantages and disadvantages of various wideband DOA estimation techniques, such as STCM-based method, and WSF technique, to name a few. The issues to address here will deal with the design, development and simulation of the proposed techniques suitable for the specific geometry(ies) that are used in real-life battlefield scenarios. The primary criterion is to develop algorithms that can be implemented in real-time. In addition, the methods should not rely on prior knowledge of the number of targets, target's dynamical information and initial conditions, and background interference and clutter.
2. We will continue our present work on subband MUSIC algorithm and extend the methodologies for different array combinations for multiple node configurations. This method can also be combined with the spatial invariance methods as described above. The subband processing and DOA estimation can substantially reduce the ambiguity due to the spatial aliasing of sparse arrays while giving accurate DOA's. We shall investigate how to resolve, with minimum ambiguity and high confidence, the DOA's associated with multiple closely spaced targets in spatially aliased data due to sparse nature of the arrays employed for this problem. This is especially important in presence of spatially colored interference and other interferences such as wind noise and environmental factors.
3. We will continue on our preliminary study on using ICA as a tool to perform blind source separation. The goal here is to investigate whether or not in tight target formations ICA could potentially determine the number of sources. Although, this method does not have the tracking ability, it is simple and does not suffer from the resolution versus aliasing tradeoff as with the DOA estimation methods. The practical suitability for this technique to our particular problem becomes indeed quite challenging when correlated noise and/or multipath is present.
4. We would also investigate the issue of track association and target classification. Track/data association can be used to remove the false peaks in the DOA estimates and obtain smooth tracks. This is particularly important in staggered formations when the tracks may be difficult to associate. Once this is accomplished, based upon the tonal/movement features of the targets classification can be

made. The recursive high order correlation method and sequential Bayes classifier developed by the PI will be employed for track association and target classification tasks.

5. The algorithms will be tested and analyzed on new data sets that will be acquired from the US Army TACOM-ARDEC. These data sets, which will be collected in different environmental conditions, include several multiple target cases that involve various target scenarios and high density of clutter and correlated interference. Additionally, we continue to generate several sets of realistic synthesized data by inserting multiple closely spaced targets in different tight formations. This would enable us to study the performance of the overall system in terms of accuracy, robustness and stability of the DOA estimation algorithms. Moreover, we shall continue to investigate how the algorithms perform under missing data or sensor failure conditions. This is extremely critical in real battlefield situations and in adverse environmental conditions. We would like to see how our physical understanding of the behavior and properties of the array-node configurations can inform the choice of algorithms to remedy these difficult problems.

References

- [1] N. Srour, "Unattended Ground Sensors-A Prospective for Operational Needs and Requirements", *ARL Report Prepared for NATO*, October 1999.
- [2] T. Pham, M. Fong, "Real-time implementation of MUSIC for wideband acoustic detection and tracking," *Proceedings of SPIE*, vol. 3069, pp. 250-256, 1997.
- [3] T. Pham and B. M. Sadler, "Wideband Array Processing Algorithms for Acoustic Tracking of Ground Vehicles," *ARL Technical Report*, Adelphi, MD, 1997.
- [4] A. L Swindlehurst, P. Stoica, and M. Jansson, "Exploiting arrays with multiple invariances using MUSIC and MODE," *IEEE Trans. on Signal Processing*, Vol. 49, No. 11, pp. 2511-2521, Nov. 2001.
- [5] S. J. Yu and J. H. Lee, "Efficient eigenspace-based array signal processing using multiple shift-invariant subarrays," *IEEE Trans. Antenna Propagation*, Vol. 47, pp. 186-194, Jan. 1999.
- [6] M. Wax, T. J. Shan, and T. Kailath. "Spatio-temporal spectral analysis by eigenstructure methods," *IEEE Trans. Acoust., Speech, Signal Processing*, Vol. ASSP-32, pp. 817-827, Aug 1984.
- [7] H. Wang and M. Kaveh, "Coherent signal subspace processing for detection and estimation of angle of arrival of multiple wideband sources," *IEEE Trans. Acoust., Speech, Signal Processing*, Vol. ASSP-33, pp. 823-831, Aug. 1985.
- [8] K. M. Buckley and L. J. Griffiths, "Eigenstructure based broadband source location estimation," in *Proc. IEEE ICASSP*, Tokyo, Japan, 1986, pp. 1869-1872.
- [9] G. Su and M. Morf, "Modal decomposition signal subspace algorithms," *IEEE Trans. Acoust., Speech, Signal Processing*, Vol. ASSP-34, pp 585-602, June 1986.
- [10] G. Bienvenu, "Eigensystem properties of the sampled space correlation matrix," *Proc. IEEE, ICASSP*, Boston MA, 1983, pp. 332-335.
- [11] Y. Grenier, "Wideband source location through frequency-dependent modeling," *IEEE Trans. Signal Processing*, Vol. 42, pp. 1087-1096, May 1994.
- [12] M. A. Doron, A. J. Weiss, and H. Messer, "Maximum likelihood direction finding of wideband sources," *IEEE Trans. Signal Processing*, vol. 41, pp. 411-414, Jan 1993.

- [13] Y. Bresler and A. Macovski, "Exact maximum likelihood parameter estimation of superimposed exponential signals in noise," *IEEE Trans. Acoust., Speech, Signal Processing*, vol. ASSP-34, pp. 1081-1089, Oct. 1986.
- [14] M. Agrawal and S. Prasad, "DOA estimation of wideband sources using a harmonic source model and uniform linear array," *IEEE Trans. Signal Processing*, Vol. 49, No. 3, March 1999.
- [15] S. M. Kay, V. Nagesh, and J. Slisbury, "Broadband detection based on two-dimensional mixed autoregressive model," *IEEE Trans. Signal Processing*, vol. 41, pp. 2413-2428, July 1993.
- [16] A. T. Moffet, "Minimum-redundancy linear arrays," *IEEE Trans. Antenna Propagat.*, vol. AP-16, pp. 172-175, 1968.
- [17] S. Pillai, Y. Bar-Ness, and F. Haber, "A new approach to array geometry for improved spatial spectrum estimation," *Proc. IEEE*, vol. 73, pp. 1522-1524, Oct. 1985.
- [18] J.-J. Fuchs, "Extension of the Pisarenko method to sparse linear arrays," *IEEE Trans. Signal Processing*, vol. 45, pp. 2413-2421, Oct. 1997.
- [19] C. Chambers, T. C. Tozer, K. C. Sharman, and T. S. Durrani, "Temporal and spatial sampling influence on the estimates of superimposed narrowband signals: when less can mean more," *IEEE Trans. Signal Processing*, vol. 44, pp. 3085-3098, Dec. 1996.
- [20] Y. I. Abramovich, D. A. Gray, A. Y. Gorokhov, and N. K. Spencer, "Positive-definite Toeplitz completion in DOA estimation for fully augmentable nonuniform linear antenna arrays," in *Proc. ICASSP*, Atlanta, GA, 1996, pp. 2551-2554.
- [21] Y. I. Abramovich, D. A. Gray, A. Y. Gorokhov, and N. K. Spencer, "Positive-definite Toeplitz completion in DOA estimation for nonuniform linear antenna arrays-Part I: Fully augmentable arrays," *IEEE Trans. Signal Processing*, vol. 46, pp. 2458-2471, Sept. 1998.
- [22] Y. I. Abramovich, A. Y. Gorokhov, and N. K. Spencer, "Positivedefinite Toeplitz completion in DOA estimation for partially augmentable nonuniform linear antenna arrays," in *Proc. SSAP*, Corfu, Greece, 1996, pp. 550-553.
- [23] S. Haykin, J. P. Reilly, V. Kezys, and E. Vertatschitsch, "Some aspects of array signal processing," *Proc. Inst. Elect. Eng. F*, vol. 139, no. 1, pp. 1-26, 1992.
- [24] Y. I. Abramovich, N. K. Spencer, and A. Y. Gorokhov, "Resolving manifold ambiguities in direction-of-arrival estimation for nonuniform linear antenna array," *IEEE Trans. Signal Processing*, Vol. 47, No. 10, 1999.
- [25] R. O. Schmidt, "A signal subspace approach to multiple emitter location and spectral estimation," Ph.D. dissertation, Dept. Elect. Eng., Stanford Univ., Stanford, CA, 1981.
- [26] M. Wax and J. Ziskind, "On unique localization of multiple sources by passive sensor arrays," *IEEE Trans. Acoust., Speech, Signal Processing*, Vol. 37, pp. 996-1000, July 1989.
- [27] C. Proukakis and A. Manikas, "Study of ambiguities of linear arrays," in *Proc. ICASSP*, Adelaide, Australia, 1994, Vol. 4, pp. 549-552.
- [28] K.-C. Tan and Z. Goh, "A detailed derivation of arrays free of higher rank ambiguities," *IEEE Trans. Signal Processing*, Vol. 44, pp. 351-359, Feb. 1996.
- [29] Y. I. Abramovich, N. K. Spencer, and A. Y. Gorokhov, "Detection-estimation of more uncorrelated Gaussian sources than sensors in nonuniform linear antenna arrays - Part I: Fully augmentable arrays," *IEEE Trans. On Signal Processing*, Vol. 49, No. 5, pp. 959-971, May 2001.

- [30] T. Liu and J. M. Mendel, "Azimuth and Elevation Direction Finding using Arbitrary Array Geometries", *IEEE Trans. on Signal Processing*, Vol. 46, pp.2061-2065, July 1998.
- [31] A.C. Barthelemy and P.K. Willett, "Volumetric Array Prewhitening", *IEEE Trans. on Signal Processing*, Vol. 46, pp.281-293, February 1998.
- [32] M.D. Zoltowski and C.P. Mathews, "Real-Time Frequency and 2-D Angle Estimation with Sub-Nyquist Spatio-Temporal Sampling", *IEEE Trans. on Signal Processing*, Vol. 42, pp.2781-2794, October 1994.
- [33] H. Krim, M. Viberg, "Two decades of array signal processing research — The parametric approach," *IEEE Signal Processing Magazine*, pp. 67-94, July 1996.
- [34] D. D. Lee and K. L. Kashyap, "Robust maximum likelihood bearing estimation in contaminated Gaussian noise," *IEEE Trans. Signal Processing*, Vol. 40, pp. 1983-1986, Aug. 1992.
- [35] P. Tsakalides and C. L. Nikias, "Maximum likelihood localization of sources in noise modeled as a stable process," *IEEE Trans. Signal Processing*, Vol. 43, pp. 2700-2713, Nov. 1995.
- [36] R. J. Kozick and B. M. Sadler, "Maximum-likelihood array processing in non-Gaussian noise with Gaussian mixtures," *IEEE Trans. Signal Processing*, Vol. 48, pp. 3520-3535, Dec. 2000.
- [37] M. Pesavento and A. B. Gershman, "Maximum-likelihood direction-of-arrival estimation in the presence of unknown nonuniform noise," *IEEE Trans. Signal Processing*, Vol. 49, pp. 1310-1324, July 2001.
- [38] S. Visuri, H. Oja, and V. Koivunen, "Subspace-based direction-of-arrival estimation using nonparametric statistics," *IEEE Trans. Signal Processing*, Vol. 49, pp. 2060-2073, Sept. 2001.
- [39] E. G. Larsson and P. Stoica, "High-resolution direction finding: The missing data case," *IEEE Trans. Signal Processing*, Vol. 49, pp. 950-958, May 2001.
- [40] A. Bell and T. Sejnowski, "An information-maximization approach to blind separation and blind deconvolution," *Neural Computation*, vol.7, pp.1129-1159, 1995.
- [41] P. Smaragdīs, "Blind separation of convolved mixtures in the frequency domain," *Neurocomputing*, vol.22, pp.21-34, 1998.
- [42] L. Parra and C. Spence, "Convulsive blind separation of non-stationary sources," *IEEE Trans. Speech & Audio Process.*, vol.8, pp.320-327, 2000.
- [43] H. Saruwatari, S. Kurita, K. Takeda, F. Itakura, and K. Shikano, "Blind source separation based on subband ICA and beamforming," *Proc. ICSLP2000*, vol.3, pp.94-97, Oct. 2000.
- [44] H. Saruwatari, T. Toshiya, and K. Shikano, "Blind source separation based on fast-convergence algorithm using ICA and array signal processing," pp. 412-417, 2001.
- [45] J. Krolik, D. Swingler, "Multiple broad-band source location using steered covariance matrices," *IEEE Trans. on ASSP*, vol. 37, no. 10, pp. 1481-1494, 1989.
- [46] P. Boettcher, J.A. Sherman, and G.A. Shaw, "Target localization using acoustic time-difference of arrival in distributed sensor networks", presented at *SPIE AeroSense'02: Unattended Ground Sensors*, Orlando, FL, April 2002.
- [47] L.M. Kaplan, Q. Le, and P. Molnar, "Maximum Likelihood Methods for Bearings-only Target Localization," *Proc. of the IEEE Inter. Conf. on Acoustics, Speech and Signal Processing (ICASSP'01)*, pp. 3001-3004, 2001.

- [48] H. Wu, M. Siegel and P. Khosla, "Vehicle Sound Signature Recognition by Frequency Vector Principal Component Analysis", *Proc. of IEEE Instrumentation and Measurement Tech. Conf.*, St. Paul, MN, May 1998.
- [49] X. Yu and M.R. Azimi-Sadjadi, "Neural Network Directed Bayes Decision Rule for Moving Target Classification," *IEEE Trans. on Aerospace and Electronic Systems*, Vol. 36, pp. 176-188, January 2000.
- [50] J. Krolik, "Focused wideband array processing for spatial spectral estimation", Chap. 6 in *Advances in Spectrum Analysis and Array Processing, Vol. II*, S. Haykin ed. Prentice-Hall, 1991.
- [51] E. D. D. Claudio, R. Parisi, "WAVES: weighted average of signal subspaces for robust wideband direction finding," *IEEE Trans. on Signal Processing*, vol. 49, no. 10, pp. 2179-2191, 2001.
- [52] J. A. Cadzow, "Multiple source location-The signal subspace approach," *IEEE Trans. on Signal Processing*, vol. 38, no. 7, pp. 1110-1125, 1990.
- [53] M. D. Zoltowski and K. T. Wong, "ESPRIT-based 2-D direction-finding with a sparse uniform array of electromagnetic vector-sensors," *IEEE Trans. Signal Processing*, Vol. 48, pp. 2195-2204, Aug. 2000.
- [54] K. T. Wong and M. D. Zoltowski, "Direction finding with sparse rectangular dual-size spatial invariance array," *IEEE Trans. Aerospace Electr. Syst.*, Vol.34, pp. 1320-1327, Oct. 1998.
- [55] M. D. Zoltowski and K. T. Wong, "Closed-form eigenstructure-based direction finding using arbitrary but identical subarrays on a sparse uniform Cartesian array grid," *IEEE Trans. Signal Processing*, Vol. 48, pp. 2205-2210, Aug. 2000.
- [56] P. Comon, "Independent component analysis, a new concept?" *Signal Processing*, vol. 36, no. 3, pp. 287-314, April 1994.
- [57] A. J. Bell, T. J. Sejnowski, "An information-maximization approach to blind separation and blind deconvolution," *Neural Computation*, vol. 7, no. 6, pp. 1129-1159, 1995.
- [58] S. Amari, "Natural gradient works efficiently in learning," *Neural Computation*, vol. 10, pp. 251-276, 1998.
- [59] J. F. Cardoso, "Blind signal separation: statistical principles," *Proceedings of the IEEE*, vol. 9, no. 10, pp. 2009-2025, 1998.
- [60] S. Haykin, *Neural Networks — A comprehensive foundation*, 2nd Edition, Prentice Hall, 1999.
- [61] A. Hyvarinen, "Survey on independent component analysis," *Neural Computing*, vol. 2, pp. 94-128, 1999.
- [62] L. Parra, C. Fancourt, "An adaptive beamforming perspective on convolutive blind source separation," book Chapter in "Noise Reduction in Speech Applications", eds. Gillian Davis, CRC Press LLC, 2002.
- [63] L. Parra, C. Alvino, "Geometric source separation: Merging convolutive source separation with geometric beamforming," *IEEE International Workshop on Neural Networks and Signal Processing*, pp. 273-282, 2001.
- [64] C. Fancourt, L. Parra, "The generalized sidelobe decorrelator," *Proc. IEEE Workshop on Application of Signal Processing to Audio and Acoustics*, 2001.
- [65] L. Parra, C. Spence, "Convolutive blind separation of non-stationary sources," *IEEE Trans. on Speech & Audio Processing*, vol. 8, no. 3, pp. 320-327, 2000.

- [66] A. Hyvarinen, "*Fast and Robust Fixed-Point Algorithms for Independent Component Analysis*", IEEE Trans. on Neural Networks, vol. 10, no. 3, pp. 626-634, 1999.
- [67] D. T. Pham, P. Garrat, and C. Jutten, "*Separation of a mixture of independent sources through a maximum likelihood approach*" In Proc. EUSIPCO, 771-774, 1992.
- [68] C. Jutten and J. Herault, "*Blind Separation of Sources. part I: An adaptive algorithm based on neuromimetic architecture*", Signal Processing, 24:1-10, 1991.
- [69] J. Karhunen, J. Joutsensalo, "*Representation and Separation of Signals Using Nonlinear PCA Type Learning*", Neural Networks, 7(1):113-127, 1994.
- [70] J.-F. Cardoso, "*Eigen-structure of the Fourth-order Cumulant Tensor with Application to the Blind Source Separation Problem*", In Proc. ICASSP'90, pp. 2655-2658, Albuquerque, NM, USA, 1990.
- [71] J.-F. Cardoso, "*Source Separation Using Higher Order Moments*", In Proc. ICASSP'89, pp. 2109-2112, 1989.
- [72] M.C. Jones, R. Sibson, "*What is Projection Pursuit?*", J. of the Royal Statistical Society, ser. A, 150:1-36, 1987.